DEVELOPMENT OF A MALDI–ION MOBILITY–SURFACE-INDUCED DISSOCIATION–TIME-OF-FLIGHT–MASS SPECTROMETER FOR THE ANALYSIS OF PEPTIDES AND PROTEIN DIGESTS

A Dissertation

by

EARLE GREGORY STONE

Submitted to the Office of Graduate Studies of
Texas A&M University
in partial fulfillment of the requirements for the degree of

DOCTOR OF PHILOSOPHY

December 2003

Major Subject: Chemistry

DEVELOPMENT OF A MALDI–ION MOBILITY–SURFACE-INDUCED DISSOCIATION–TIME-OF-FLIGHT–MASS SPECTROMETER FOR THE ANALYSIS OF PEPTIDES AND PROTEIN DIGESTS

A Dissertation

by

EARLE GREGORY STONE

Submitted to the Office of Graduate Studies of
Texas A&M University
in partial fulfillment of the requirements for the degree of

DOCTOR OF PHILOSOPHY

Approved as to style and content by:

_____
David H. Russell
(Chair of Committee)

_____ _____
Gyula Vigh
(Member)

J. Martin Scholtz
(Member)

_____ _____
Simon W. North
(Member)

Emile A. Schweikert
(Head of Department)

December 2003

Major Subject: Chemistry

ABSTRACT

Development of a MALDI–Ion Mobility–Surface-Induced Dissociation–Time-of-flight–Mass Spectrometer for the Analysis of Peptides and Protein Digests. (December 2003)

Earle Gregory Stone, B.S., University of Texas at San Antonio

Chair of Advisory Committee: Dr. David H. Russell

Peptide sequencing by surface-induced dissociation (SID) on a MALDI-Ion Mobility-orthogonal-TOF mass spectrometer is demonstrated. The early version of the instrument used for proof-of-concept experiments achieves a mobility resolution of approximately 20 and TOF mass resolution better than 200. Peptide sequences of four peptides from a tryptic digest of cytochrome c (*ca.* 1 pmol deposited) were obtained. The advantage of IM-SID-o-TOFMS is that a single experiment can be used to simultaneously measure the molecular weights of the tryptic peptide fragments (peptide mass mapping) and partial sequence analysis, (real time tandem mass spectrometry.) Optimization of the MALDI–IM–SID–o-TOF mass spectrometer for peptide sequencing is discussed. SID spectra

obtained by using stainless steel, Au grids, and fluorinated self-assembled monolayers (F–SAM) on Au are compared. Optimum collision energies differ for the various surfaces.

The fragmentation patterns observed for a series of peptides and protein digests using the Nd:YAG laser (355 nm) for MALDI ion formation and an FSAM surface for ion activation is compared to the fragmentation patterns observed for CID and photodissociation. The fragmentation patterns observed in all cases are strikingly similar. Photodissociation produced a greater abundance of ions resulting from side-chain cleavages. As a general rule optimized SID spectra contain fewer immonium ions than either photodissociation or CID.

Evaluation of an instrument incorporating a new hybrid drift cell is discussed. Spectra for a digest of hemoglobin is compared to that acquired with an ABI 4700 TOF-TOF. The performance of the instrument is also evaluated using a micro-crystal Nd:YAG laser (355 nm) for MALDI operated at 400 Hz. Experiments were performed to determine the sensitivity and overall performance of the instrument. The reproducibility of the MS/MS spectra for gramicidin S is shown to be 94% run-to-run. The best mobility resolution obtained for a neat deposition of the dye Crystal Violet was 60 $t/\Delta t$.

Sensitivity was tested with the peptide fibrinopeptide A (m/z 1537, AA sequence ADSGEGDFLAEGGGVR). Data acquired for sixty seconds with approximately sixty femtomoles deposited. Abundant $[M+H]^+$ ions where observed as well as $[M+H]^+$-NH_3 ions. The S/N for this short run was insufficient to identify any SID fragments.

DEDICATION

This dissertation is dedicated to my mother, Ivy Mae Stone, who gave unstintingly the love, support, and understanding that only a mother can provide throughout the long years of my pursuit of two undergraduate degrees and one graduate degree.

ACKNOWLEDGEMENTS

I would like to thank Dr. David H. Russell for making available the support and resources necessary for this research to be realized, and have the research presented to a worldwide audience. I would like to express my gratitude and recognize Dr. Zee-Yong Park, Dr. Iddys Figueroa, and Dr. Sergei Dikler for their help and advice. I would like to thank Dr. Stephan B.S. Bach for encouraging me to pursue a graduate degree and selecting me to do undergraduate research because he was looking for a tinkerer, for, if he hadn't, I would not be writing this.

I would like to thank Dr. Vicki Wysocki and her group for their invaluable assistance in providing the FSAM material and surfaces used in the SID experiments. I would also like to acknowledge the assistance of Dr. Zee-Yong Park and Dr. John McLean for providing the protein digests.

And I would like to recognize all the students who endured the freshman major and honors labs I had the pleasure of teaching. In this regard I would like to also thank Dr. Frank Kola for his assistance and Dr. Michael Rosynek for giving me the opportunity to continue to teach these labs and to develop as an instructor.

TABLE OF CONTENTS

CHAPTER Page

LIST OF FIGURES

FIGURE Page

FIGURE Page

FIGURE Page

FIGURE Page

FIGURE Page

FIGURE Page

LIST OF TABLES

CHAPTER I

INTRODUCTION

The Problem

Recombinant DNA technology has opened the book on the interplay between genotype and phenotype at a molecular level and has had the consequent effect of increasing the need for analytical instrumentation.[1] Any advances in biotechnology, specifically those to address the growing need for protein identification and characterization (e.g. proteomics), are limited by the means, the analytical instrumentation and techniques, necessary to uncover the information in so rich a source. The response in regards to instrument development has been the design of more rapid, efficient mass spectrometry techniques (biological mass spectrometry among others) to replace pre-proteomics methodologies, all in an effort to speed the delivery of the information contained in the genome to the volume of scientific knowledge.[2,3,4,5] The health and longevity of a program designed to develop new analytical instrumentation for

———————————————————

This dissertation follows the style and format of the *Journal of Mass Spectrometry*.

proteomics is evidenced by the emergence of programs such as “The PepTalk Conference” (http://www.chi-peptalk.com/) where leading thinkers in the field of proteomics help other potential end users of this technology come to grips with the nuts and bolts issues of how to properly exploit these emerging technologies. Because of the enormity of the protein expression of any given genotype the primary consideration for the design of instruments intended for use in the fields of biotechnology must be that they possess a high throughput capacity. High throughput can best be accomplished by providing for (1) simple, limited purification of small amounts of proteins from complex mixtures, and (2) sensitive, rapid generation of the necessary information sufficient for structural determination.

Current Trends in Proteomic Technology

The rapid growth in the field of biological mass spectrometry and especially the area of proteomics is directly attributable to the development of ionization sources capable of introducing large, thermally labile molecules into the gas phase (*i.e.* matrix-assisted-laser-desorption-ionization (MALDI) and electrospray ionization (ESI).)[6] HPLC and capillary electrophoresis[7,8] have taken center stage in meeting challenge (1) as stated above, and when combined with an

ESI-mass spectrometer (e.g. LC/MS[9,10,11,12] and CE/MS[13,14]) are capable of addressing both challenges (1) and (2). These current state-of-the-art bioanalytical techniques provide efficient on-line separations with excellent sensitivity (subpicomole amounts of material can be analyzed), and the amino acid sequence information needed to determine the structure of peptides, proteins, oligonucleotides, and other large biomolecules is obtained.

The development of MALDI time-of-flight mass spectrometry (TOFMS), as conceived by Hillenkamp and Karas,[15] has proven equally effective and efficient as LC/MS and CE/MS in fulfilling conditions (1) and (2). Briefly, MALDI is a pulsed ionization method (ca. 5 ns pulse width), thus the ions are formed over a very short time span, and predominately singly charged $[M+H]^+$ ions with relatively low internal energies are formed.[16,17,18,19,20] MALDI as compared to ESI has some distinct advantages, *i.e.* the sensitivity of MALDI for peptides is excellent, as it exhibits both low detection limits (femtomole to sub-femtomole, attomole detection levels have been reported),[21,22,23,24] the ability to handle complex mixtures, and a relatively high tolerance of contaminants commonly found in biological samples (including salts, buffers, and detergents added for sample processing) MALDI is also advantageous instrumentally as it is a pulsed beam technique

that does not require any gating that might result in some of the limited amount of analytes of interest typically available from biological samples being discarded. Additionally, the utility of MALDI as a high pressure ionization method has been demonstrated previously and is especially useful for experiments discussed in this dissertation.[25] The use of MALDI is even more appealing for high throughput protein analysis in light of recent developments in sample preparation such as Zip Tips™ coupled with MALDI,[26,27] digestion of proteins employing organic solvent systems,[28] and on plate digestion.[29,30]

The combination of MALDI or ESI with enzymatic digestion has proven to be an excellent tool for the rapid identification of proteins; providing information that takes effective advantage of the extensive protein databases (PDB) already in existence.[31,32,33] In particular, the mass analysis of MALDI formed ions by TOFMS has evolved as an efficient tool for the analysis of these thermally labile, non-volatile biological compounds, *e.g.* peptides, RNA and DNA, and especially mixtures of peptides resulting from the tryptic digests of proteins.[34,35] The technique referred to as peptide mass mapping (PMM) by MALDI-TOFMS is rapidly becoming the method of choice for proteomics;[36,37] however, identification of proteins that are not listed in a database or

that are post-translationally modified may not be possible using only PMM.[38,39] Clearly, these problems motivate the continued development of tandem mass spectrometry (MS/MS) which provides an attractive, logical solution for identifications of unknown proteins.[40,41]

Since the introduction of MALDI and ESI, not only has the methodology of protein identification and characterization witnessed dramatic and substantial changes, the instrumentation used for tandem MS has also rapidly evolved. For example, the original tandem mass spectrometers were either triple quadrupoles or magnetic sector instruments;[42] but in the last few years tandem MS instruments such as quadrupole ion traps, reflectron TOF, and various hybrid instruments using a combination of quadrupoles, ion traps, and TOFs have been developed.[43,44,45] The ideal tandem mass spectrometer would be capable of simultaneously acquiring partial sequence information (MS2 spectra) on all the peptides in the PMM (MS1 spectra),[46] and to date this goal has not been achieved as current state-of-the-art MS/MS instrumentation relies upon sequential peak interrogation for peptide sequencing. With respect to proteomics, the inability of traditional tandem MS to simultaneously acquire MS1 and MS2 spectra is a significant limitation. For example,

several minutes are required for interrogation of each sample, or even longer depending upon the number of peptides in the PMM and the number of laser shots required to achieve an acceptable S/N level. [47] Typically the mass spectrometer (MS1) is scanned to acquire the mass spectrum of the intact analytes, *i.e.* PMM, and MS1 is then used to select specific ions of interest. The mass selected ions are then activated and fragmented by using collision-induced dissociation,[48] photodissociation,[49] spontaneous decay (metastable ions),[50] or surface-induced dissociation (SID),[51] and the fragment ion spectra of the selected ion is acquired using a second mass spectrometer (MS2). The sequential analysis of the PMM places a high demand on analytes which may be of limited abundance. It would therefore be useful not only for purposes of increasing throughput but also for reasons of decreasing the amount of analyte required to acquire both the PMM and partial sequence information simultaneously. The necessity of interrogating each intact analyte ion individually, by scanning electric or magnetic fields, limits sample throughput of complex mixtures. The simultaneous acquisition of all product ions from a mixture of analytes is possible and has been demonstrated using FT–ICR multiplexing schemes.[52] However, the information obtained by the FT-ICR experiment is limited by the lack of a correlation between the

MS2 ions and precursor $[M+H]^+$ ions for highly complex biological mixtures such as whole cell analyses of yeast as demonstrated by Smith *et al*.[52]

Separation / MS Timescale Compatibility

Given an ideal tandem MS instrument capable of simultaneous acquisition, as noted above, the sample throughput requirements for proteomics must still be met. An emphasis on rapid, efficient separation methods is of primary concern. The limiting factor in the methods discussed above is the disparity in the timescale of current separation methods and the timescale of the mass analyzer. The timescales for HPLC and CE separations, the currently favored methods of separation, are really not compatible with the timescale of MS.[53] Typical HPLC analysis of biological materials requires several minutes to hours, whereas the mass spectral data can be acquired at Hz to kHz rates depending on the type of mass spectrometer that is used. The time scale for separation thus necessarily limits the sample throughput, and is an inefficient use of the mass spectrometer.

Although CE separations are more rapid than HPLC, minutes are still required with the mass spectral data acquired at much higher rates.[54] Ion Mobility (IM) separation, on the other hand, can be performed in milliseconds per separation requiring only a minute or

even less to achieve a useful signal-averaged spectra. This allows the MS data to be collected at rates in excess of 50 kHz.

Background for Ion Mobility

The ion mobility instrument is composed of an ion source, a series of rings to provide a linear acceleration field and a neutral bath gas, and a mass analyzer. Separations are based on a repetitive series of accelerations and decelerations prior to elution or detection. The ions are accelerated by the electric field and then experience a deceleration that results from collisions with the bath gas. As a result, a steady-state drift velocity is obtained as the energy imparted by the electric field is quenched by the collisions and the ions obtain a near thermal equilibrium state with the bath gas. A "one-temperature" approximation can then be assumed as long as the field strength, E, is low enough and the gas pressure, P, is sufficiently high enough that there are sufficient collisions, or $E/P \leq 2$ V cm^{-1} $torr^{-1}$, known as the "low-field" limit. Under these conditions the mobility of the ion (K, expressed in the units cm^2 V^{-1} sec^{-1}) can be considered to be constant, thus ion mobility separations are based on the collisional cross-section (σ) of the ions. The relationship between ion mobility and collisional cross-section is illustrated by Mason and Revercomb:[55]

$$K = \frac{3e}{16N}\left[\frac{1}{m}+\frac{1}{M}\right]^{1/2}\left[\frac{2\pi}{kT}\right]^{1/2}\frac{1+\Delta}{\pi r_m^2 \Omega^{(1,1)*}} \qquad \text{(Equation 1)}$$

Where *m* is the ionic mass, M is the neutral bath gas mass, $\Omega^{(1,1)*}$ is the first order collision integral, Δ is a correction term for higher order approximations. $\Omega^{(1,1)*}$ contains both a hard sphere collision term and a term for ion-neutral interactions, but the ion-neutral interaction term for peptide ions interacting with atomic and small molecule bath gases is very small and can be neglected. Total drift times, t_d, can be calculated for these as a function of K, field strength (E), and drift cell length (d) by:

$$t_d = \frac{d}{KE} \qquad \text{(Equation 2)}$$

Drift times for ions in a mass range for peptides generated by tryptic digestion of proteins (m/z 500 to 3000) is on the order of microseconds to milliseconds.

Equation 1 can be reduced to:

$$K^{-1} \alpha k(\mu\Omega)/z \qquad \text{(Equation 3)}$$

And since for larger molecules μ is a constant:

$$K^{-1} \alpha \Omega/z \qquad \text{(Equation 4)}$$

It is important to note that for larger molecules $\Omega \alpha$ surface area ($Å^2$).

$$K^{-1} \alpha Å^2/z \qquad \text{(Equation 5)}$$

The implication of Equation 5 then is that ions with a larger $Å^2$, will arrive at the detector later than ions with a smaller $Å^2$.

As previously stated, with a mass spectrometer acquiring at 100 kHz, drift times of milliseconds allow a very efficient use of the mass spectrometer. The dead time between acquisitions is reduced (see the section on high repetition rate lasers later in this chapter), but the transit times of ions in the drift cell are sufficiently long that all the ions from each ionization event can be mass analyzed. This is an important consideration when designing MS/MS experiments that are necessary for structural determinations of peptides using “soft” ionization techniques. To take advantage of the ion sampling efficiency of IM for an MS/MS experiment it is assumed that the drift cell functions analogously to a mass spectrometer. The mobility selection is roughly equivalent to MS1, prior to activation and subsequent mass analysis, MS2. At high mass, mobility drift times are dominated by collision-cross section not mass, as seen in Equation 1; however, for a near homologous series of peptides a relationship between mass and total drift time can be observed (See Figure 1)[56] as in work involving cytochrome c. Additionally, ion

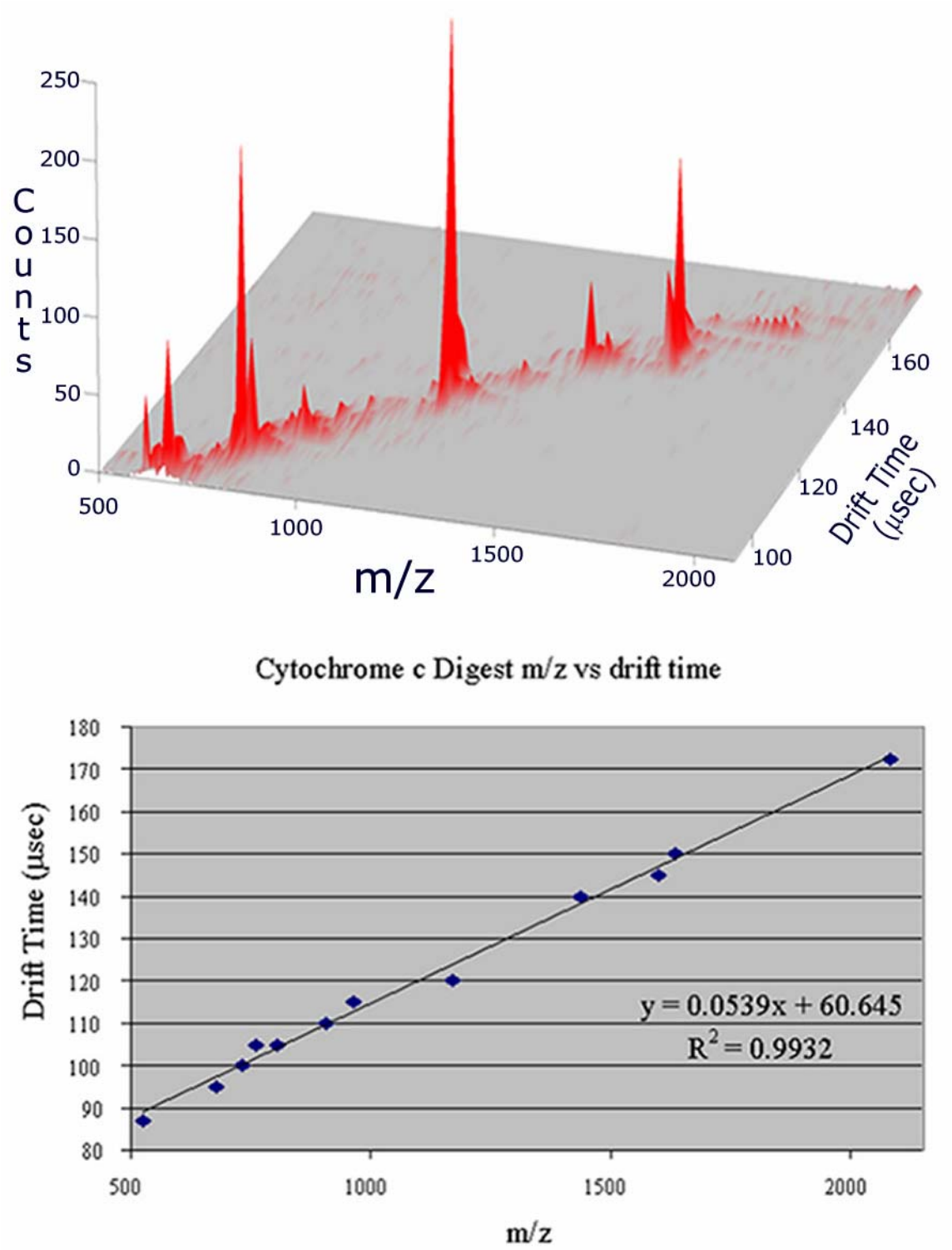

Figure 1: A MALDI/IM/o-TOF spectrum of a tryptic digest of cytochrome c and a plot of m/z vs. total drift time for twelve selected peaks

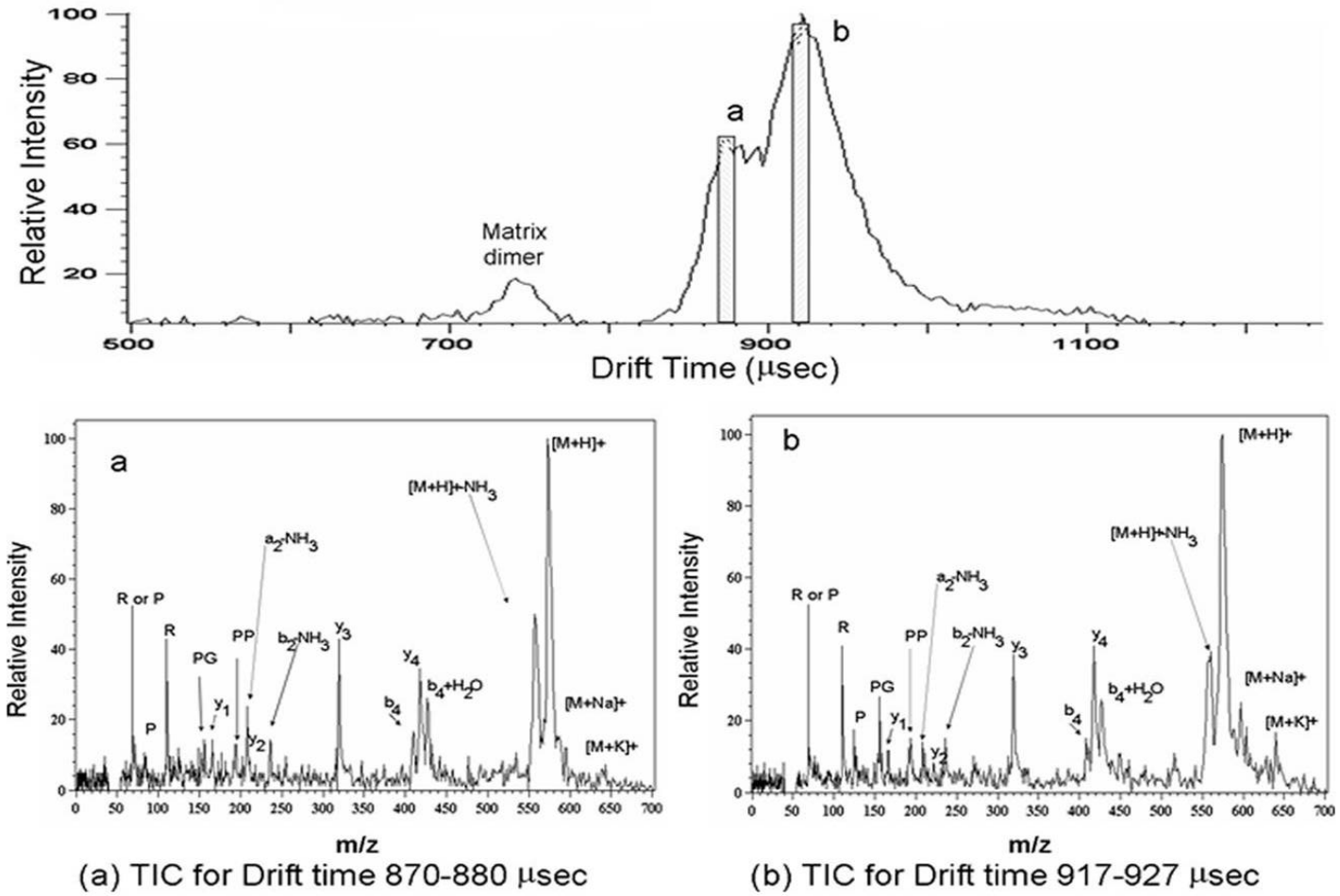

Figure 2: Top, an integrated mobility spectrum for all mass spectra acquired from 500 to 1100 msec. Bottom, integrated mass spectra extracted as indicated by the highlighted boxes in the mobility spectra.

mobility allows for an added dimension of information with the capability of observing the gas-phase conformation of the ions.[57,58]

IM allows for an added dimension of information not available in other MS/MS experiments, viz. the ability to observe different gas-phase conformations for the same ion.[59] Bradykinin fragment 1-5 (AA sequence RPPGF) is an excellent example. At low field strengths the two observed conformations do not interconvert and the fragmentation patterns for the two isomass conformations can be observed, Figure 2. The SID spectra for each of the bradykinin fragment 1-5 $[M+H]^+$ ions, where the conformations are induced by intramolecular hydrogen bonds, are identical. However, the possibility exists for species that possess two conformations due to cationization by metal ions or covalent cross linkers that the fragmentation would be different and without IM there would be no way to know what fragments corresponded to which conformer as the parent ions are isomass.

The Case for IM

One approach to the ideal tandem mass spectrometer is to couple IM to TOF mass spectrometry.[60] IM appears to be the single technique capable of high-speed separations, thereby reducing the amount of time required for cleanup of biological samples.[61] IM,

which can be considered to be a gas-phase analog of electrophoresis,[62] shows considerable potential to provide useful separations that are congruous with a mass spectrometric time scale. IM separations can be achieved in 100 μs to 20 ms per elution cycle with separation achieved on the basis of size, *viz.* surface area-to-charge ($Å^2/z$) (assuming that as stated previously that the interaction potential is negligible).[63] IM drift times can be adjusted with judicious instrument design and choice of experimental parameters to be two to three orders of magnitude longer than the mass spectrometric flight times. It is therefore possible to take advantage of the kHz data acquisition rate of the mass spectrometer while allowing for a sufficiently long elution profile to simultaneously acquire the mobility (e.g. MS1) and TOF (e.g. MS2) mass spectra. The slight differential in time scales between the IM separation and the TOF mass analysis effectively provides the ability to interrogate all the ions resulting from a single ionization event. This dissertation will demonstrate that MALDI–IM–TOFMS can simultaneously acquire the PMM and partial peptide sequence information when coupled by SID, *i.e.* the Fellgett advantage (See Figure 3.)

The marriage of IM and TOF for MS/MS experiments is facilitated by the near-linear relationship (for a relatively narrow m/z

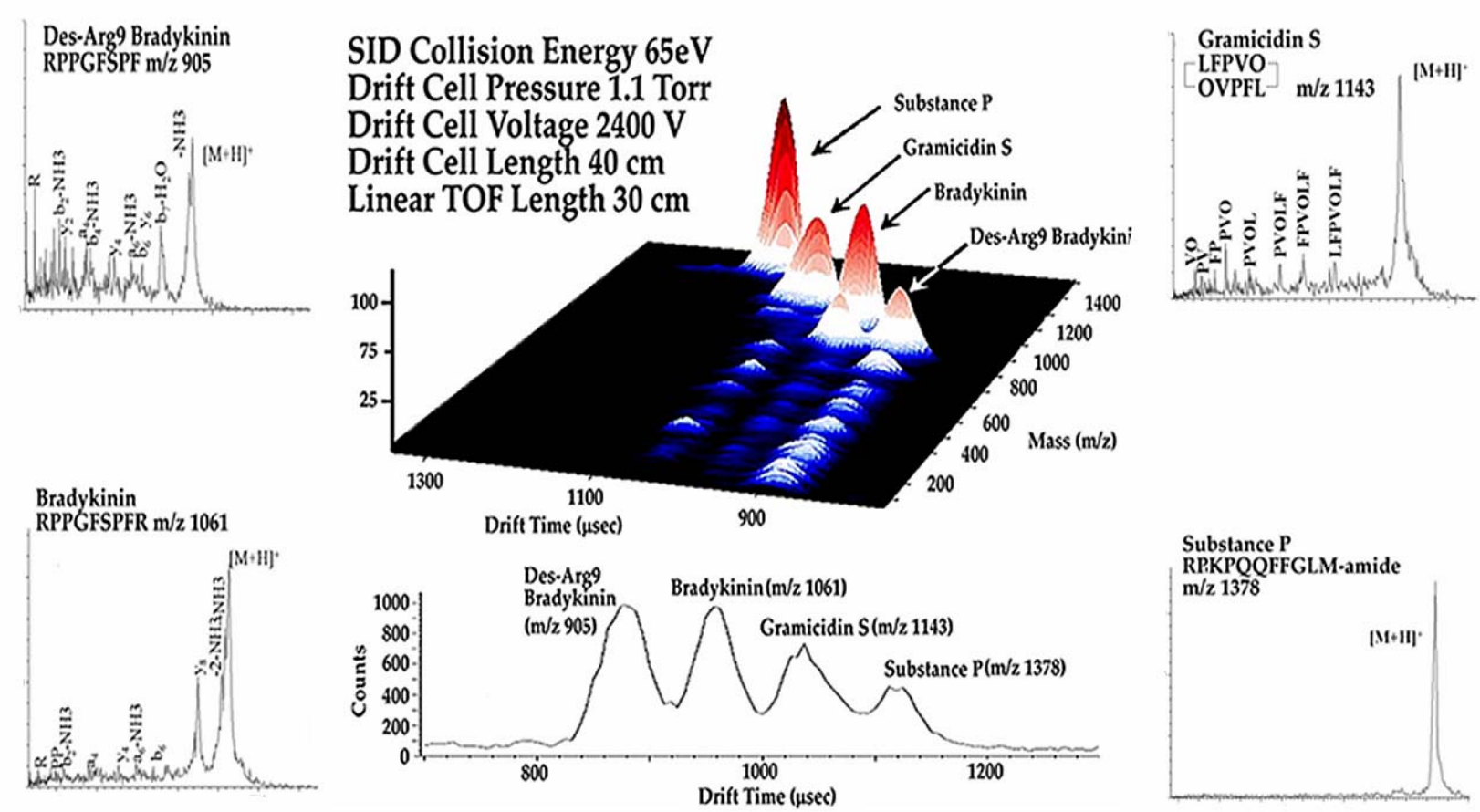

Figure 3: Shown is a 3D mass-mobility plot typical for a MALDI-IM-SID-TOFMS experiment. To aid visualization the peptide mass map (lower left) and partial sequence information for a mixture of peptides (four insets on the right) are extracted from the 3D plot using an analysis software package, Fortner Transform. Notice that the smallest peak in the mobility plot, Substance P, has the greatest precursor parent ion intensity in the series of mass spectra shown top right. The greater mobility intensity for the other three analytes in this sample is due to the simultaneous arrival of the fragment ions in the TOF analyzer with their respective precursor [M+H]+ ion.

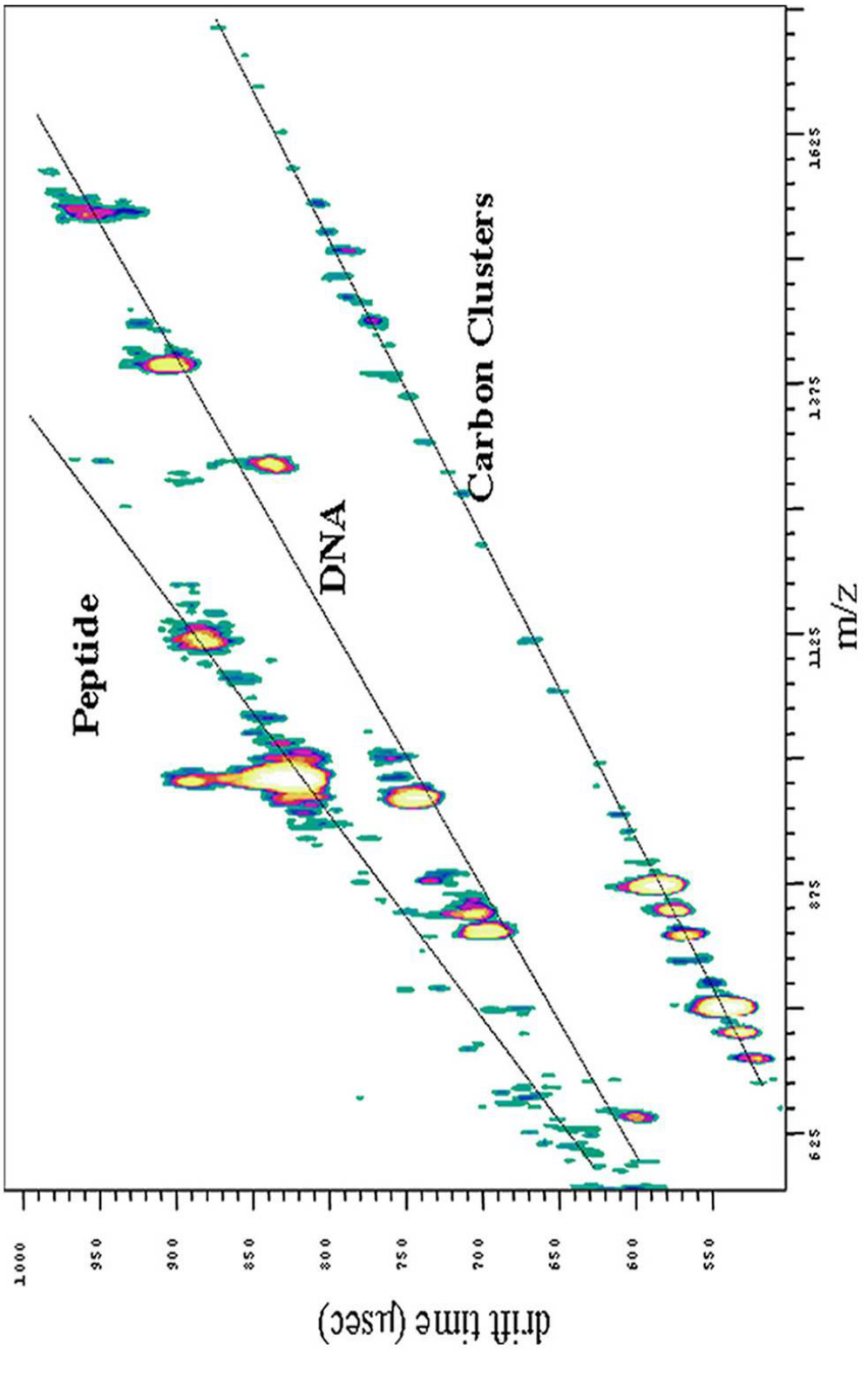

Figure 4: Ion mobility separated classes of structurally related compounds. Lines are added to ease visualization of related ions.

range) between total drift time and m/z for the typical mass range of peptides resulting from tryptic digestion, e.g., m/z 500 – 3000 (See Figure 1), and variations from a linear relationship, are due to the different packing efficiencies of the peptide sequence. For example, Griffin *et al.* showed that the mobility of structurally related compounds decreases almost linearly with mass and the standard error in a mass-mobility correlation can be as low as $\pm$2 %.[64] Karpas *et al.*[65] also showed that a mass- mobility correlation exists and that inclusion of an empirical, mass-dependent correction factor in Mason's collision cross-section equation gave quantitative agreement between mobilities and mass. The resolution, 30 – 200M/ΔM, typically attainable with simple drift cells used in ion mobility experiments is also amenable to the described experiment as the resolution provides a sufficiently wide peak for adequate ion statistics.

The fact that IM is capable of separating complex biological samples on the basis of compound class (see Figure 4) provides additional benefits. It has been shown that the gas-phase confirmations of peptides, lipids, nuclear material, and typical biological sample contaminants can be separated into structurally related classes of compounds, that is different classes have a different k, *i.e.*, $K^{-1}\alpha k\Omega/z$ and therefore $K^{-1}\alpha k\text{Å}^2/z$. This capability has a direct

relation to the peak capacity of the IM-MS experiment.[66,67] Even though IM separation of peptides is very closely related to mass, the IM-MS experiment has a peak capacity approximately five times larger than that of a TOF-TOF experiment, or any MS1 experiment of comparable mass resolution, because for even a near homologous series such as the peptides generated by the tryptic digestion of a protein there are small differences in the gas-phase conformation of the peptides.[58] Structural differences that result from post translational modification or for helical peptides can be considered compound classes, which can be distinguished on the basis of their drift time-m/z. The ability of IM to separate the compound increases the comparative peak capacity by the number of compound classes in the sample as long as the compound classes do not overlap in the IM-MS space, *i.e.* the addition of another compound class to the sample is additive to the total peak capacity. Furthermore, the multiple charge states typical for ESI formed ions are also separated by IM and add to the total peak capacity. The utility of this separation of compound classes includes separating matrix related ions for the analytes, thus the partial sequence information can be expanded to include immonium ions which are typically masked with matrix ions and matrix ion fragments (See Figure 5.)

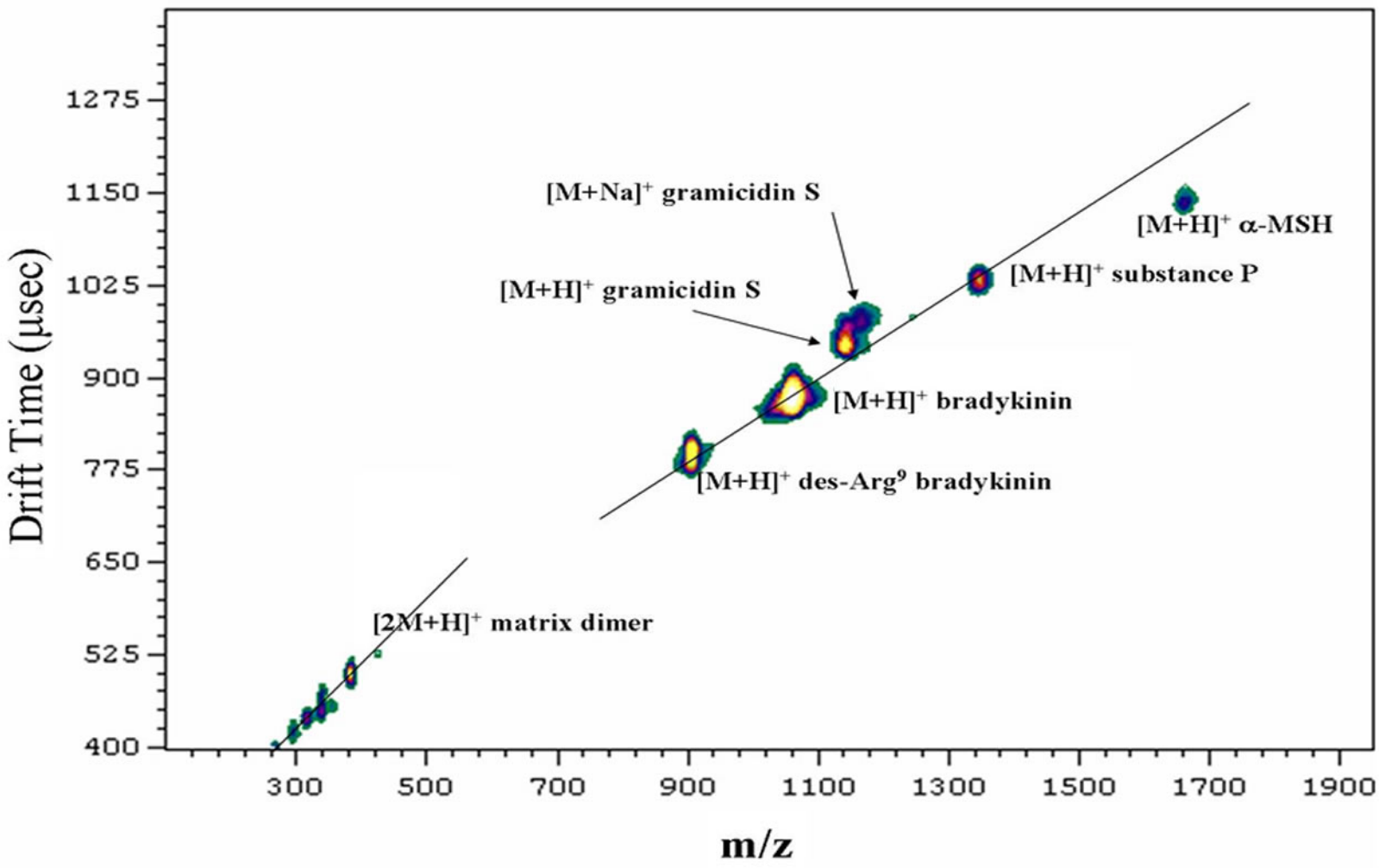

Figure 5: A typical 2D mass mobility plot for a model peptide mixture. The class separation of matrix ions from peptide ions leaves the associated mobility time slice for the low mass region of each peptide free of interfering matrix related ions. This facilitates unambiguous identification of low mass partial sequence information.

A further benefit is the capability of using isomass internal calibrants. Accurate mass measurement is of great importance when mapping complex mixtures. Absolute mass determination requires mass calibration using either an external or internal standard.[68,69] The primary problem with use of external standards can lead to ambiguous results over an extended mass range such as that for a typical tryptic digest. The same is true for matrix calibrants. Internal calibrants are used to correct for affects of changing instrumental variables. As in the case of matrix monomers and dimers the signal from internal calibrants can often be much more intense than peptide signals which can often occur in only trace amounts. The use of peptides or proteins to bracket higher masses may also overlap with the analyte signal or may be difficult to find a suitable pair when the masses of peptides of interest are unknown. Montaudo *et al.* developed a method using self-calibration for polymers, but it requires knowledge of the repeating unit.[70,71] Nelson *et al.* have developed two methods for internal calibration of protein digests using the over sampled amino acids as internal calibrants which can be correlated with the calculated amino acid sequence.[72] Furthermore, these methods require prior knowledge of the analyte, and this may not be possible when analyzing protein digests that contain unknown or

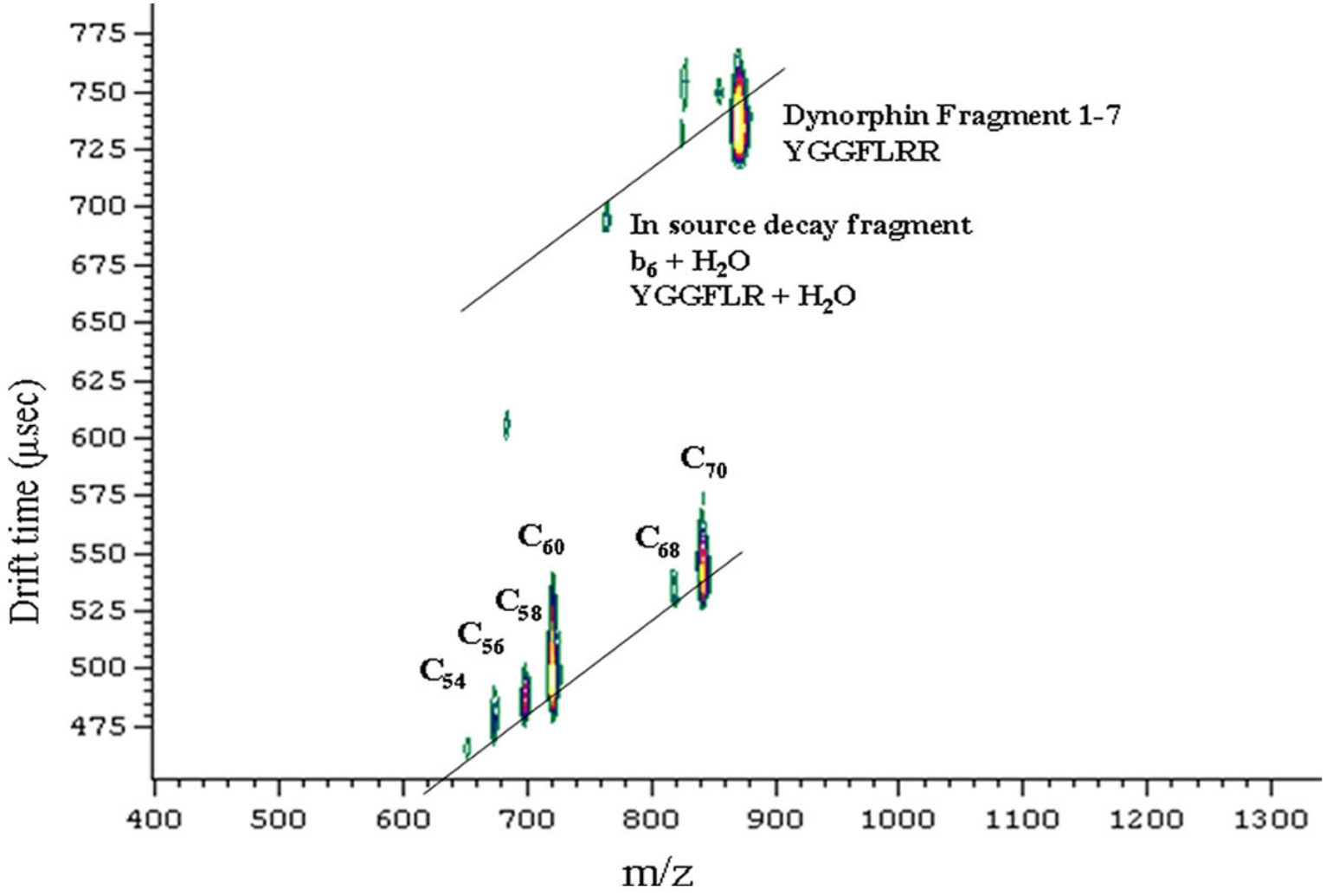

Figure 6: 2D mass-mobility plot illustrating the internal calibration of a peptide sample using C_{60} so-deposited with the matrix/analyte mixture.

modified proteins. On the other hand, carbon cluster ions formed by laser desorption and co-deposited with the matrix/peptides, can be used for high precision mass calibration in the IM-TOF experiment. As IM separates ions based on collisional cross-section ($Å^2/z$), a difference in collisional cross-section between a near homologous series of peptides and a homologous series of carbon or salt clusters results in separate mass-mobility groupings for each being observed. Carbon and salt clusters possess a different change in mobility drift time with respect to m/z ($\Delta\tau/(\Delta m/z)$) than the isomass peptides thereby eliminating the overlap and the consequent loss of peptide signals by the internal. (See Figure 6)

Background for SID

The molecular weights of the peptides can be obtained from the peptide mobility–mass map, and fragmentation of the peptide ions between the mobility drift cell and TOF ion source yields fragment ions that provide partial or complete sequence of the peptide. SID is advantageous for activation of the eluting ions prior to mass analysis of the fragment ions as the combination of SID with MALDI, IM and TOF provides considerable benefits and flexibility in terms of instrument design when compared to CID.

Significant progress has been made in the last few years to better understand SID and to improve reliability as a structural probe for gas–phase ions.[50] SID has been shown to exhibit specific advantages over the more established method of CID.[73] In SID coupled MS/MS experiments other than IM-TOF, selected ions are collided with solid surfaces at collision energies of 10-100 eV. For example, Laskin and Futrell claim that the internal energies of greater than 10 eV are possible by SID, making it the method of choice for fragmentation of large biomolecules. More importantly, the internal energy of the excited ions has a narrow distribution[74] and is easily controlled by the collision energy, which is a function of surface material and ion velocity. It has been shown[75] for cyclic peptides that fragment ions leave the surface after collision with a common velocity and that the dissociation event occurs away from the collision surface.[76] However, since the ions leave the surface with a wider range of kinetic energies, with the distribution of energies increasing with mass, it is expected that there will be some loss of mass resolution. The degradation of mass resolution though should not be a problem as it has been demonstrated that proteomic software packages on the Internet can successfully identify a peptide given the mass of the digest parent ion and as few as two fragment ions of that

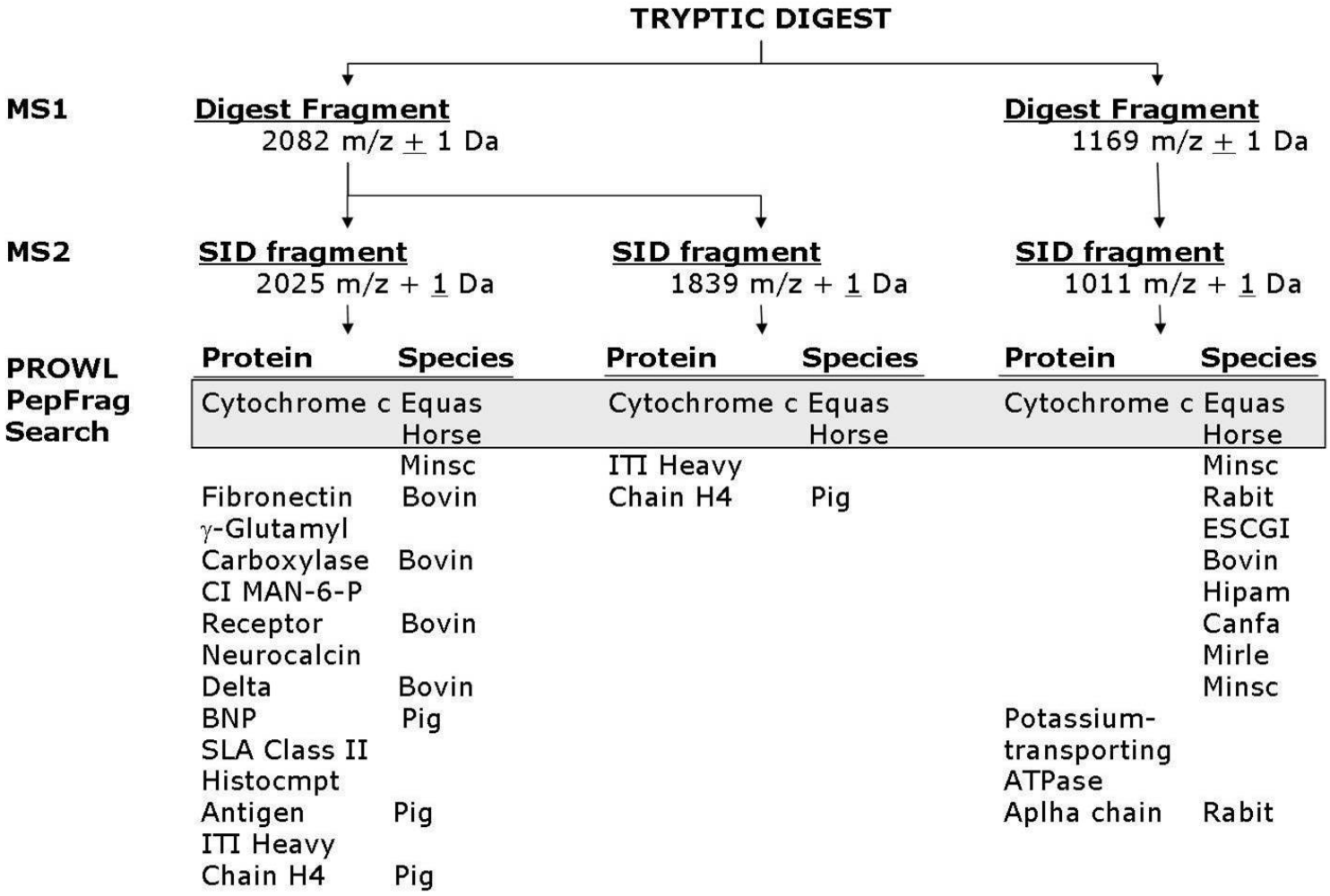

Figure 7: A flow chart illustrating the methodology for identifying a tryptically digested protein.

parent provided with a modest mass accuracy of ±1 Da. Using the PepFrag routine provided in PROWL,[77] it can be shown with a mass accuracy of ± 1 Da[78] that protein identification can be accomplished with only two tryptic digest fragments over mass 1000 with one or two corresponding SID fragments (Figure 7). The following search criteria were employed: the Kingdom field was set to other mammalia, trypsin was selected as the digestion enzyme, the digest fragment type was selected as the $[M+H]^+$, number of protein matches was set to 100, average mass was selected, and the mass accuracy for both digest fragment and SID fragment was set to ± 1 Da. Total search times averaged two seconds.

As IM drift tubes and TOF analyzers are relatively simple to design and construct, SID does not add any additional complexity as it does not require expensive lasers like those needed for photodissociation nor the introduction of a bath gas, increasing vacuum requirements in the mass analyzer, and gas controllers as with CID. In addition to the value of the instrument configuration for sequencing peptides, the pulsed nature of the MALDI–IM experiment provides a new dimension to fundamental studies of the utility of SID. For example, time based studies applied to SID experiment can reveal differences between ions undergoing quasi–elastic scattering, inelastic

scattering, or capture and thermal desorption providing insight to the partitioning of translational energy into the three post–collision modes; conversion to internal energy, transfer to the surface, and scattering energy.

The Case for SID

The generation of partial sequence information from MALDI formed ions presents a small challenge to instrument design as well. As MALDI is a relatively "soft" ionization technique the abundance of structurally significant fragment ions is low and steps must be taken to induce fragmentation of the protonated peptide ions, $[M+H]^+$, to determine peptide sequences or sites of post-translational modifications. Fragmentation of the ions can be increased by judicious choice of the MALDI matrix[79] or by using an ion activation process, *e.g.,* collision-induced dissociation (CID),[80] photodissociation (PD),[81] or surface-induced-dissociation (SID)[82] with subsequent mass spectrometry analysis of the fragment ions, so-called MS-MS or tandem mass spectrometry.

As implied above, the increased throughput, efficiency, and dimensionality of information observed using IM/MS can be further enhanced when coupled in an MS/MS experiment utilizing surface-induced dissociation (SID), collision-induced dissociation (CID), or

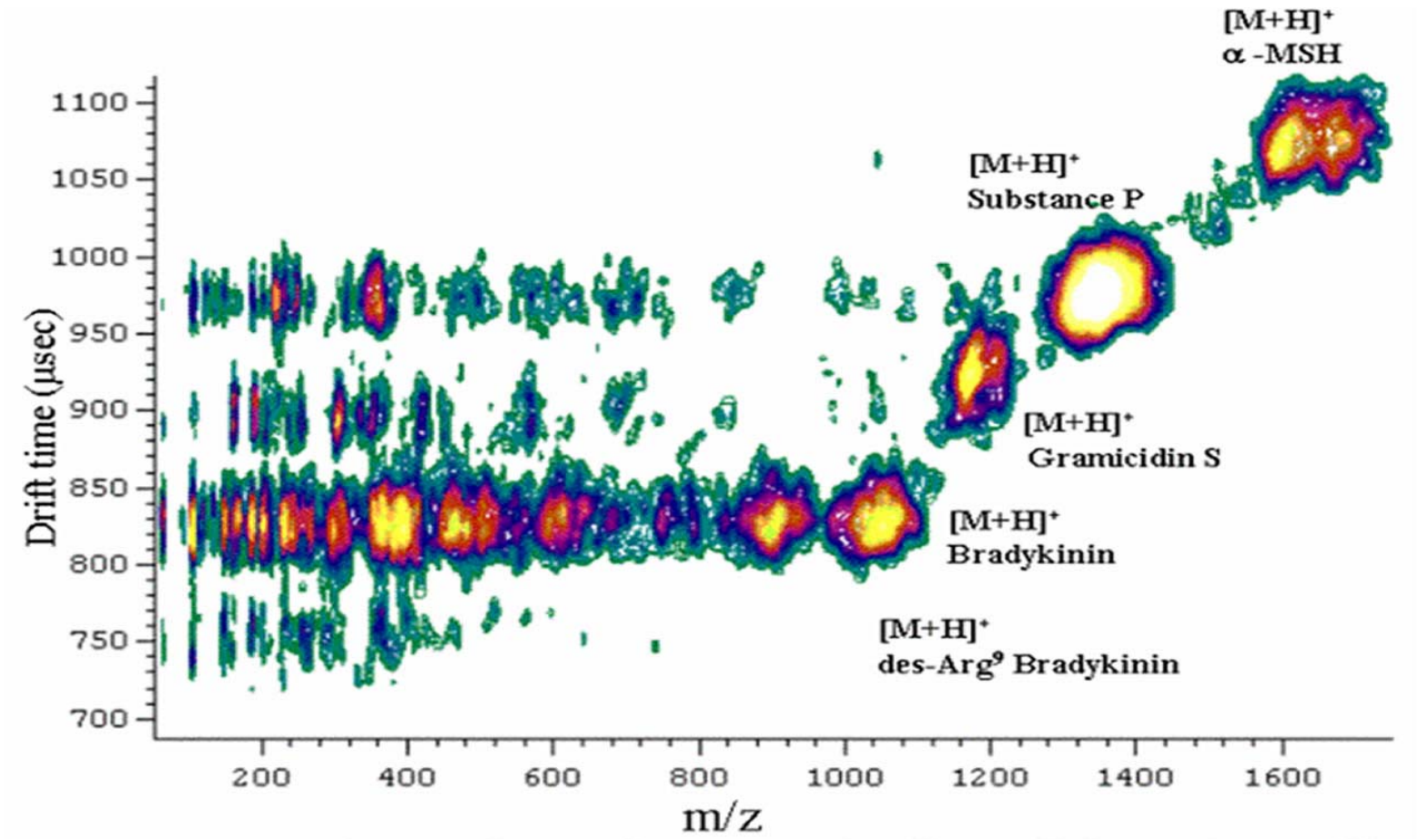

Figure 8: A mobility/mass plot of a simultaneously acquired MS/MS spectrum for a model peptide mixture; des-Arg^9 bradykinin, bradykinin, gramicidin S, substance P, and α-melanocyte stimulating hormone. Collision energy for SID is 70 eV with a perfluorinated C_{13} self-assembled monolayer. The mass-activation energy dependence is clearly shown. A complete sequence for bradykinin is observed and at lower energy a complete sequence for des-Arg^9 bradykinin. A larger kinetic shift barrier and an insufficient flight time post-SID did not permit the observation of fragments for α-MSH.

photodissociation (PD). IM-TOF is of particular interest for MS/MS experiments as both IM and TOF can be used as time–domain m/z separators. Fragment ions arising from protonated peptides that dissociate following mobility separation will arrive in the TOF ion source simultaneously such that a drift–time correlation between the fragment ions and the precursor $[M+H]^+$ ion is established. The m/z value of $[M+H]^+$ and fragment ions are measured using the TOF analyzer. The resulting plot of mobility drift time vs. m/z (TOF) (See Figure 8) simultaneously yields both a series of mobility separated $[M+H]^+$ ions (the peptide mass map) and the fragment ion spectra associated with a particular $[M+H]^+$ ion (peptide sequence information.)[40,41] Additionally, Laskin and Futrell have reported dramatic improvement in S/N for their FT–ICR SID studies, which is important for biological samples where often the signal of interest is one for a peptide of low counts or may be lost in the biological, or matrix background.[83]

High Repetition Rate Lasers

With significant improvements in the compatibility of timescales for separation and mass analysis of proteomic samples using the MALDI-IM-SID-TOFMS, the limiting factor now becomes the repetition rate of the laser typically used for MALDI. The acquisition

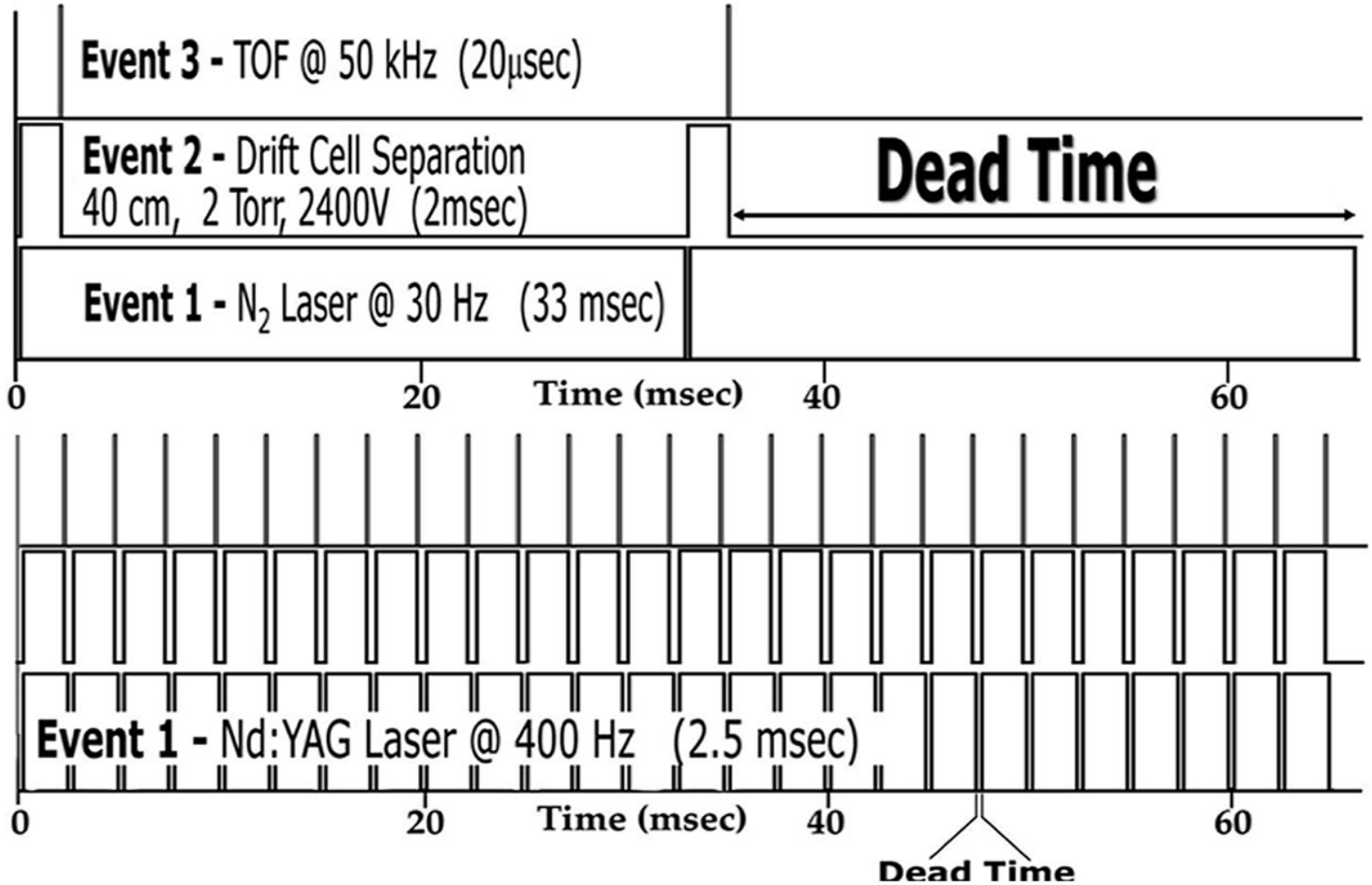

Figure 9: A schematic illustrating the effect on throughput with respect to the duty cycle of the mass analyzer (TOFMS), the separation technique (IM), and the ionization technique (MALDI laser repetition rate.)

time for simultaneous acquisition of the PMM and associated SID spectra is less than five minutes per digest sample using a nitrogen laser operated at 20-30 Hz. This acquisition time can be further reduced to less than a minute with the incorporation of a high repetition rate frequency tripled micro-crystal Nd:YAG (355nm) laser operated at 400 Hz (See Figure 9.)

The IM-MS experiment is composed of three events, the MALDI event, the IM separation, and the TOF mass analysis. The duty cycle of the instrument then is determined by the slowest repeating event. For a typical MALDI experiment this is set by the rate of the laser, 30 Hz or once every 33 msec. With the IM separation occurring on a 1-2 msec cycle this means that there is approximately 30 msec of dead time waiting for the laser to fire again before another packet of ions can be separated by IM. Dead time between laser shots is reduced by a factor greater than ten when operated at 400Hz, 2.5 msec between laser shots, using the high repetition rate micro-crystal laser. The dead time is now reduced to 0.5 msec. The sampling rate determination is now limited by the time it takes to elute a MALDI ion packet through the drift cell, 1-2 msec, as the micro-crystal laser can be operated at kHz rates.

Additional Considerations

Beyond the scope of this dissertation, but still a factor to be considered is the development of expert systems to analyze the greater abundance of data obtained resulting from the increase in throughput, as evidenced by material available at web sites for proteomic conferences (http://www.chi-peptalk.com/pnf.asp), and indeed as the bioanalytical instrumentation and methodologies of MALDI/TOFMS, LC/MS, and CE/MS are improved and consequently the ability of biotechnologists[84,85] to explore increasingly complex systems is expanded, a push has been made to include the automated analysis. Yates et al.[86] developed such an instrument utilizing HPLC, electrospray, tandem TOFMS, and the SEQUEST software package. Using such systems researchers are able to load multiple samples in the evening before going home and then returning in the morning to review the results. To make such an instrument useful in the age of the computer and the Internet several other design factors need to be considered. The instrument design should be capable of accessing protein or DNA databases and the operational software should provide data analysis capability before and after being connected to a database. This automated analysis capacity can be accomplished with the inclusion of computer algorithms capable of peak harvesting,

identification of secondary modifications, and translating and linking DNA sequences from the databases with the protein structural information obtained using mass spectrometry, *i.e.* amino acid composition, mass fingerprints, and/or peptide sequences.

Conclusion

The higher throughput for the MALDI-IM-SID-TOFMS is possible because (1) IM separation (at low pressures, 1-5 Torr He) is very compatible with the mass analyzer time scale (μsec), and (2) IM separates gas-phase ions on the basis of collision cross-section(σ)-to-charge (z) ratio (σ/z), that is, to a first approximation *m/z* is proportional to an ion's volume (size) and therefore the drift time for the ion.[87] Thus, for approximately 90%[88] of peptides resulting from a tryptic digest a near-linear mass-mobility correlation exists.[89] Additionally, the SID fragment ions arising from protonated peptides that dissociate following mobility separation in a field free region of the instrument in the TOF ion source arrive simultaneously establishing a drift-time correlation between the fragment ions and any precursor $[M+H]^+$ ions surviving activation.[90] The clear correlation between SID fragment ions and precursor $[M+H]^+$ ions permits unambiguous assignment of sequence information to the PMM. The time-resolved nature of the IM-SID-TOF experiment

results in a 2D IM-MS plot that yields both a series of mobility separated $[M+H]^+$ ions (the peptide mass map) and the fragment ion spectra associated with a particular $[M+H]^+$ ion (peptide sequence information.)[27,91] Additionally, the pulsed nature of the MALDI–IM experiment provides for fundamental studies of SID. For example, time based studies applied to SID experiment can reveal differences between ions undergoing quasi-elastic scattering, inelastic scattering, or capture and thermal desorption providing insight to the partitioning of translational energy into the three post-collision modes; conversion to internal energy, transfer to the surface, and scattering energy.

CHAPTER II

EXPERIMENTAL

MALDI-IM-TOFMS Instrumentation

MALDI, IM, SID, and TOF mass spectrometry are well suited to tackle bioanalytical problems. A home-built instrument, with simplicity and robustness as the key features, designed around a practical combination of these analytical techniques was built for the proof-of-concept experiments (Figure 10.) The instrument is comprised of a drift cell and ionization region (design pressure in the range of 1-100 Torr), a mass/mobility analyzer region (high vacuum), the necessary electronics to power and control the drift cell and analyzer region, and the appropriate computer hardware and software.

The MALDI event has been demonstrated as compatible with the higher operating pressures[92,93,94,95] of the drift-cell and was incorporated into the drift cell design to simplify the overall instrument construction. Ions are formed in the drift cell at its operating pressure on the direct insertion probe with the output from a focused nitrogen laser (337nm, 20 Hz pulse frequency.) The angle

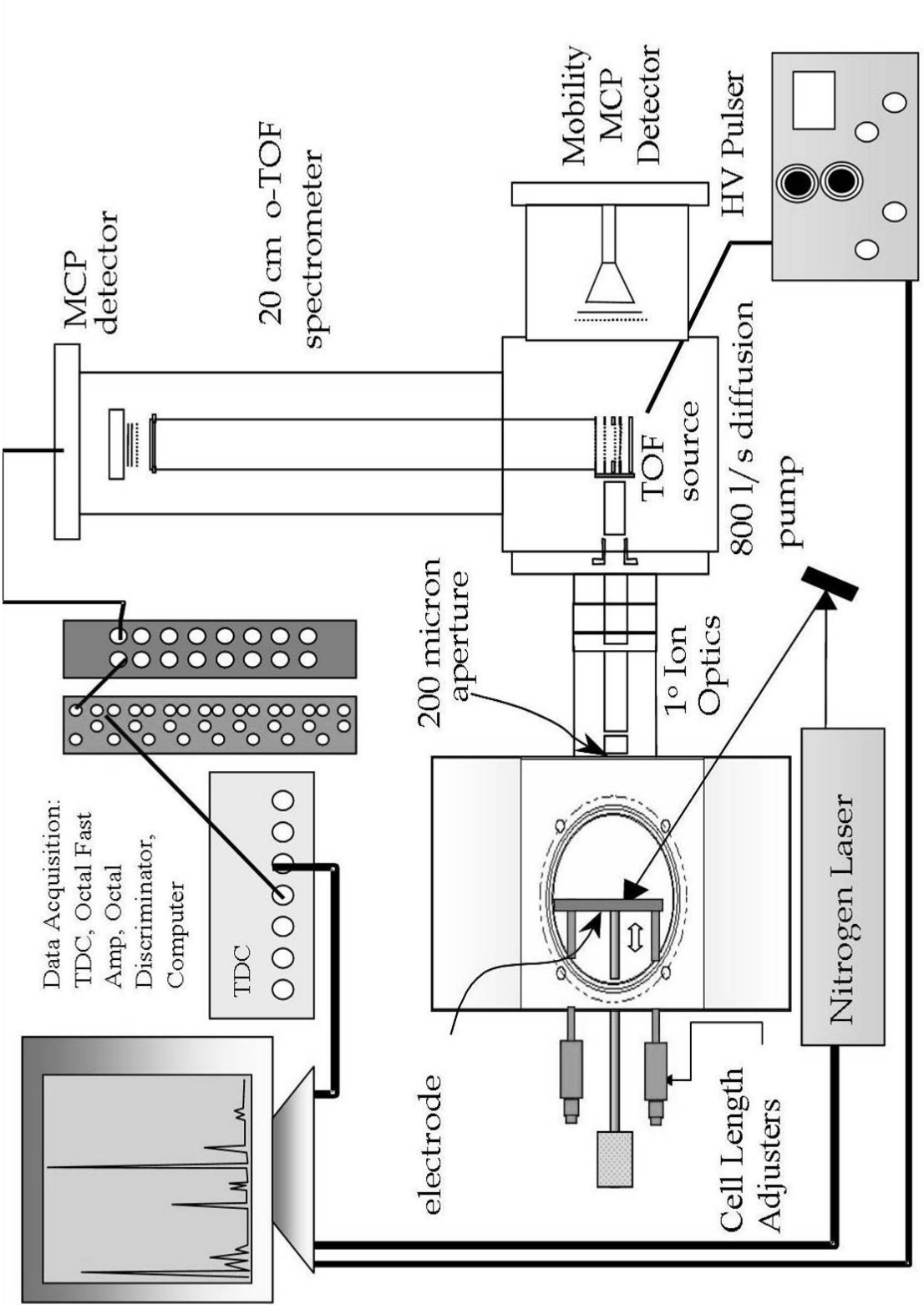

Figure 10: A drawing of the prototype MALDI-IM-TOFMS instrument.

of laser incidence was adjusted as close to normal to the probe tip sample deposition surface as instrument design allowed in order to control the laser spot size and to maximize the simplicity of the ion optics and the instrument.

Interfacing the ion mobility drift cell to the analyzer region of the instrument was accomplished using a .005 inch thick plate with a single orifice laser machined into the center. The orifice size was varied from 200 to 500 microns to limit the flow of gas in order to maintain a reasonable vacuum (5×10^{-5} Torr or better) in the mass analyzer by not overloading the available vacuum system for a given configuration, and remain large enough to not limit the sensitivity by decreasing the ion transmission. After exiting the orifice separating the drift cell from the analyzer region, ions were focused into an axial mobility detector or the extraction region of the TOF analyzer orthogonal to the drift cell axis by a series of electrodes. The o-TOF analyzer was designed to maintain a pressure of 5×10^{-6} to 5×10^{-5} Torr.

Detection of ions for both mass and mobility analysis was performed using micro channel plate (MCP) detectors and the detector signals were processed in a single ion counting mode using a time-to-digital converter (Ionwerks Model TDCX4). The start signal to

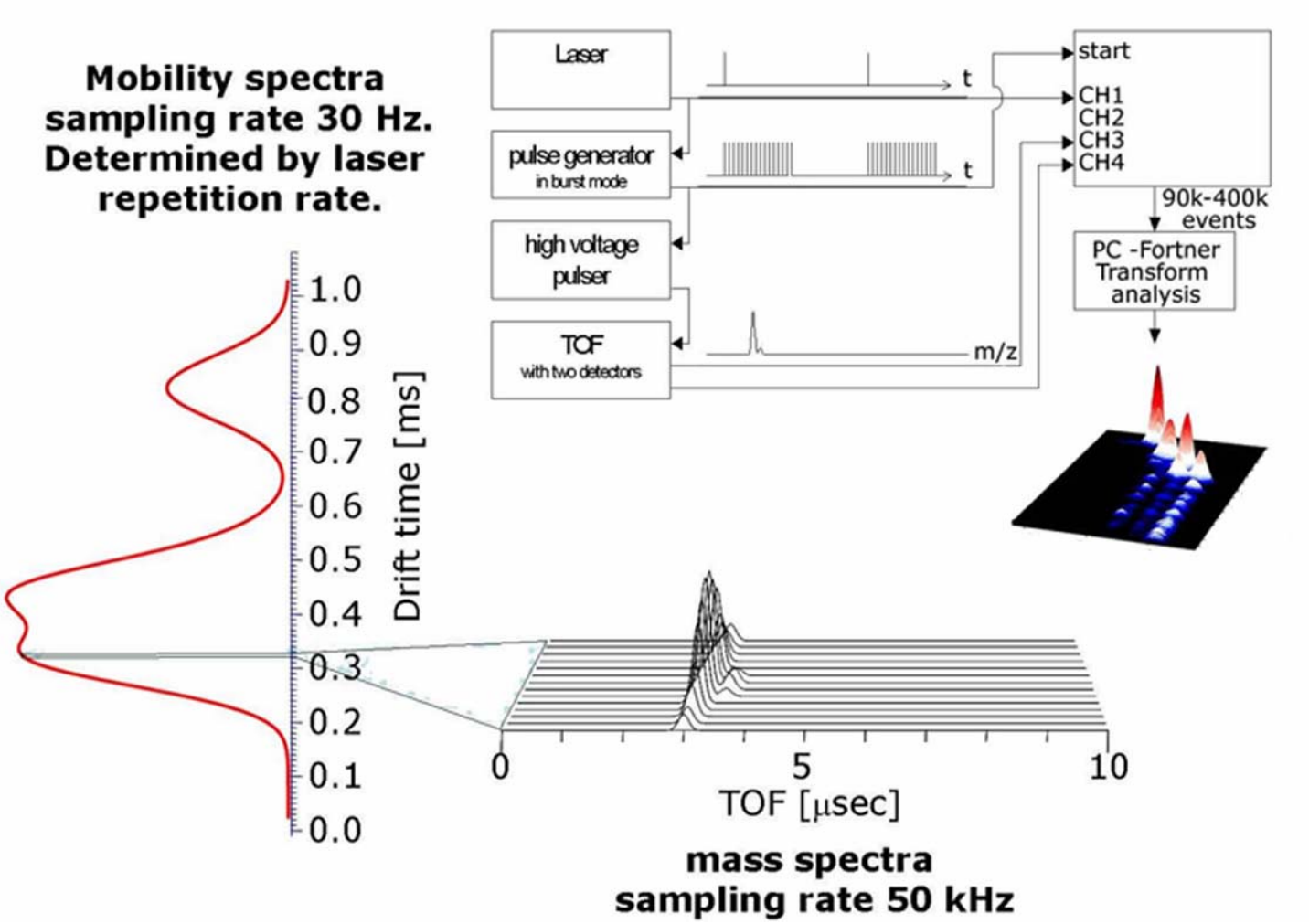

Figure 11: Pictogram of data acquisition and relationship of m/z to drift time.

measure the TOF is coincident with pulsing the extraction region (See Figure 11.) The ions extracted orthogonally and accelerated into the mass analyzer are detected by a 4-anode MCP detector (Ionwerks). Data handling is similar to GC-TOF or LC-TOF instruments and the mobility sampling rate is limited to laser firing rate, and the TOF sampling rate is limited by flight time of heaviest ion and flight tube length, for an ion of m/z 5100 ion the flight time in a 20 cm linear TOF is 20 μs. At 5 Torr the drift times are in the range of 1 -2 ms. Because the drift time through the o-TOF extraction region is shorter than the flight time in the linear TOF a theoretical duty cycle (for ions exiting the skimmer) of up to 100% exists.

Data acquisition starts coincident with the trigger pulse sent to the laser by initiating a series of pulse bursts that can be delayed by an amount of time greater than or equal to the drift time of a non-retained species. Each pulse within a burst is a complete TOF spectrum. 1000-3000 laser shots were signal averaged to increase S/N, with a complete mobility spectrum acquired for each laser shot. Because the drift time of the ions through the extraction region is shorter than the flight time in the TOF, theoretically 100% of the ions eluting from the drift cell can be sampled in quick succession. This makes provision for later experiments to simultaneously observe

several parent ions and their mobility associated SID fragment patterns in the same spectra.[96]

As the TDC will be operated in list mode, the data acquired will be exported directly to a graphing program and displayed in “real-time”. Initially data will be analyzed manually with peak lists input into PROWL protein identification programs. Data analysis was accomplished using Grams/32 (Thermo Galactic, Salem, NH) or Fortner Transform Version 3.3 (Research Systems, Boulder CO) software packages. Fortner Transform was used to generate two-dimensional contour plots with mobility separation shown as total drift time on the y-axis, m/z information shown on the x-axis, and brighter colors, yellow to white, indicating higher ion counts (hereafter denoted as a mass-mobility plot). The data acquired using the Ionwerks TDC was smoothed for all contour plots.

MALDI was performed in the IM drift cell (Figure 10) at a pressure of 5 – 10 Torr helium using a 337 nm nitrogen laser operated at near-threshold desorption levels with a repetition rate of 20 Hz. UHP helium was purchased from Praxair (Danbury, CT) and used without further purification or drying.

The TOF mass spectrometer was calibrated using a mixture of six peptides: HLGLAR (MW 665.8), des-Arg^{9}-bradykinin (MW 904.0),

neurotensin fragment 1-8 (MW 1030.1), gramicidin S (MW 1141.5), substance P (MW 1347.6), and RRLIEDAQKAARG (MW 1519.7). Studies were performed on single peptides, peptide mixtures, and protein digests.

MALDI-IM-SID-TOFMS Instrumentation

Figure 12 is a cutaway drawing of the first instrument incorporating a periodic focusing drift cell designed to improve ion transmission efficiency. An additional benefit of the new drift cell is an improved mobility resolution, approximately 50 to 100 $t/\Delta t$. The ion mobility chamber was operated between 1 to 5 Torr He with a field strength of 10 to 40 V cm^{-1}.The instrument was further modified for preliminary SID experiments by positioning a hydrocarbon coated (adventitious pump oil) gold grid (Buckbee-Mears, St. Paul, MN) in-line (perpendicular to the ion beam) (See Figure 12 A) between the mobility drift cell and the extraction plates of the o-TOF source.[97, 98] For these experiments two grids, 300 lines per inch, 90% transmittance, were overlaid to reduce the transparency to ~80%. SID was performed at a grazing incidence angle[99] to the surface and at collision energies ranging from 20 to 90 eV in the experiments using the gold grids.

This design was chosen based on convenience for performing

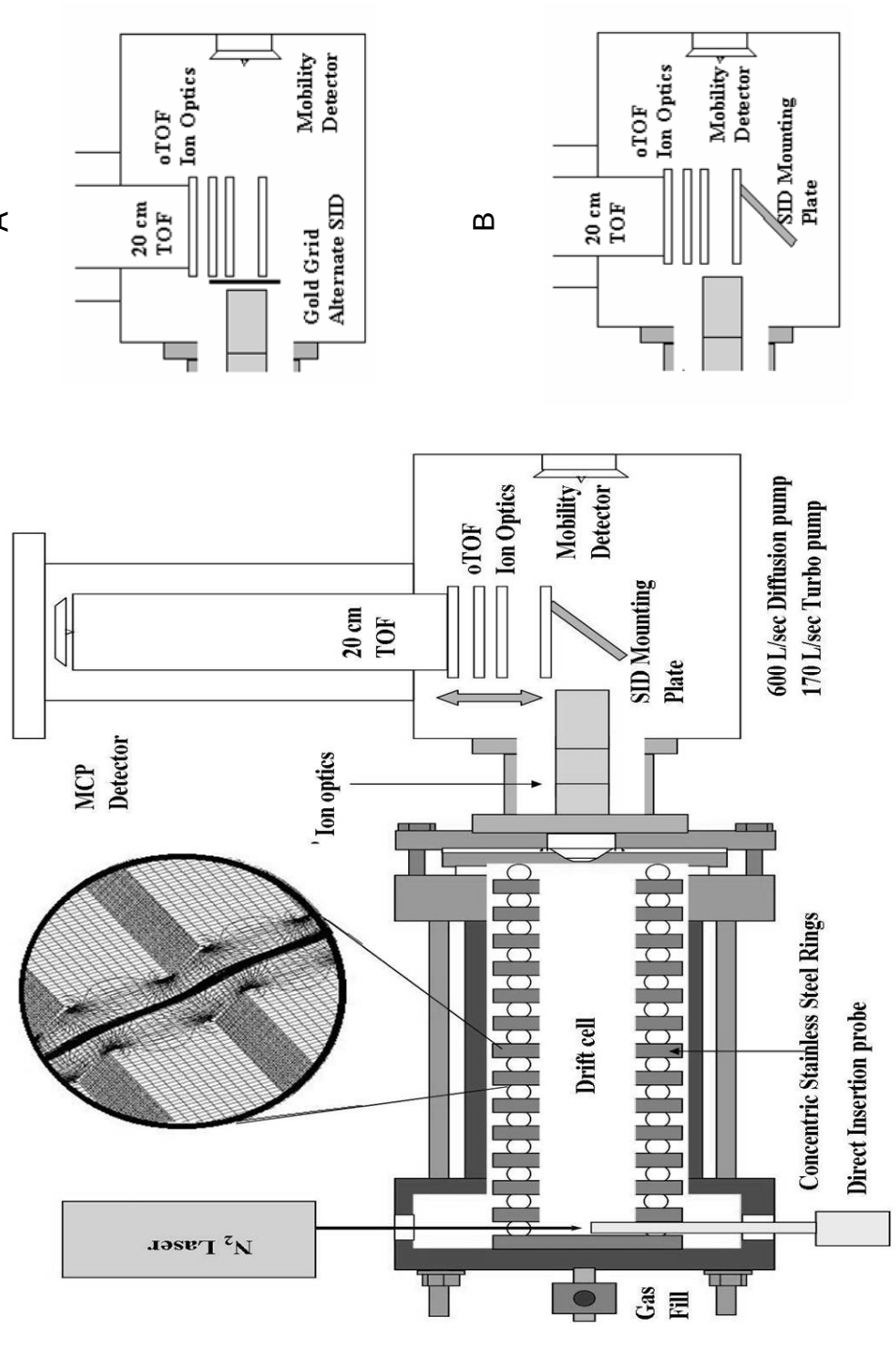

Figure 12: A cutaway drawing of the MALDI–IM–SID–o-TOF mass spectrometer used in these experiments. Inset A shows the instrument configuration used to perform the gold grid SID experiments. Inset B shows the current instrument configuration in non-SID mode.

SID and IM-TOF measurements on the same instrument. The probe tip surface in this second generation instrument was normal to the drift cell axis in order to take advantage of the drift cell gas pressure's tendency to flatten the usual cone of the laser-desorbed plume and minimize loss of drift resolution due to the increased diameter of the flattened plume

SID was also accomplished using an adventitious hydrocarbon coated stainless steel surface or an F–SAM (Figure 12). These surfaces were positioned 40^0 to the incident ion beam and 1 cm directly below a gridded TOF extraction plate (angled plate drawn in Figure 12). This is similar to the early instrument configurations employed by the Cooks group.[100] The length of the new periodic focusing drift cell was increased to 29.5 cm. The instrument was further modified to allow the movement (see arrow Figure 12) of the 20 cm o-TOF such that the SID surface could be lowered out of the ion beam and allow the acquisition of non-SID spectra (Figure 12 B.)

SID incident energies, 20 – 100 eV, were adjusted using the primary ion optics with the extraction plate bias voltages adjusted to optimize mass resolution ($m/\Delta m$, FWHM). The mass resolution for non-SID fragment ions was greater than 200 and decreased to less than 100 for SID experiments. Therefore the $[M+H]^+$ and $[M+Na]^+$

ions are not completely resolved and the SID spectra could contain fragment ions from both species. We do not detect abundant fragment ions in the SID spectra that we would expect for the $[M+Na]^+$ precursor ions, and this is probably due to the higher activation energies required to fragment the adduct ions. Data was acquired for 1 – 2 minutes using the 20 Hz nitrogen laser.

Next Generation MALDI-IM-SID-TOFMS Instrument

Figures 13 is a drawing of the next generation instrument incorporating a hybrid drift cell of the first and second instrument designed to improve the MALDI source conditions of a periodic focusing drift cell. A photo of the actual instrument is shown in Figure 14. This design opens up the MALDI region and employs an on axis near uniform field pre-separation region at focuses the ions into the periodic focusing section of the drift cell. The pre-separation region is of a lower field strength than the periodic focusing region. The large volume ion source and the lower field strength reduce ion loss due to space charge resulting in an overall increase in sensitivity without decreasing the mobility resolution. MALDI formed ions were separated by their mobility in a low pressure gas (~1-2 Torr He) and activated by collisions with an FSAM surface in a field free region of the instrument for this instrument configuration.

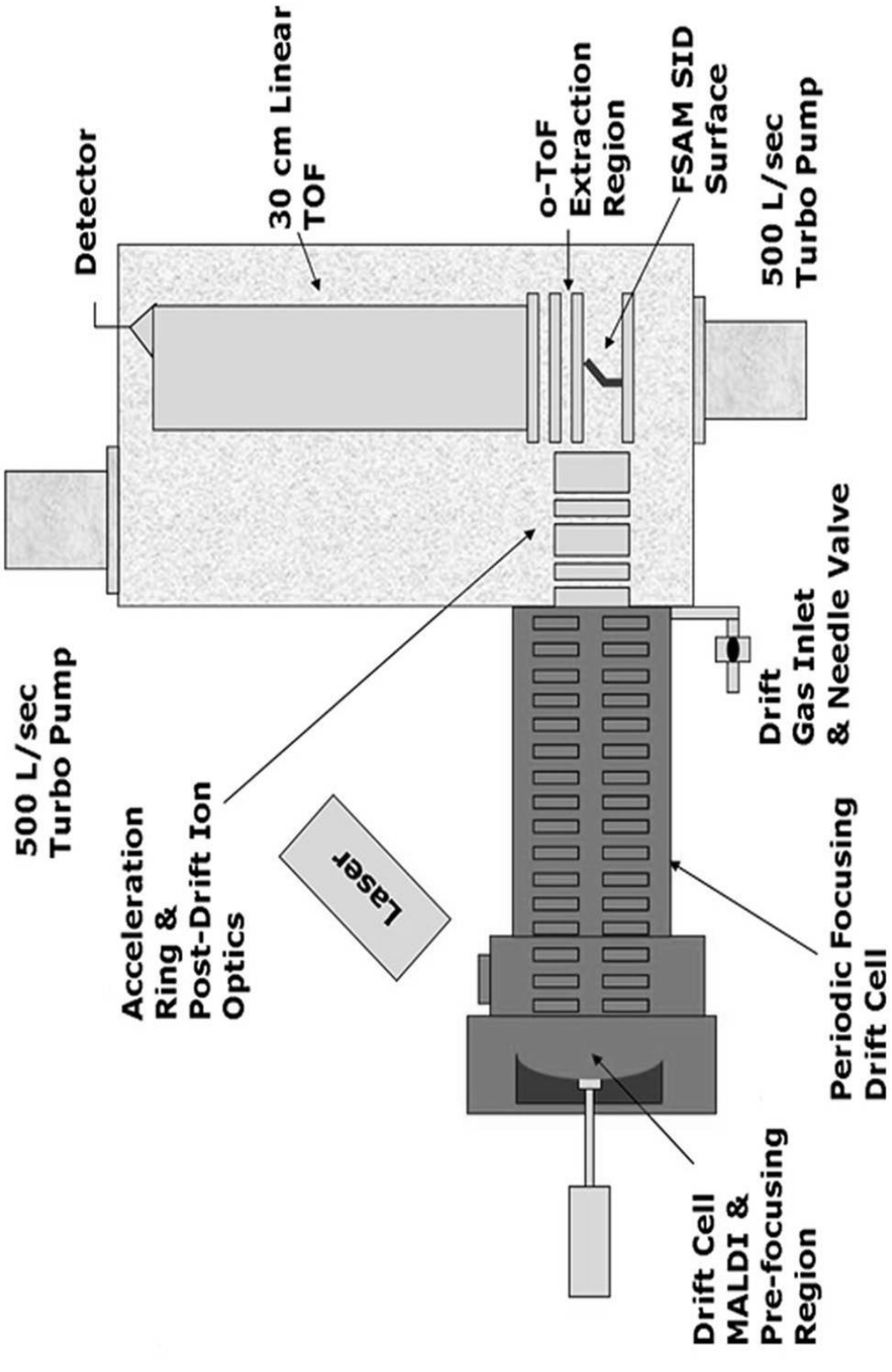

Figure 13: A drawing of the next generation MALDI-IM-SID-TOFMS instrument with a hybrid drift cell.

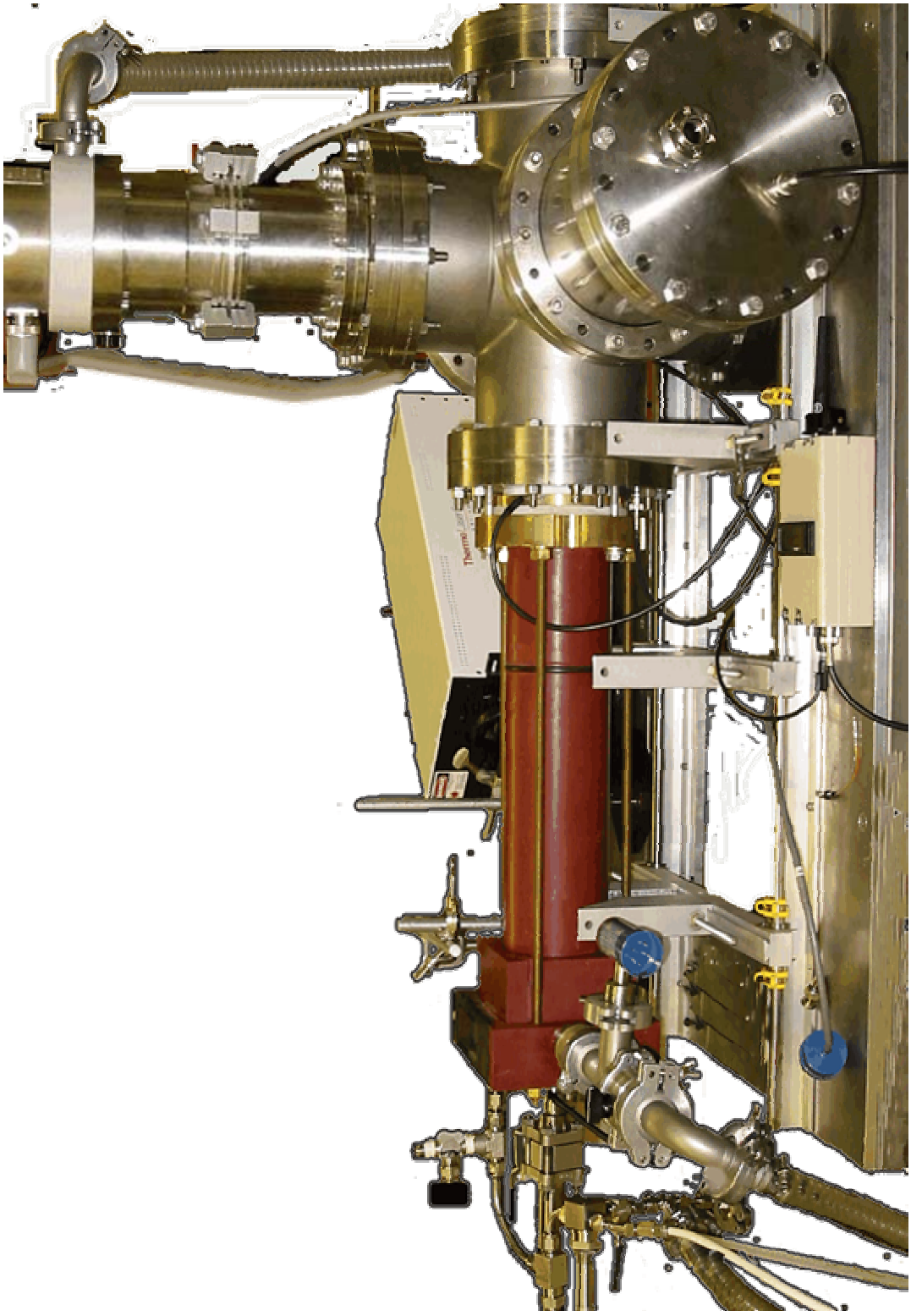

Figure 14: A picture of the MALDI-IM-SID-TOFMS instrument with a hybrid drift cell.

The sample probe was brought back in line along the axis of the drift cell. The sample surface is refreshed by simply rotating the sample probe. Provisions in this design were also made to accommodate a micro-crystal kHz laser manufactured by JDS Uniphase (San Jose, CA). The drift cell, ion optics, and TOF mass analyzer were built in-house.

Experimental Procedure

The performance of the instruments was evaluated using a series of peptides varying in mass (500-2100 *m*/z), RKEVY (MW 693.81), des-Arg^9 bradykinin (AA sequence RPPGFSPF, MW 904.05), bradykinin (AA sequence RPPGFSPFR, MW 1060.24), gramicidin S (AA sequence cyclo-LFPVOLFPVO, MW 1141.5), substance P (AA sequence RPKPQQFFGLM-NH_2, MW 1346.6), and α-melanocyte stimulating hormone (α-MSH) (AA sequence Ac-SYMEHFRWGKPV-NH_2, MW 1664.9), purchased from Sigma (St Louis, MO) and used as delivered upon mixing 1 mg per 1 mL of methanol. Mixtures of model peptides and peptide mixtures generated by proteolytic digestion of proteins, *e.g.* cytochrome c, bovine serum albumin, myoglobin, and chicken egg white lysozyme purchased from Sigma (St Louis, MO) and dissolved in methanol without further purification, were also used to evaluate instrument performance.

Digestion was accomplished according to a protocol developed in the research group[101]. Briefly the proteins were dissolved in aqueous a 50mM ammonium bicarbonate solution to make a 1 μM protein solution, then incubated at 90^0C for 20 minutes in an airtight micro-centrifuge tube. Following incubation, the protein was placed in an ice water bath to quench the denaturation. The thermally denatured protein was then digested with trypsin at 37^0C for 4 hours using a 40/1 (weight of substrate/weight of trypsin) concentration. A 50/50 solution of 2',4',6'-trihydroxy-acetophenone and fructose was added to the protein solution to obtain a protein/matrix solution with a 1000/1 matrix to analyte ratio. The inclusion of fructose increases sample homogeneity and durability.[102] Samples will be deposited to the probe tip using the dried droplet method.[103] Ions will be mobility selected, activated using SID, and mass analyzed. Data handling is similar to that of LC-TOF instruments (Figure 11).

Protein and peptide coverage was calculated and compared to spectra acquired using a PerSeptive Biosystems Voyager Elite XL TOF, operated in linear mode, an ABI 4700 TOF-TOF, and an in-house built MALDI-photodissociation-TOFMS employing identical sample preparation procedures. All samples, with the exception of limit of detection studies, were prepared by diluting the peptide solution with

a matrix solution composed of 11 mg of α-cyano-4-hydroxycinnamic acid and 11 mg of fructose in 1 mL of methanol. 2 – 4 μL of the analyte/matrix solution, corresponding to a few hundred picomoles of material, were deposited by the dried droplet method onto the direct insertion probe tip.

In the case of digests, 2 μL of the digestion solution, without further cleanup, desalting, or separation, was added to 20 μL of the α-cyano/fructose matrix solution. Approximately 100 femtomoles of analyte were deposited on the sample probe using the dried droplet method at a 1000:1 matrix to analyte ratio.

MALDI ions were formed at near-threshold levels using a 337 nm nitrogen laser operated at 20 Hz. Data was collected and signal averaged for 1 to 2 minutes. Data analysis was accomplished using Grams 3D and PROWL protein identification programs.

CHAPTER III

PRELIMINARY STUDIES ON THE HYPHENATION OF MALDI, IM, SID, AND TOFMS

Analysis of Model Peptides

Before analyzing complex peptide mixtures, a series of single component samples were analyzed to show that flight times through the drift cell increase near-linearly with increasing m/z of the peptide, *i.e.* to demonstrate that IM can be used as the primary mass analyzer.

The mass-dependent mobilities for peptide ions are dominated by the hard-sphere collision cross-section term, *i.e.* surface area-to-charge ($Å^2/z$), and the ion-neutral interaction potential term can be neglected.[63] Figure 15 contains a plot of experimentally measured drift time vs. m/z for twelve peptide fragment ions (determined using the peak centroids in the 3D plot, see figure page 56) obtained by digestion of cytochrome c with trypsin (*vide infra*). The error for the m/z is determined to be $\pm$ 1 amu. It has been shown by Ruotolo and coworkers that the maximum deviation from a linear trend is $\pm$11% when the data set is extended from twelve peptides to 234 peptides.[66]

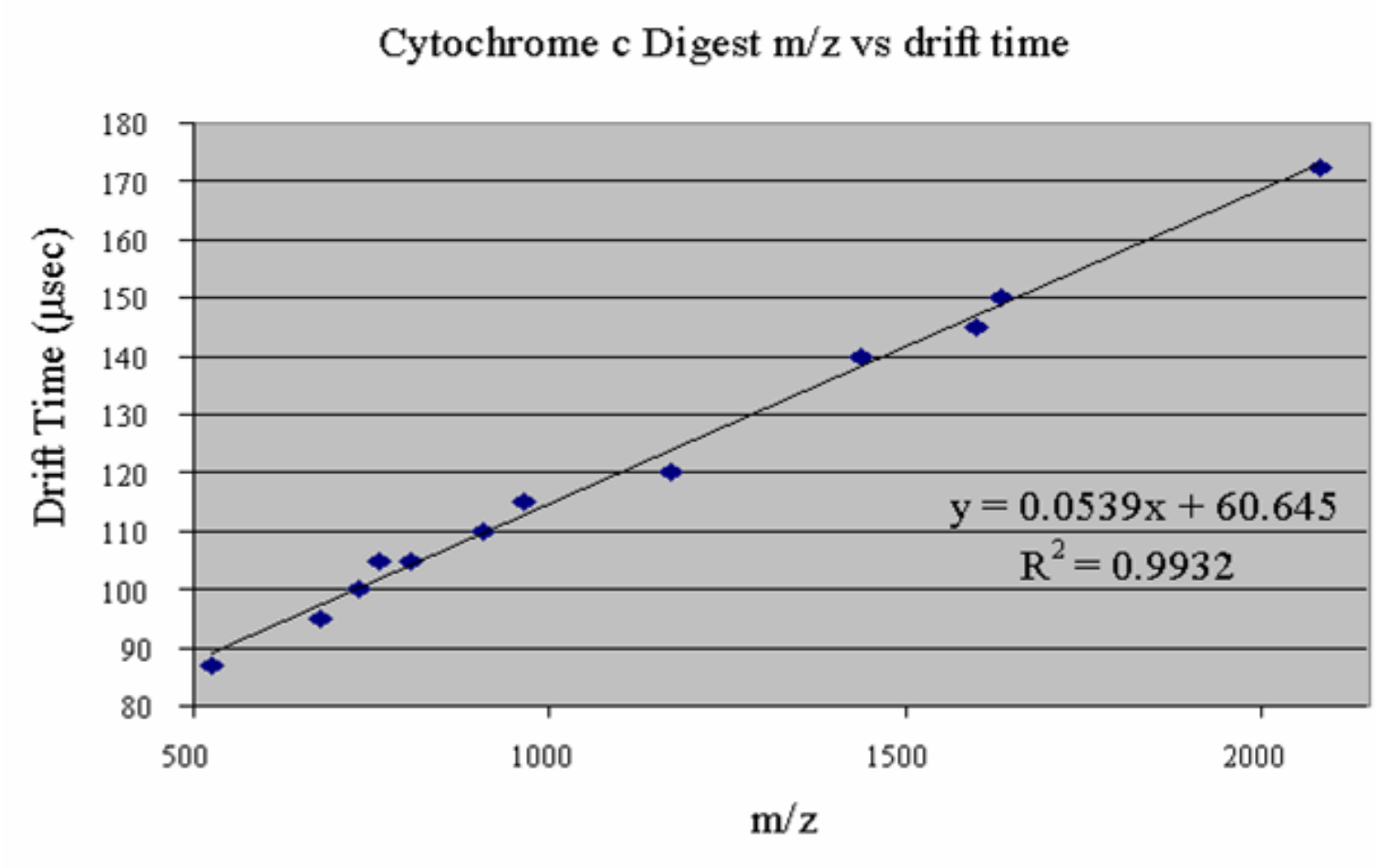

Figure 15: A plot of drift time vs. m/z value for selected peptide fragment ions formed by tryptic digestion of cytochrome c, taken from data shown in Figure 19. A linear relationship can be seen for the near homologous series of peptides for the mass range typically observed for tryptic digest fragments.

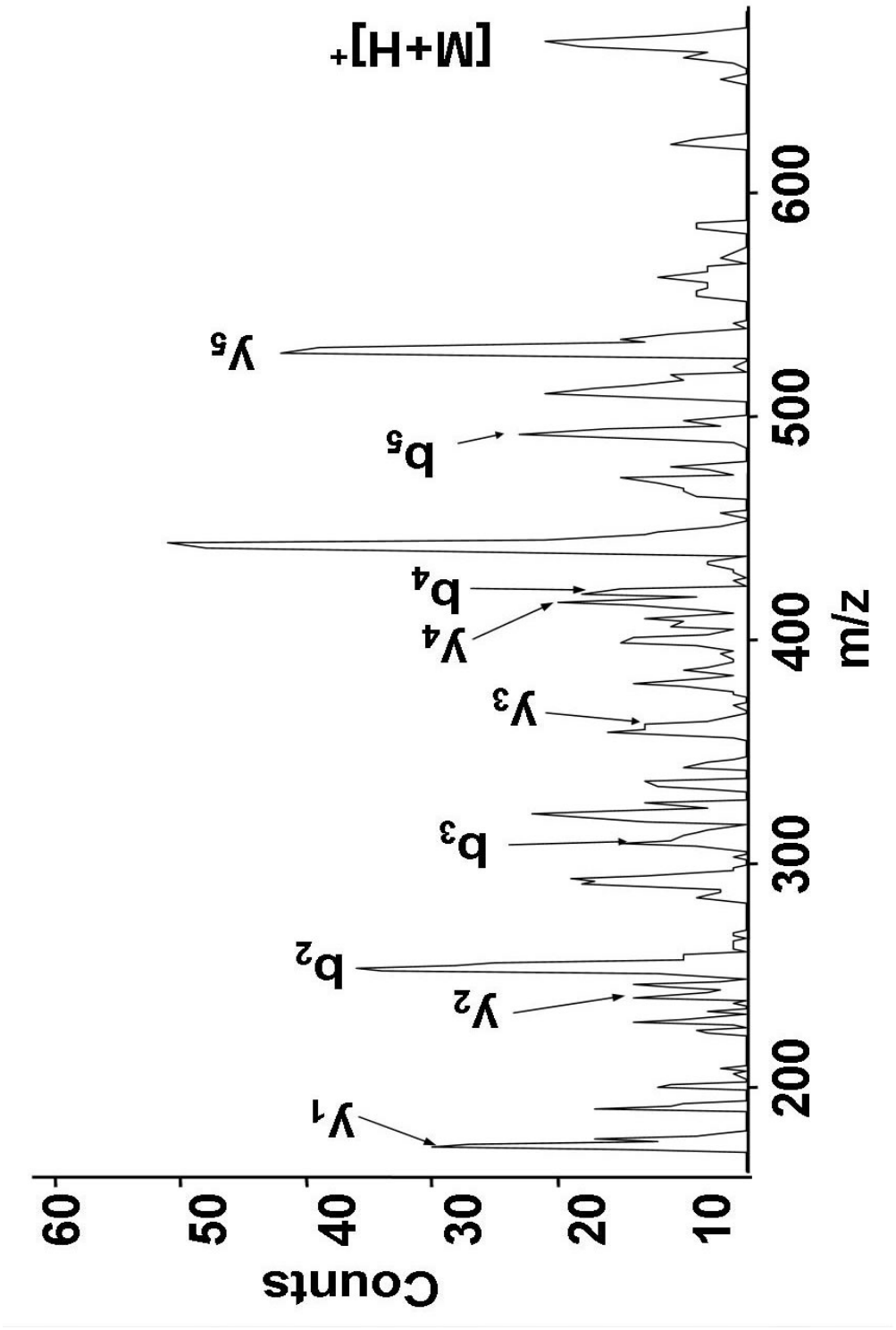

Figure 16: MALDI-IM-SID-o-TOF spectrum of HLGLAR. Mass accuracy for labeled SID fragments are $\pm$ 1 amu. Collision energy is ~20 eV. A complete y_j series and a near complete b_i series are shown. SID fragments resulting from small neutral losses (H_2O and NH_3) are not labeled.

The y-intercept in Figure 15 corresponds to the flight time of an ion in the absence of a neutral bath gas. Clemmer and coworkers have shown similar data for singly charged peptide ions formed by electrospray ionization,[104] and the results shown in Figure 15 simply confirm their observations and the earlier work by Griffin[64] and Karpas.[65] SID experiments were also performed on three model peptides to illustrate SID fragmentation efficiency and types of fragment ions produced from the digest fragment ions created by MALDI. The SID results for peptides are very comparable to results reported previously by Wysocki.[105] Figure 16 contains the SID spectrum of the hexapeptide HLGLAR (m/z 666.8). For simplicity only the b- and y-fragment ions are labeled. Unassigned peaks are largely due to the loss of water or ammonia from the SID fragment ions. The loss of small neutrals is common through out all the SID spectra acquired for arginine and lysine containing peptides as is also the case with CID and photodissociation.[106] The spectra were acquired under conditions (20 eV collision energy) that are sufficient to obtain an almost complete SID fragmentation series for a low mass parent. The results are in excellent agreement with those of Kaiser *et al.*[107] The spectrum contains a complete series of y-type fragment ions (y_1-y_5)

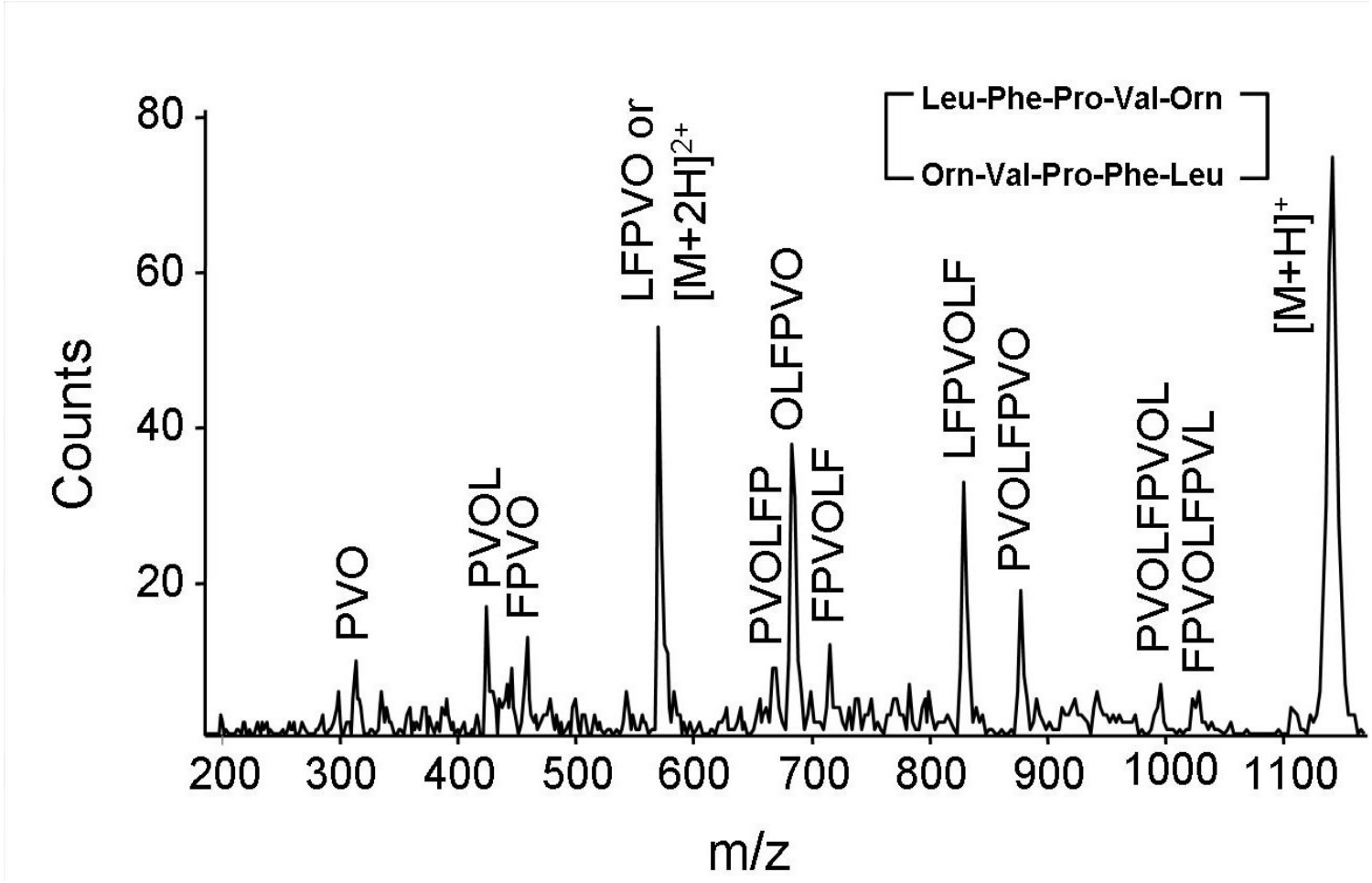

Figure 17: MALDI-IM-SID-o-TOF spectrum of gramicidin S. Mass accuracy for labeled SID fragments are ± 1 amu. Collision energy is ~20 eV. Note the near complete series of proline N-terminal fragments. The pentapeptide fragment VLOFP may be a combination of all five possible N-terminal fragments and the $[M+2H]^{2+}$ parent ion, but is most likely LFPVO.

and most of the expected b-type (b_2-b_4) fragment ions. The complete y-type fragment ion series is anticipated due to the presence of the C-terminal arginine. Figure 17 contains the SID spectrum of the cyclic peptide gramicidin S (m/z 1142.5). This spectrum is very similar (in terms of fragment ion yields) to the SID spectrum of gramicidin S reported by McLafferty and coworkers.[108] The spectrum in Figure 17 id that of the singly charged parent while the parent investigated in McLafferty's work is the $[M+2H]^{2+}$. As a result the intensity of the hexapeptide (and larger) fragment ions were of greater abundance in the spectrum in Figure 17 than in McLafferty's work. Because gramicidin S is a cyclic peptide, the SID fragment ions produced depend upon the site of ring opening as opposed to the amino acid sequence; therefore, this spectrum is included to illustrate the efficiency of SID for producing fragment ions from a relatively stable peptide ion.

Figure 18 contains the SID spectrum of protonated bovine insulin b chain (m/z 3495.5). In addition to the single and doubly charged parent ions the y_{15} through y_{29} fragment series and the b_{16} through b_{29} fragment ions are observed. The doubly charged β-chain ion is formed by the SID process, because the appearance of this ion

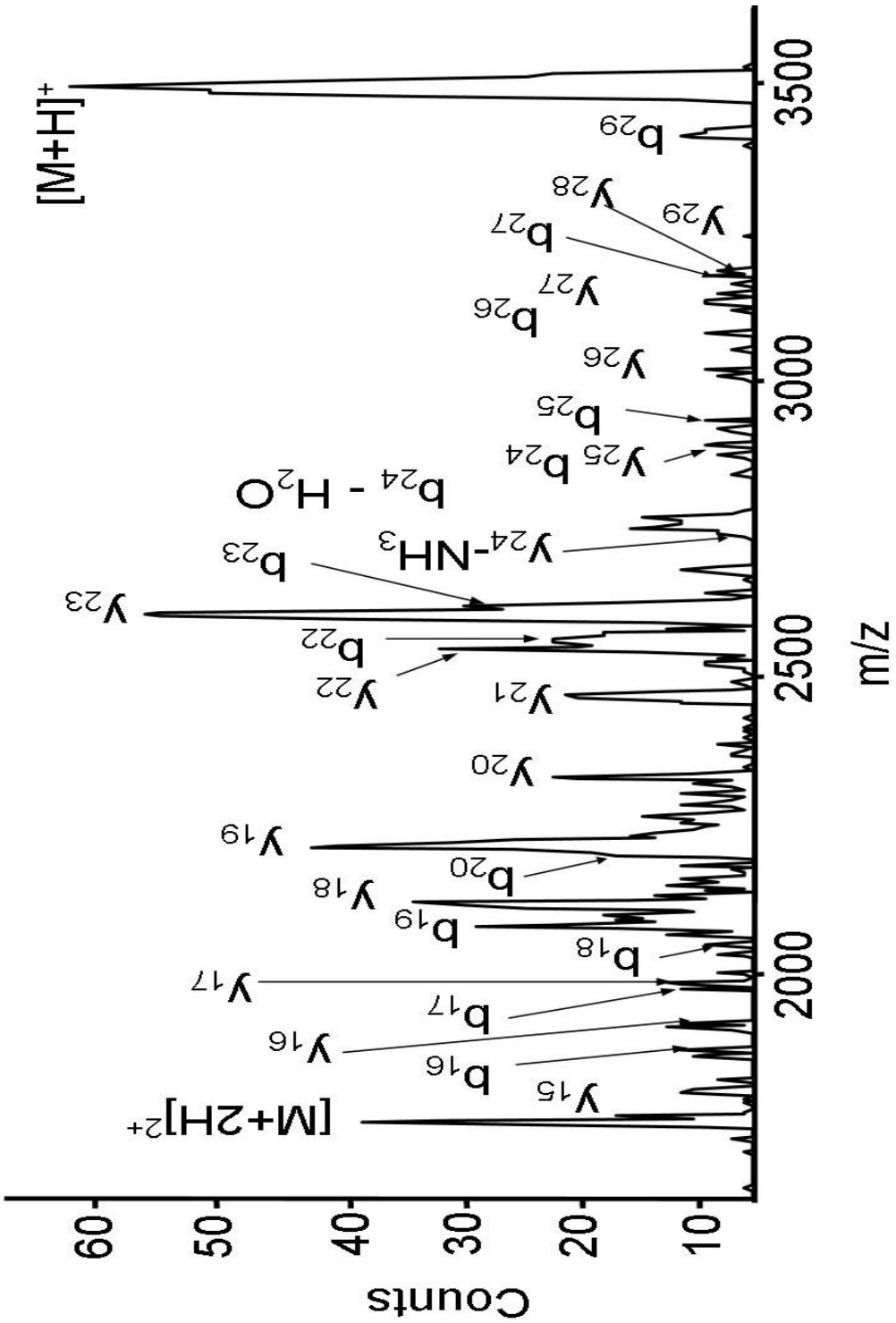

Figure 18: MALDI-IM-SID-o-TOF spectrum of bovine insulin b chain. The presence of the $[M+2H]^{2+}$ ion is attributed to protonation of the $[M+H]^{+}$ during or immediately following the SID event. Mass accuracy for labeled SID fragments is $\pm$ 1 amu. Collision energy is ~20 eV.

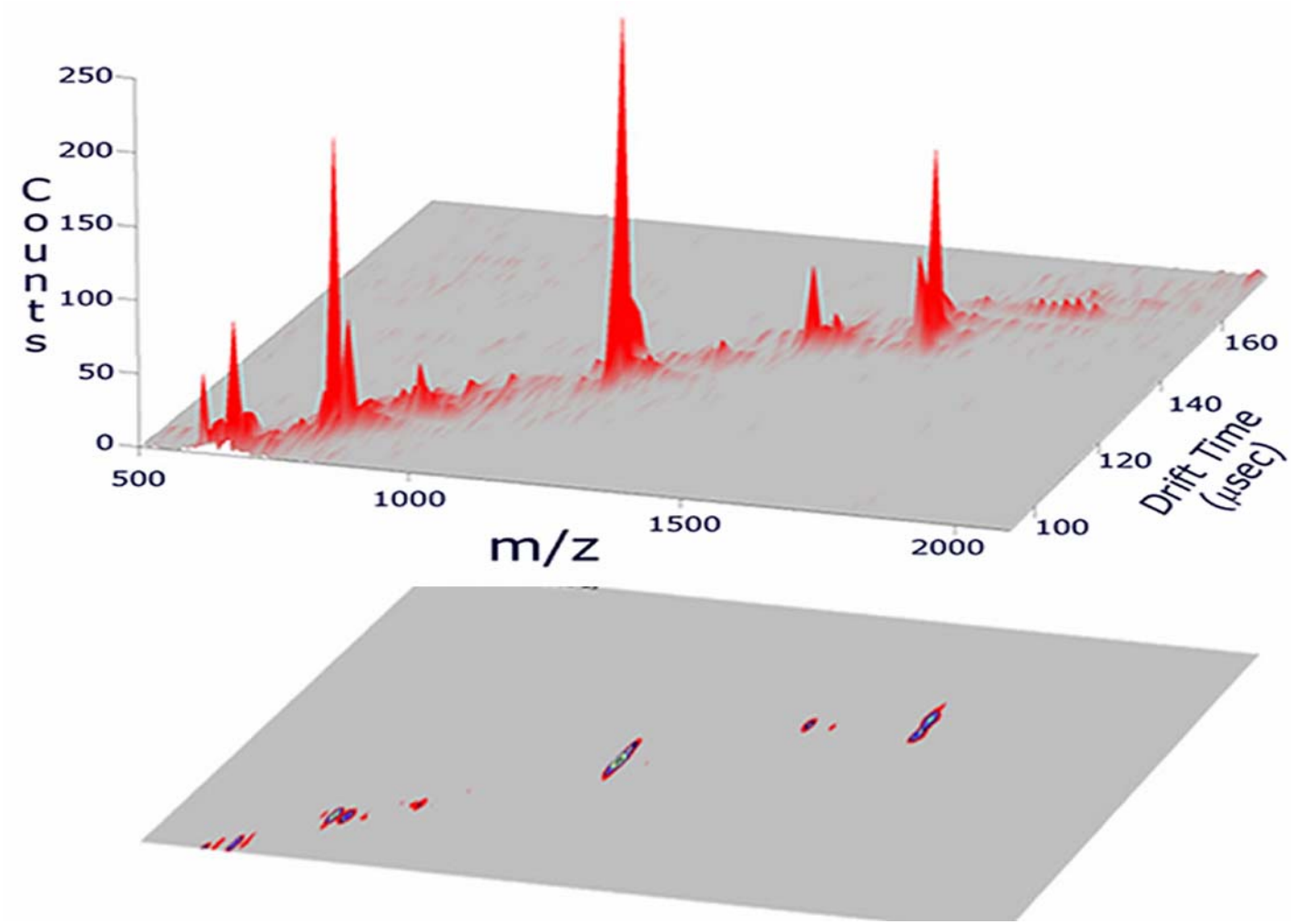

Figure 19: MALDI-IM-o-TOF of an "in-solution" digest of cytochrome c illustrating peptide mass mapping capability of the current instrument configuration. All ions entering the extraction region of the o-TOF are mass analyzed.

in the mass spectrum is not accompanied by an appearance in the mobility spectra. The mechanism of forming the $[M+2H]^{2+}$ ion is not known, but this suggests two possibilities. The first is that the protonation is occurring upon impact with the surface, *i.e.* ion/surface reaction. Experimental evidence for the transfer of atoms or groups of atoms, in particular hydrogen atom(s) from hydrocarbons, from or to the surface has been shown by Cooks *et al.*[109] The second is the possibility of a doubly charged dimer arriving simultaneously in drift time with the singly charged as suggested by Clemmer.[110] . The partial y-type and b-type ion series observed provide a complete sequence of the peptide. For example, the y_{15}-y_{29} fragment ions can be used to determine the first 14 amino acids from the N-terminus, whereas the b_{16}-b_{29} ions identify the remaining amino acids.

Analysis of a Model Protein Digest

Figure 19 contains a plot of MALDI-IM-o-TOFMS data for an "in-solution" digest of cytochrome c. M/z data is represented on the x-axis, the y-axis is the total drift time for each digest fragment ion, and the z-axis is the total ion count. This data format is actually a 2-D (mobility and m/z) display of a peptide mass map. The data shown are typical for thermally denatured tryptic protein digests.[111]

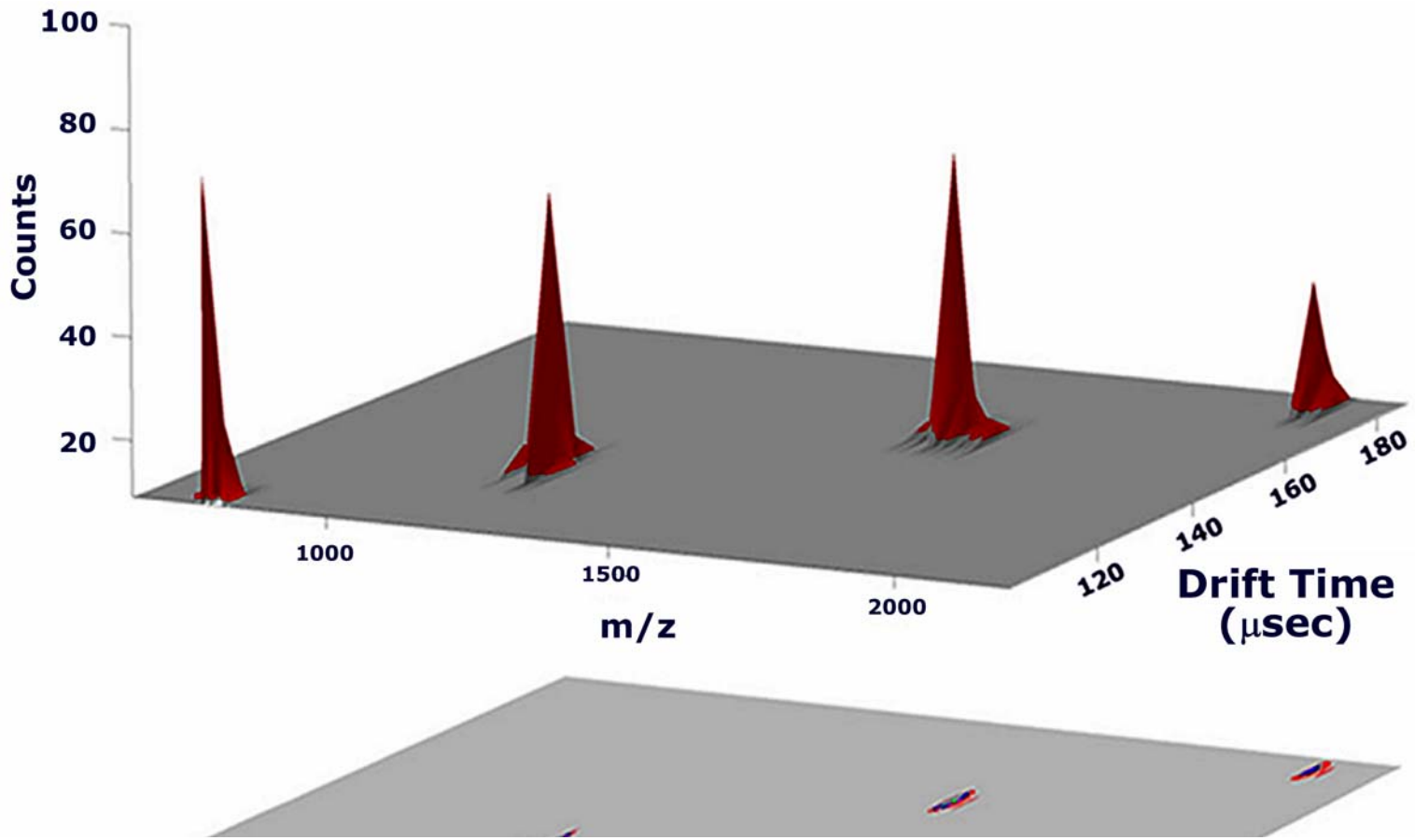

Figure 20: MALDI-IM-o-TOF of four mobility-selected tryptic fragments from an "in-solution" digest of cytochrome c. Mobility selection of ions eluting from the drift cell for subsequent mass analysis is accomplished using the arrival times predicted by the trend observed in Figure 15 to operate the extraction plates of the o-TOF mass spectrometer.

The digest and SID fragments listed in Table 1 were identified by searching the protein database (Swis-Prot) and using the Protein Prospector MSFit program. These peptide fragments account for 91 of the 104 (87.5% coverage) amino acids present in cytochrome c. Four prominent digest fragments in the 2-D peptide mobility/mass map (Figure 20) were selected by ion mobility (MS^1), subjected to SID, and then analyzed by o-TOFMS. The SID fragment ions have the same mobility as the parent ion, because the fragment ions are formed after the $[M+H]^+$ ions elute the drift cell. The time scale of an IM separation, 100 us to 20 ms, is one to two orders of magnitude longer than the flight times in the mass spectrometer (10-100 us). Consequently, it is possible to acquire SID fragment ion spectra for all ions eluting the drift cell from a single ionization event. The SID was performed using the same methods as was used for the single component peptide samples. The SID collision energy was held constant (20 eV); however, since the fragmentation efficiency is a function of velocity, it would be useful to program a voltage ramp (*e.g.,* increasing SID energy with increasing m/z for more fragmentation coverage) into this experiment. Figure 21 contains a 2-D plot of the IM-SID-o-TOF spectra, and Table 1 contains a list of the m/z values and assignments for the fragment ions. Note that the

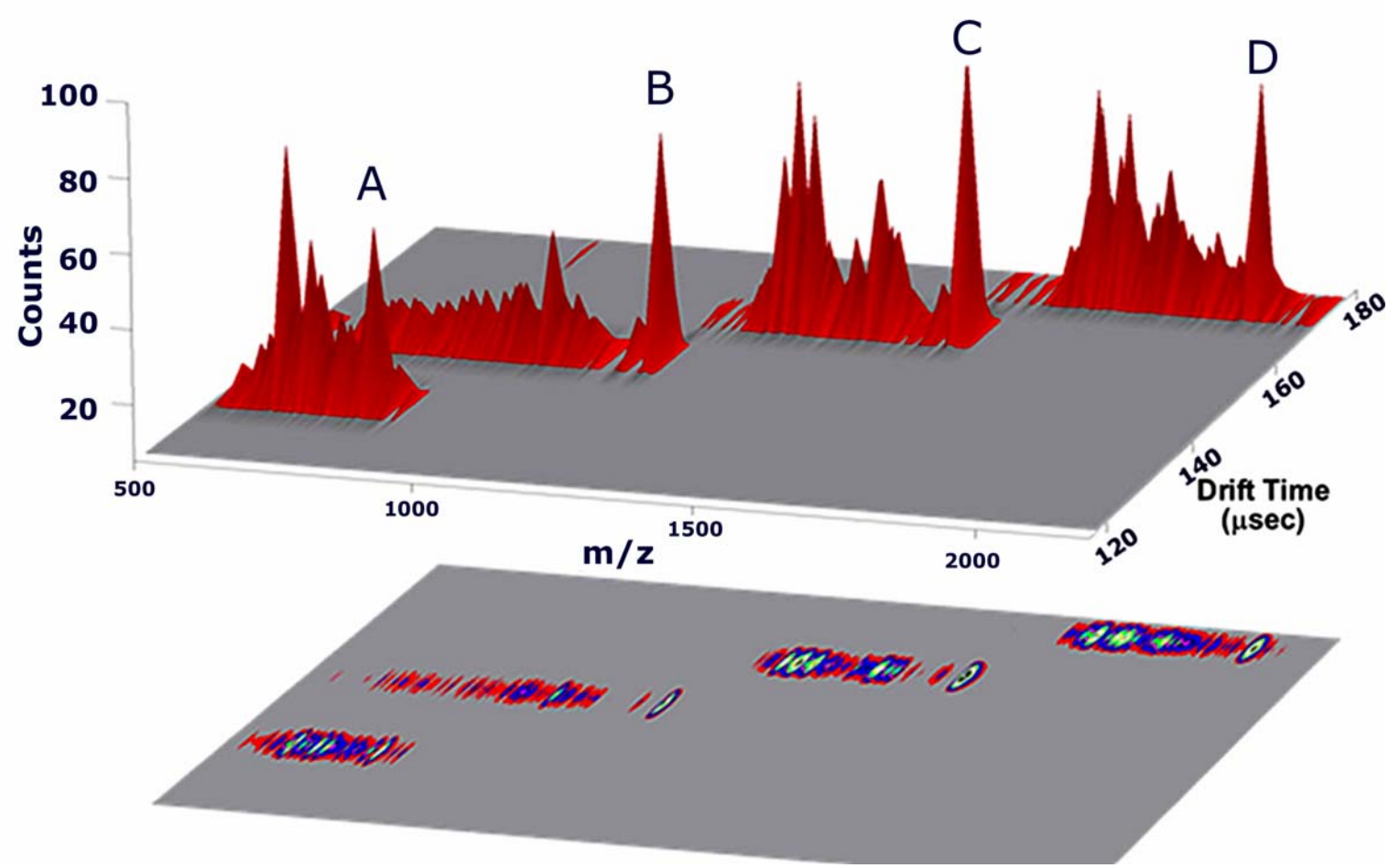

Figure 21: MALDI-IM-SID-o-TOF spectra of four mobility selected peaks from an "in-solution" digest of cytochrome c. Mass accuracy for labeled SID fragments are $\pm$ 1 amu. Collision energy is ~20 eV. SID fragments are associated by total mobility drift time with the parent digest fragment. The data handling package allows for any of the four spectra to be observed in a format similar to the other figures for ease of peak assignment.

range of ions observed for digest peaks A and B in Figure 21 covers the mass range from m/z 500 up to the parent and that this is not the case for peaks C and D. We attribute the lack of low mass ions in C and D to an insufficient energy deposited in the parent ion due to the orientation of the SID surface. The grazing incidence angle does not permit energy conversion similar to that for FSAM coated surfaces positioned at an angle to the incident ion beam. It is also high likely that MALDI formed ions have considerable excess internal energy and that this affects the SID fragment ion yields. We see similar results for photodissociation of MALDI formed ions.[112] It should be noted that we do observe that low m/z fragment ions increase in abundance at higher translational energies. For SID energies above 500 eV, Reiderer does not observe large y- or b-type fragment ions seen in Figure 21, but rather significant single amino acid residue and immonium ion production.[113] Also notice the similarity between the fragmentation patterns and parent peak intensity observed for peak A (m/z 780) and that for HLGLAR (666.8) in Figure 16, peak B (m/z 1169) and gramicidin S (m/z 1142.5) in Figure 17, and peak D and bovine insulin b chain in Figure 18.

We have not listed all the fragment ions detected in the SID spectrum in Table 1. In particular we omitted fragment ions that

Table 1: A list of assigned fragment ions, m/z values and amino acid sequence of peptide fragments from the tryptic digestion of cytochrome c.

Digest/SID Fragment	m/z [M+H]$^+$ Calc	Exp	Amino Acid Sequence
Digest Peak A	780.0	778.9	MIFAGIK
y_6	648.8	648.0	IFAGIK
b_6	633.8	633.7	MIFAGI
y_5	535.7	534.4	FAGIK
Digest Peak B	1169.3	1168.6	TGPNLHGLFGR
y_{10}	1068.2	1068.4	GPNLHGLFGR
y_9	1011.2	1010.6	PNLHGLFGR
b_{10}	995.1	994.2	TGPNLHGLFG
b_9	938.1	937.5	TGPNLHGLF
y_8	914.1	913.5	NLHGLFGR
y_7	799.9	799.6	LHGLFGR
b_8	790.9	789.8	TGPNLHGL
y_6	686.6	685.9	HGLFGR
b_7	677.4	678.7	TGPNLHG
b_6	620.7	619.9	TGPNLH

Digest/SID Fragment	m/z [M+H]$^+$ Calc	Exp	Amino Acid Sequence
Digest Peak C	1634.9	1635.2	CAQCHTVEK+ heme
y_8 + heme	1531.8	1530.9	AQCHTVEK+ heme
b_8 + heme	1488.7	1487.8	CAQCHTVE+ heme
y_7 + heme	1460.7	1461.1	QCHTVEK+ heme
b_7 + heme	1359.6	1360.1	CAQCHTV+ heme
y_6 + heme	1332.5	1311.6	CHTVEK+ heme
b_6 + heme	1260.5	1259.8	CAQCHT+ heme
Digest Peak D	2082.4	2083.2	GITWKEETLMEYLENPK
y_{16}	2025.3	2026.0	ITWKEETLMEYLENPK
b_{16}	1936.2	1936.8	GITWKEETLMEYLENP
y_{15}	1912.2	1913.1	TWKEETLMEYLENPK
b_{15}	1839.1	1840.2	GITWKEETLMEYLENPK
b_{14}	1725.0	1725.7	GITWKEETLMEYLE

involved loss of H_2O and NH_3 from b_i and y_j sequence fragment ions. The ions listed are sufficient to identify the peptides and the protein from which the peptides are generated. For the data base searches, TOF mass accuracy was set to $\pm$ 1 Da for both $[M+H]^+$ ions and the m/z values of the SID fragment ions, and ion types were limited to b_i and y_j fragments. SID fragments were manually identified by matching experimentally measured fragment ion m/z values with predicted m/z values. We are currently developing a computer algorithm to perform this task.

The m/z 649 SID fragment from digest fragment A (Figure 21; m/z 780) corresponds to loss of a methionine residue (y_6). If we search the data base using the m/z of the $[M + H]^+$ ion and the y_6 fragment using PROWL's PepFrag routine, we obtain a match against 17 proteins, where 10 of the matches are cytochrome c. If we add two additional SID fragments, *e.g.,* m/z 634 (y_5) and m/z 536 (b_6), the number of protein matches is reduced to 11, where 10 are species non-specific cytochrome c. The sequences returned were MIFAGIK for cytochrome c and MIMKEK for IL4_TURTR Interleukin-4 precursor. Because the MIFAGIK digest fragment is conserved from species to species the database identified proteins would not be species specific.

The same procedures were used to identify the remaining three peaks in the 2-D peptide mass map. Digest fragment labeled B (m/z 1169) was identified using m/z 1068 and 1011 SID fragment ions, and we obtained 10 matches, where 9 of the matches were conserved sequences for cytochrome c. If we added the m/z 995 SID fragment to the search, 10 species non-specific matches for cytochrome c were obtained. The complete sequence for peak B can be determined from the fragment ion spectrum (Table 1), e.g.; the fragment ion series b_6-b_{10} and y_6-y_{10} can be used to identify the complete sequence.

The data base search to identify peak C (m/z 1634) resulted in zero matches for m/z 1532, 1489, 1461, and 1359; however, we previously reported that the m/z 1634 ion was most probably a heme containing fragment ion.[114] Subtracting the isotope-averaged mass of heme (615.7) from the measured m/z values, including the $[M+H]^+$ ion, yields m/z 915.2 (1530.9-615.7), m/z 872.1 (1487.8-615.7), m/z 845.4 (1461.1-615.7), and m/z 744.4 (1360.1-615.7), and the data base search produces 10 matches all of which are cytochrome c. Thus the peptide sequence for peak C is CAQCHTVEK+heme, which corresponds to amino acid residues 14-22. Peak D was identified as Equine cytochrome c on the basis of the $[M + H]^+$ ion, m/z 2082, and three SID fragments, m/z 2025, 1935, 1912. The use of fewer

numbers of SID fragment ion m/z values for peak D resulted in identification as non-species specific cytochrome c.

Conclusions

It has been demonstrated that peptide mass mapping and sequencing can be accomplished with MALDI-IM-SID-o-TOFMS. The peptide mass mapping and SID peptide data is comparable to that obtained using more conventional mass spectrometry techniques. The advantages of MALDI-IM-SID-o-TOFMS are sample throughput and simultaneous acquisition of the peptide mass map and sequence analysis. Future work will be directed toward improving both mobility and mass resolution of the prototype instrument, automation of sample handling, and comparison of collision-induced dissociation, photodissociation and SID for peptide sequencing.

CHAPTER IV

OPTIMIZATION OF THE MALDI-IM-SID-TOFMS EXPERIMENT

Figures 22, 23, and 24 contain SID spectra acquired using adventitious hydrocarbon coated gold grids, (Figure 12, A concerning positioning of the grids.) These spectra were recorded using collision energies of approximately 20 eV. The spectrum (Figure 22) of RKEVY contains a complete series of a-, b-, and y-type fragment ions as well as signals for the loss of small neutral molecules such as H_2O and NH_3 from many of the fragment ions. A complete set of a-, b-, and y-type fragment ions are also observed for des-Arg^9 bradykinin (Figure 23), with the exception of fragment ions resulting from cleavage of the pro-gly amide bond (a_3, b_3, and y_5 ions). The spectrum of bradykinin (Figure 24) is very similar to that for des-Arg^9 bradykinin, and fragment ions resulting from cleavage of the pro-gly amide bond (a_3, b_3, and y_6 ions) are also absent. The absence of fragment ions resulting from cleavage of the pro-gly amide bond contradicts suggestions that proline lowers the bond dissociation energy for the adjacent amide backbone bond.[115] The apparent contradiction is probably a result of stabilizing interaction between the N-terminal

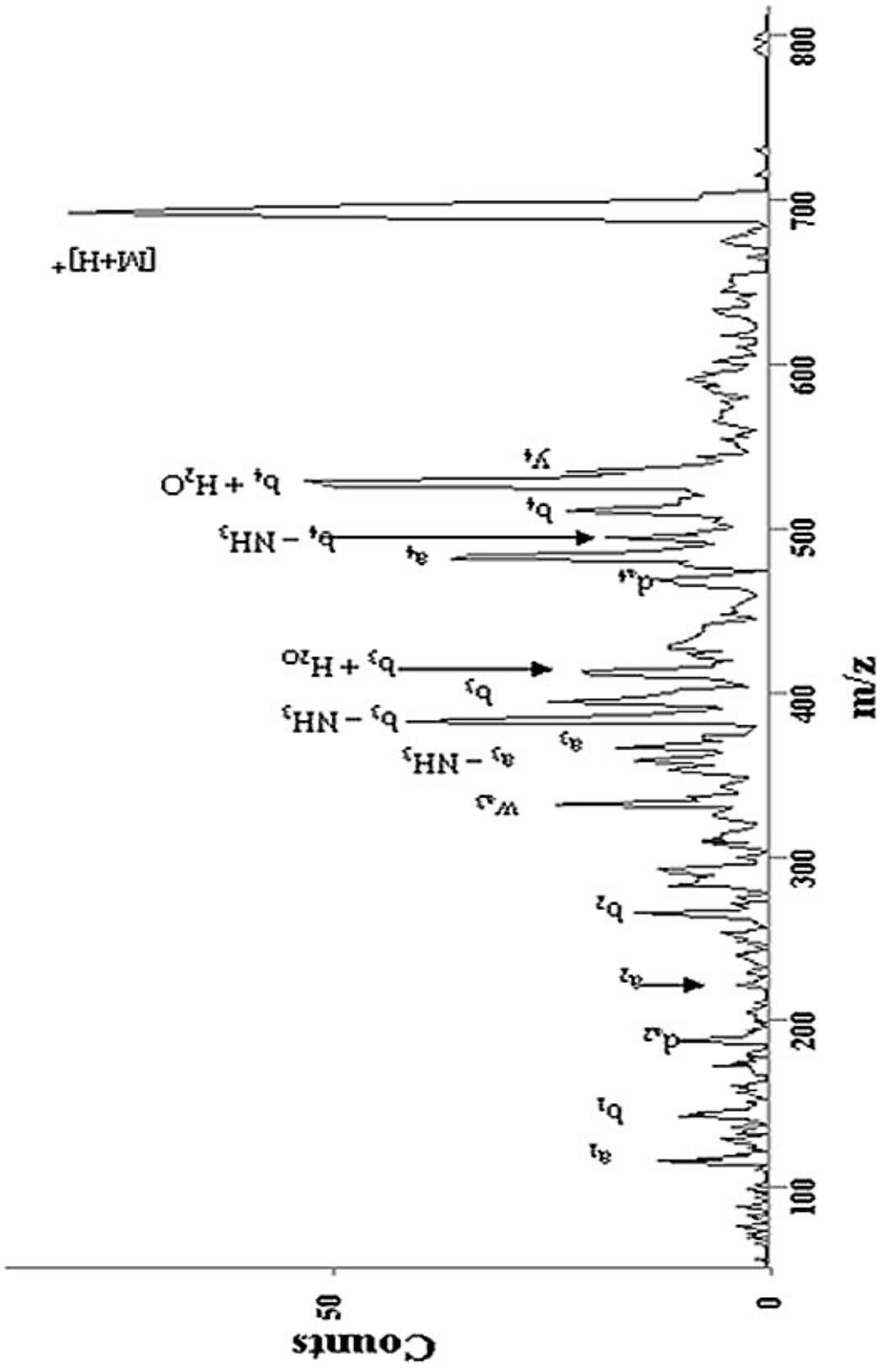

Figure 22: A MALDI–IM–SID–o-TOF mass spectrum of the pentapeptide RKEVY. This spectrum was acquired using the gold grid arrangement in Figure 12 Inset A. Data was acquired for 2 minutes and analyzed using GRAMS/32. Mass resolution, m/ΔM at FWHM, is better than 200. Mobility resolution is better than 20.

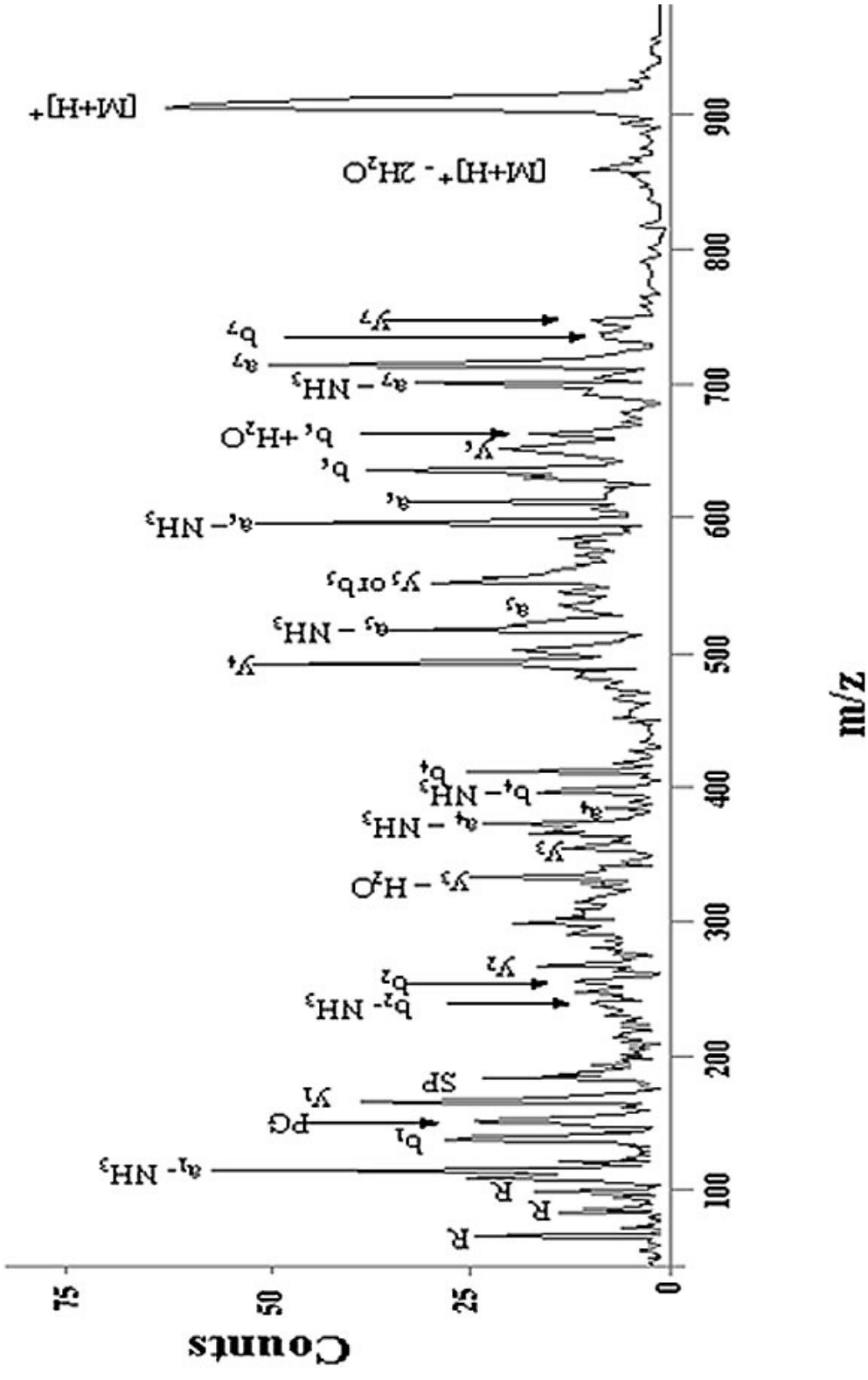

Figure 23: A MALDI–IM–SID–o-TOF mass spectrum of des-Arg[9] bradykinin. This spectrum was acquired using the gold grid arrangement in Figure 12 Inset A. Data was acquired for 2 minutes and analyzed using GRAMS/32. Mass resolution, m/ΔM at FWHM, is better than 200. Mobility resolution is better than 20.

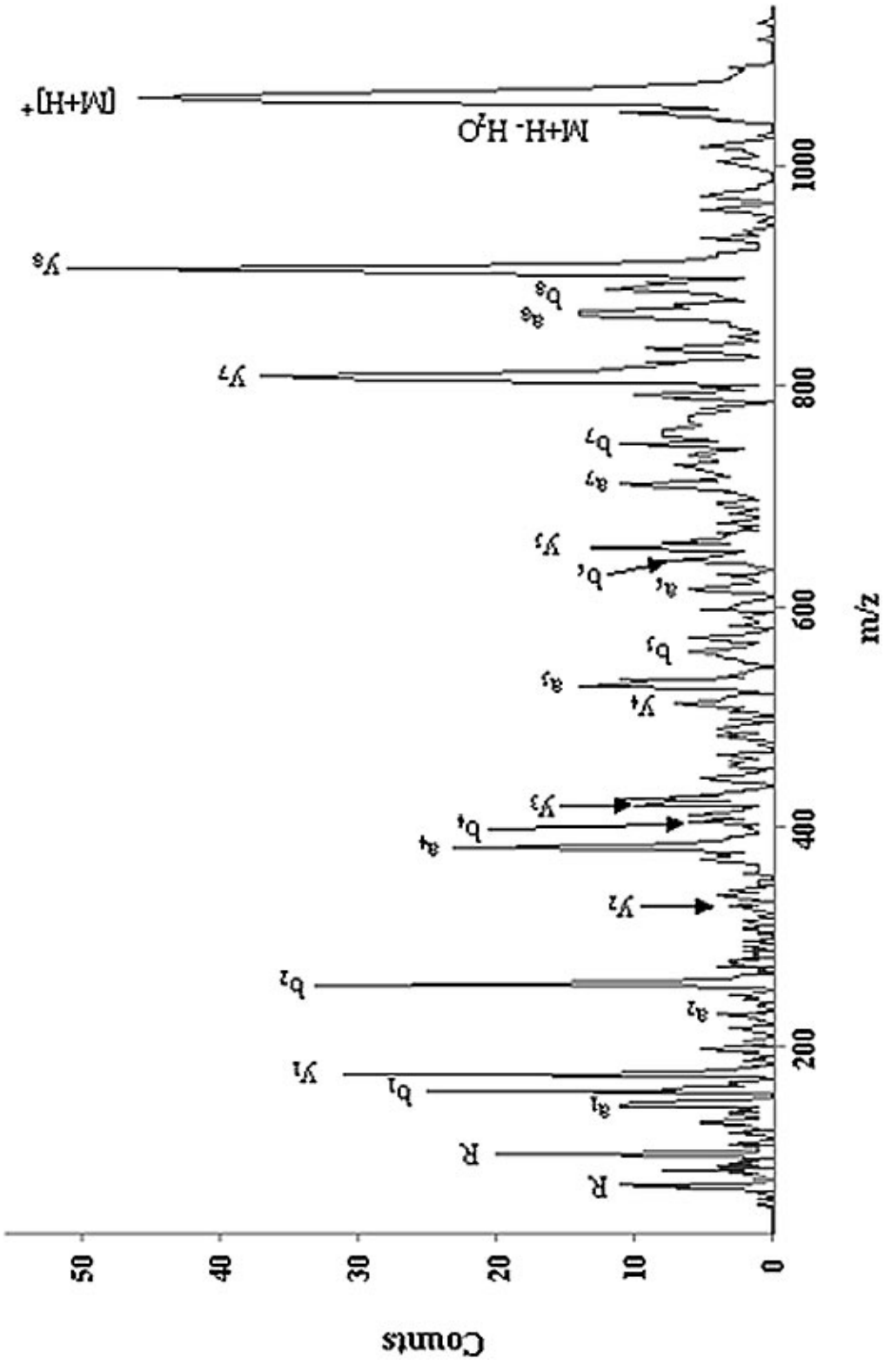

Figure 24: A MALDI–IM–SID–o-TOF mass spectrum of bradykinin. This spectrum was acquired using the gold grid arrangement in Figure 12 Inset A. Data was acquired for 2 minutes and analyzed using GRAMS/32.

arginine and the C-terminus,[116,117,118] rather than some underlying feature related to the surface activation process.

Optimization of Instrumental Design

To increase the resolution and transmission efficiency of IM we designed and constructed a longer, periodic focusing drift cell.[119] Figure 25 contains a mass-mobility plot of a mixture of five peptides composed of des-Arg^9 bradykinin, bradykinin, gramicidin S, substance P, and α-MSH. A mobility resolution of 50-75 was obtained using the new drift cell as compared to 20-30 for a conventional IM drift cell. The data shown in Figure 25 was acquired using near-threshold MALDI laser fluence, which primarily yields $[M+H]^+$ or $[M+Na]^+$ ions. The gramicidin S $[M+Na]^+$ ion is observed as a weak signal with a slightly longer drift time and higher m/z relative to the $[M+H]^+$ ion signal. Note that a plot of drift time vs. m/z yields a near-linear correlation for structurally related compounds.[90] For example, the slopes, hereafter denoted as “trend-lines”, for matrix ions is very different from that for peptide $[M+H]^+$ ions.[120] The near-linear mass-mobility relationship provides the basis for using IM as MS^1 in the MS-MS mode.[90] The mass-mobility plot is also used to correlate the fragment ions to their respective precursor ions. That is, fragment

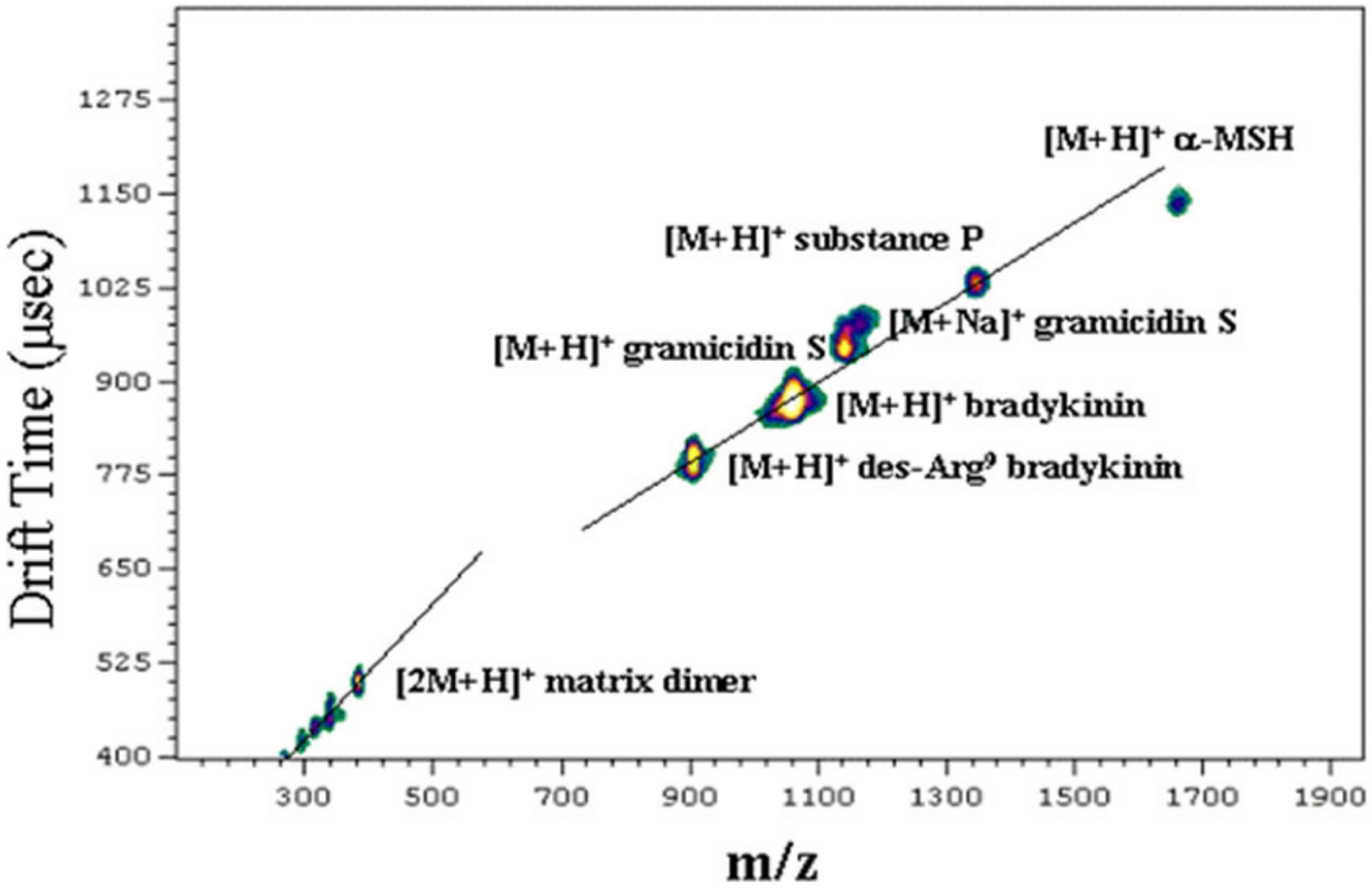

Figure 25: A mass-mobility plot of a five-peptide mixture composed of des-Arg^9 bradykinin, bradykinin, gramicidin S, substance P, and α-MSH taken with the instrument adjusted for non-SID mass-mobility data collection. Trend lines are added as a visual aid.

ions that are formed after the precursor ions elute the drift cell have the same apparent drift time as the precursor ion. On the other hand, fragment ions that are formed upon ionization appear at a drift time characteristic of that ion, and fragment ions that are formed during the time the ions are drifting through the drift cell have a broad, ill-defined arrival time distribution. The lack of observable fragment ions in Figure 25 demonstrate that the $[M+H]^+$ ions elute from the drift cell without excess internal energies.

Optimization of Parameters Affecting IM–TOFMS/MS

Figure 26 contains an SID mode mass-mobility plot for a five peptide mixture using an adventitious hydrocarbon coated stainless steel surface, positioned as shown in Figure 12, at a 90 eV collision energy. Fragment yields using the surface positioned 40^0 to the extraction plates of the TOF were much higher (a minimum of an order of magnitude higher) when compared to the fragment yields of the in-line arrangement. The increased fragmentation efficiency (intensity of ions observed) is primarily attributed to the fact that all ions must impact the surface for the surface positioned 40^0 to the mass spectrometer, whereas as much as 80% of the ion beam in the in-line experiments may not have collided with the gold mesh. Four of the five peptides yield fragment ions that can be used to determine

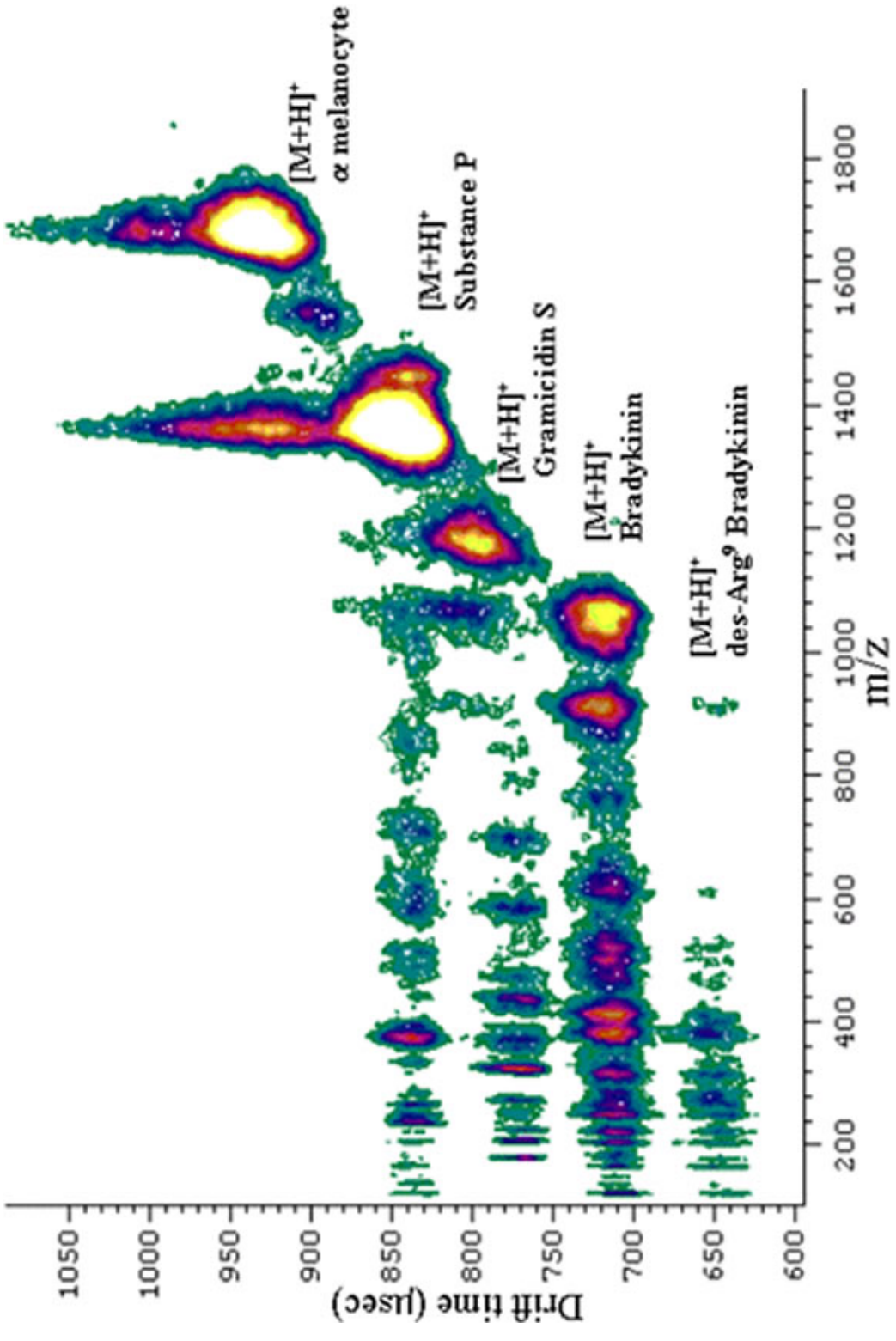

Figure 26: Mass-mobility plot of a five-peptide mix acquired using an adventitious hydrocarbon coated stainless steel surface at ~90 eV collision energy. The correlation of fragment ions to precursor ions is illustrated.

the amino acid sequence. The des-Arg^9 $[M+H]^+$ ion does not survive activation at this collision energy and the only fragment ions that are detected are the b_2, y_2, a_4, and b_4. On the other hand, bradykinin $[M+H]^+$ ions yield an entire series of a-, b-, and y-type fragment ions, with the exception of a_3, b_3, and y_6 fragment ions. The gramicidin S SID spectrum is dominated by proline terminated fragment ions, *i.e.* PV (m/z 197), FP (m/z 245), PVO (m/z 311), LFP (m/z 358), PVOL (m/z 425), PVOLF (m/z 572), and PVOLFP (m/z 669). Similarly, the SID spectrum of substance P $[M+H]^+$ ions contains a complete sequence for b_1 – b_8 and y_1 – y_8 fragment ions; however, the lack of d_{10} or w_2 fragment ion does not permit distinction between the isomeric amino acid residues of leucine and isoleucine. At these collision energies we do not observe fragmentation for α-MSH.

Figure 27 contains a series of SID mass-mobility plots for bradykinin $[M+H]^+$ ions obtained using an F–SAM surface. Spectra are shown for SID collision energies ranging from 40 to 100 eV in 20 eV increments. At 40 eV collision energies the fragmentation series is incomplete and the spectrum is dominated by y_8, b_8, a_8, b_6, a_6, y_4, b_4, a_4, and y_1 fragment ions. Increasing the collision energy to 60 eV results in a more complete fragmentation series with greater individual abundances. The fragment ion abundances are very similar

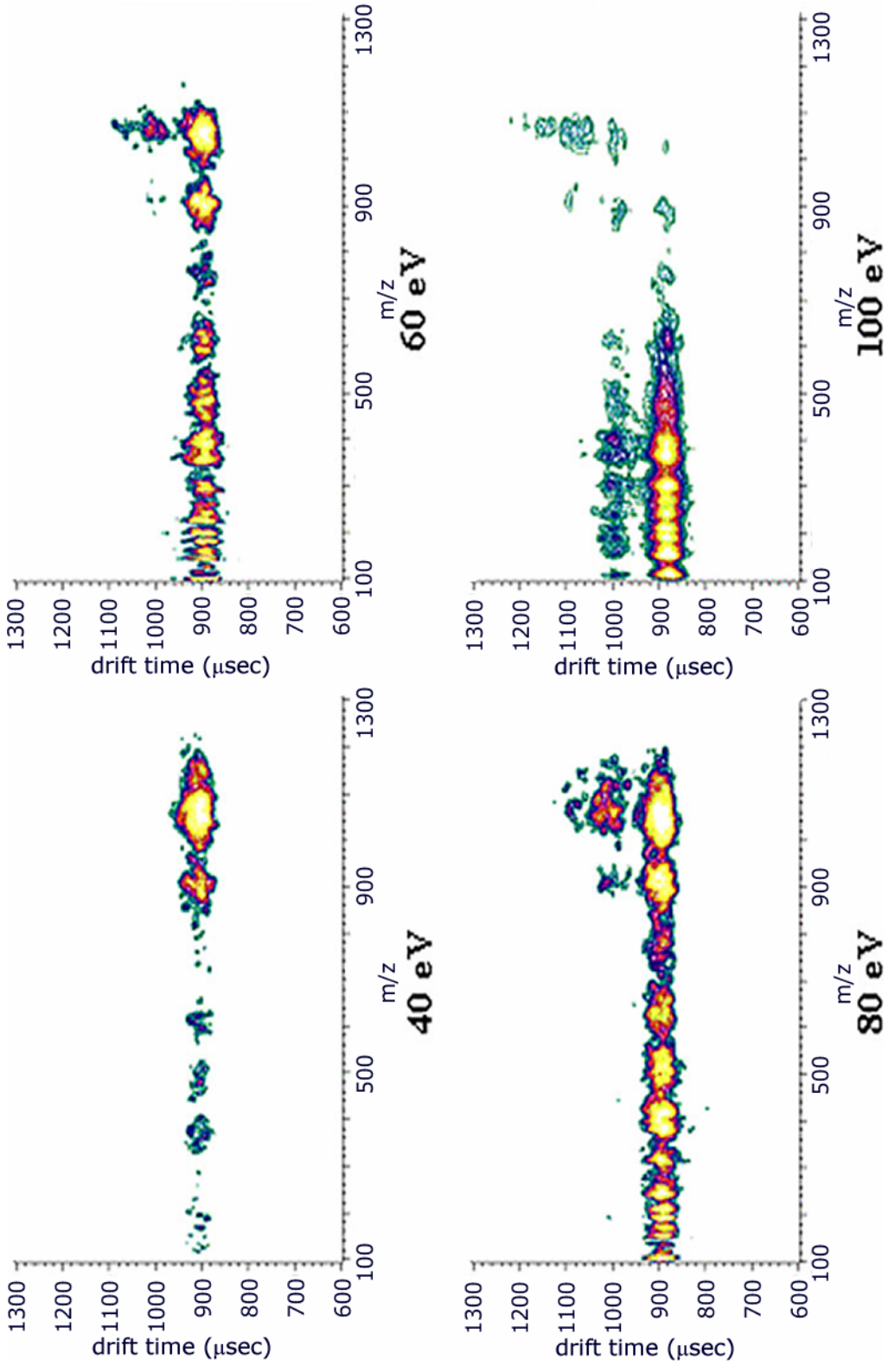

Figure 27: Series of 2D mass-mobility plots of bradykinin at increasing collision energies (40 – 100 eV) with an F–SAM surface. The depletion of the precursor ion and the abundances of the fragment ions increase near linearly with collision energy.

to that obtained for bradykinin $[M+H]^+$ ions at 90 eV collision energies from a stainless steel surface; however, the ratio of the integrated areas for the peak corresponding to the y_8/b_8+H_2O fragment ions to $[M+H]^+$ ion, is 1:1 for the F–SAM and 1:10 for the stainless steel surface. Increasing the collision energy to 80 eV increases the relative fragment ion abundances but no new fragment ions are observed and the overall mass resolution is decreased. At 100 eV collision energies the abundances of the $[M+H]^+$ and y_8 fragment ions are reduced and low m/z and immonium ions dominate the spectrum. This result is consistent with the observations made by Riederer that SID fragment ion types are dependent on impact velocity.[121]

The most sequence informative fragmentation appears to be observed between 40 and 60 eV collision energies for the F–SAM surface, and this corresponds to approximately a 30% reduction in collision energy relative to that for adventitious hydrocarbon-stainless steel. This observation as well as the specific types of fragment ions produced is consistent with work performed by Cooks, Wysocki, and others regarding the overall value of F–SAMs for SID experiments.[122],[123] In addition, the reproducibility of the SID spectra

is excellent, which greatly affects the analytical utility of F–SAMs for high throughput proteomic studies.

Evaluation of Established Parameters

Figure 28 contains a mass-mobility plot for F–SAM SID of a five peptide mixture using a collision energy of ~50 eV. Using these conditions a complete set of a-, b-, and y-type fragment ions, with the exception of a_3, b_3, and $y_{5,}$ are observed for des-Arg^9 bradykinin, and similar results, a complete set of a-, b-, and y-type fragment ions, with the exception of a_3, b_3, and $y_{6,}$ are observed for bradykinin. Note, however, that the abundances of the low m/z fragment ions are reduced with respect to those for des-Arg^9 bradykinin. The total number of fragment ions is also reduced for gramicidin S when compared to the results obtained using 90 eV collision energies and a stainless surface. The ratio of the integrated peak area of the precursor ions to the sum of the integrated peak areas of the associated fragment ions is provided in Table 2.

Figure 29 contains an F–SAM SID mass-mobility plot obtained using 70 eV collision energy. Only a small fraction of des-Arg^9 bradykinin $[M+H]^+$ ions survive activation, and the only SID fragment ions observed have m/z values of < 650. This result agrees well with spectra shown in Figure 27 for bradykinin $[M+H]^+$ ions where an

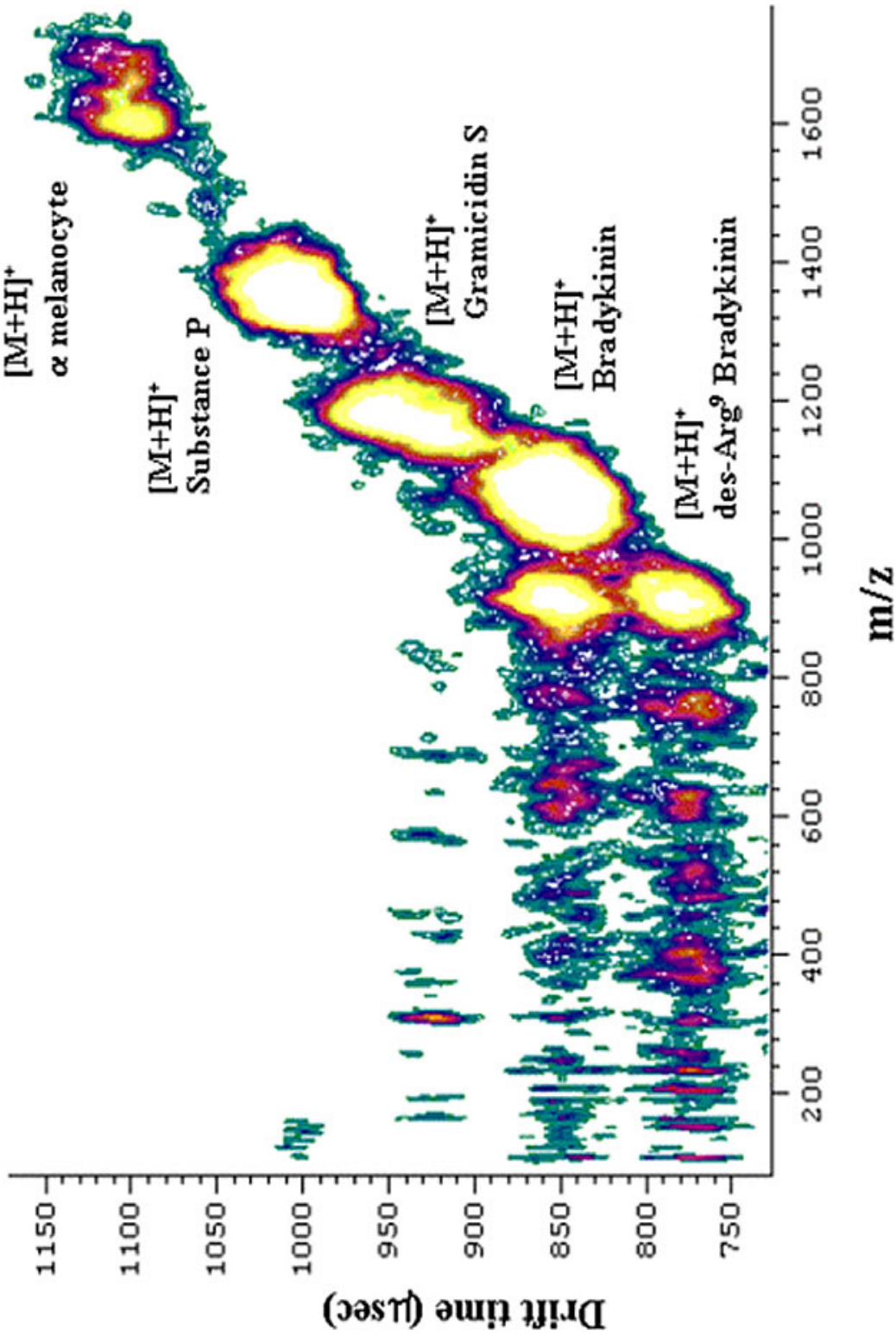

Figure 28: Mass-mobility plot of a five-peptide mix acquired at ~50 eV collision energy with an F–SAM surface.

Table 2: Ratio of integrated area of precursor ion to the sum of integrated areas for all fragment ions.

Surface/ collision energy	des-Arg^9	bradykinin	gramicidin S	substance P
Stainless 90 eV	1:11	1:4.5	1:2.7	1.4:1
F-SAM 50 eV	1:3	1:1.0	2:1.0	1:0.1
F-SAM 70 eV	1:23	1:7.0	1:3.5	1:1.3

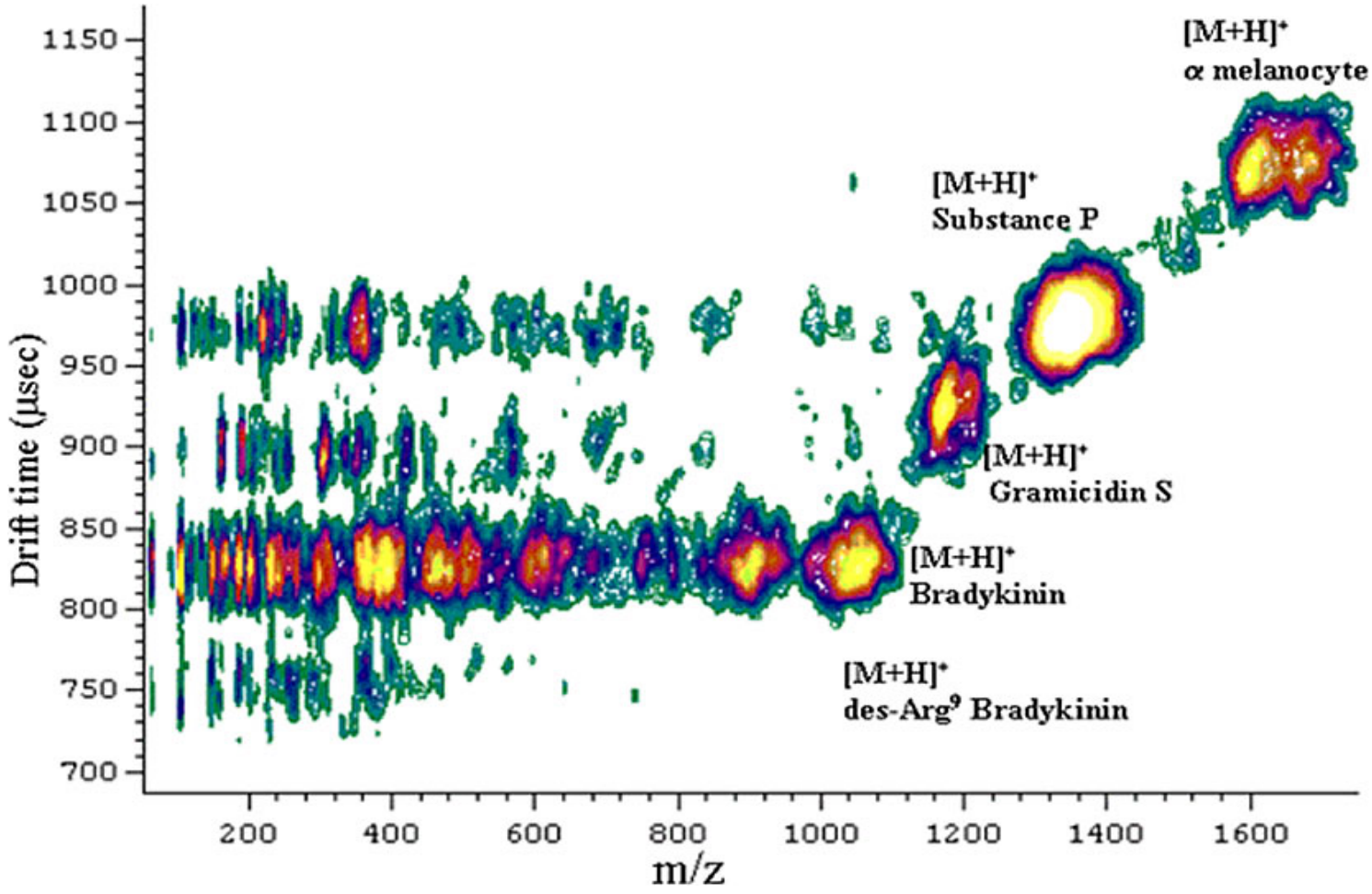

Figure 29: Mass-mobility plot of the five-peptide mix acquired at ~70 eV collision energy with an F–SAM surface showing an improvement in signal quality over a stainless steel surface. Abundances of the most abundant fragment ions are nearly equal to the precursor ions.

increase in collision energy resulted in a depletion of the precursor ion. Similar behavior is also observed for gramicidin S, *e.g.,* an increase in SID fragment ion abundance and a reduction in the $[M+H]^+$ ion abundance is observed as collision energy is increased. Similar results are obtained for substance P, which exhibits a near complete fragment ion series, a_1, a_2, a_5, b_1, b_2, $b_4 - b_8$, y_1, $y_3 - y_8$, and the usual losses of small neutrals at higher collision energies. The observed fragmentation at 70 eV collision energy with an F–SAM surface is comparable to that observed at 90 eV (Figure 26) using a stainless steel surface. The ratio of integrated peak area for the precursor ion to that of the SID fragment ions, listed in Table 2, is improved over that at 50 eV with an F–SAM.

A comparison of Figures 26 through 29 underscores an important feature of SID, *viz.,* that ions activated by SID possess a narrow distribution of internal energies. From the results shown here the use of a single collision energy appears to limit the range, ~300 m/z, where both the $[M+H]^+$ ion survives and sufficient sequence informative SID fragment ions are formed. It may be possible to overcome this limitation by ramping the collision voltage during the course of the experiment. In addition, instrument design may also be an important factor. For example, the F–SAM surface is positioned

approximately one cm from the extraction region for these studies and there may be insufficient time, less than 10 μsec, for a large m/z ion (greater than m/z 1500) to undergo dissociation. Wysocki has shown that the rate constants for the decomposition of peptides using H-SAM and F-SAM surfaces at a 35 eV collision energy are $2x10^4$ to $40x10^4$ s^{-1}, or an order of magnitude longer than the transit time from the surface to the extraction region for the instrument used in these studies. [124] Evan Williams has shown in BIRD experiments that the decomposition rates constants for peptides larger than m/z 1600 in the rapid energy exchange (REX) limit, where the internal energy distribution of a population of ions is a Boltzmann distribution, is on the order of 0.001 to 0.200 s^{-1}.[125] This means that the fragment ion spectra is not only dependent on the internal energy deposited into the precursor $[M+H]^+$ ion and its mass, but also on the flight time from the collision surface to the extraction region of the mass spectrometer.[126] The transit time from the F–SAM surface to the extraction region 1 cm away for an m/z 1500 ion having a scattered kinetic energy of 14 eV would be 4 -5 microseconds. This short flight time requires higher collision energy to achieve similar fragmentation patterns than is typically observed by Wysocki.[117] Recent work and RRKM modeling by Laskin *et al.* shows additionally that at the higher

collision energies and shorter unimolecular dissociation time scales that the internal energy distribution maps closely with the Boltzmann distribution at the REX limit as described by Williams.[127,128,129]

Additional Benefits of F–SAM Surfaces

The importance of using F–SAM surfaces for IM–SID–TOFMS is clearly illustrated by the peak tailing observed in Figure 26. Nearly identical fragmentation patterns for protonated peptides between m/z 900 and 1350 using a stainless steel at 90 eV (Figure 26) were observed for an F–SAM at 70 eV (Figure 29). The peak tailing (peaks appearing at the same mass but later drift times) observed for substance P and α-MSH using the stainless steel surface is significantly reduced for the F–SAM surface. It should be noted, however, that even with an F–SAM the choice of collision energy yields further improvements in the spectrum. That is, we see that collision energy affects peak tailing even for an F–SAM surface (see Figure 27.) By controlling the collision energy it should be possible to completely eliminate the peak tailing and thereby improve the mobility resolution.

The amount of tailing appears to be a function of the nature of the surface, the nature of the impacting ion, and the collision energy. One possible explanation is that the ions “soft-land” onto the surface

and are desorbed by later arriving ions. The data shown for bradykinin precludes this possibility as there are no other ions resulting from a single laser shot and subsequent laser shots are separated by 50 msec (20 Hz repetition rate). Even at 100 eV the latest arriving ions occur approximately 300 μsec after the first mobility appearance time. Another possibility is that multiple-charged multimers, such as $[(M+H)_n^+]^{n+}$, are formed and upon impacting the surface the ions decompose to from $[M+H]^+$ ions. We have not ruled out this possibility; however, we have measured the arrival time distribution of bradykinin ions using high-resolution ion mobility and we do not observe multiple peaks.[130]

Experiments with a dendrimer (Figure 30) shed some light on this matter. Shown in Figure 31 is the spectra acquired from a neat sample of the dendrimer prepared similarly to the bradykinin in Figure 27 at 100 eV. A single set of mobility correlated SID fragment and $[M+H]^+$ ions was anticipated, but five distinct ion species were observed separated by a fixed increase in drift time. The base peak for each of the five drift time separated species (A through E) was determined to be the $[M+H]^+$ ion minus four t-butyloxycarbonyl, (t-BOC, mol. wt. 101) protecting groups with the cleavage occurring at the amide bond similar to that for a b or y type cleavage in a peptide.

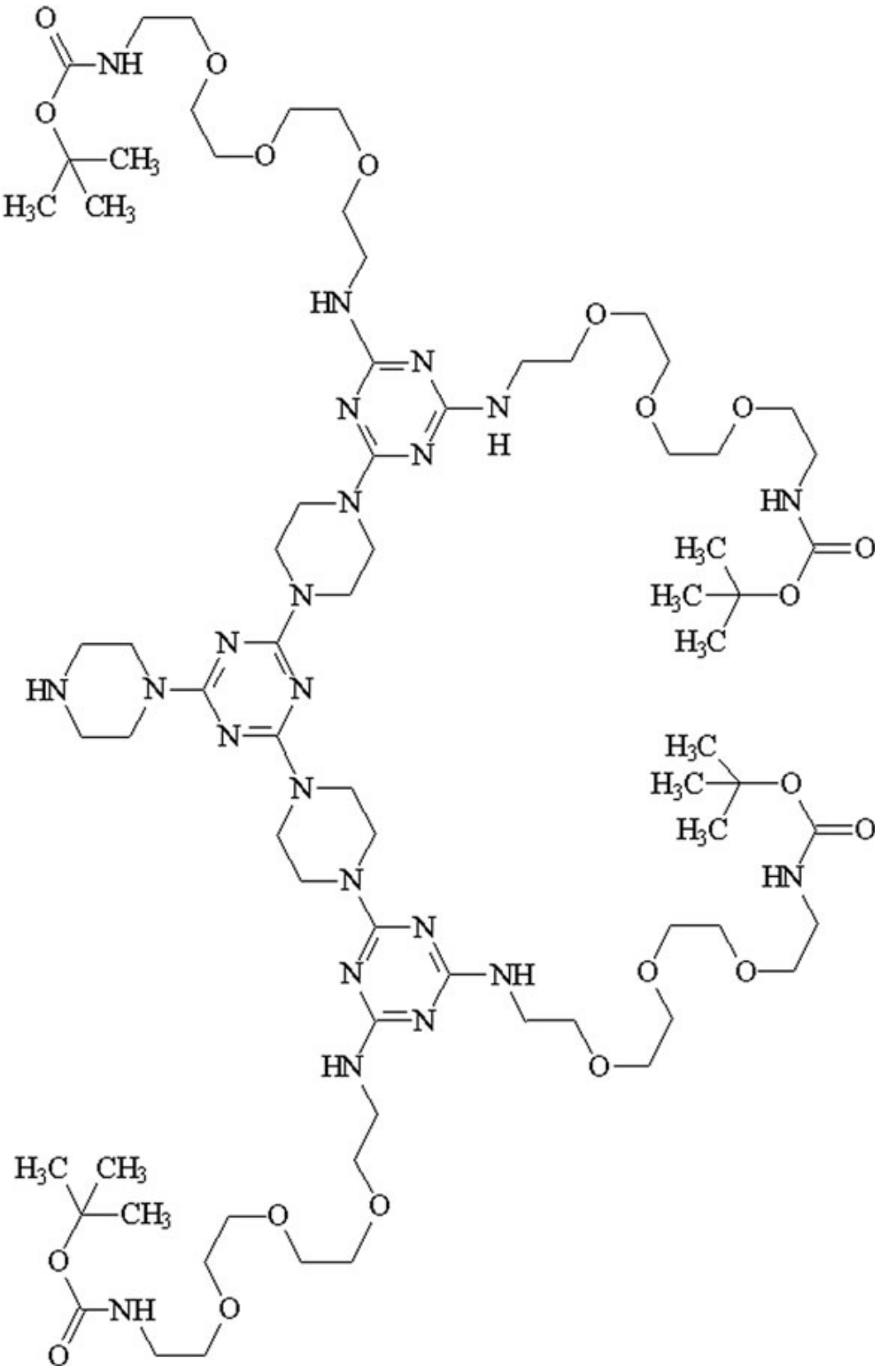

Figure 30: Structural formula for the dendrimer ($C_{73}H_{133}N_{23}O_{20}$ MW 1653) synthesized by M. McLean and E. Simanek.

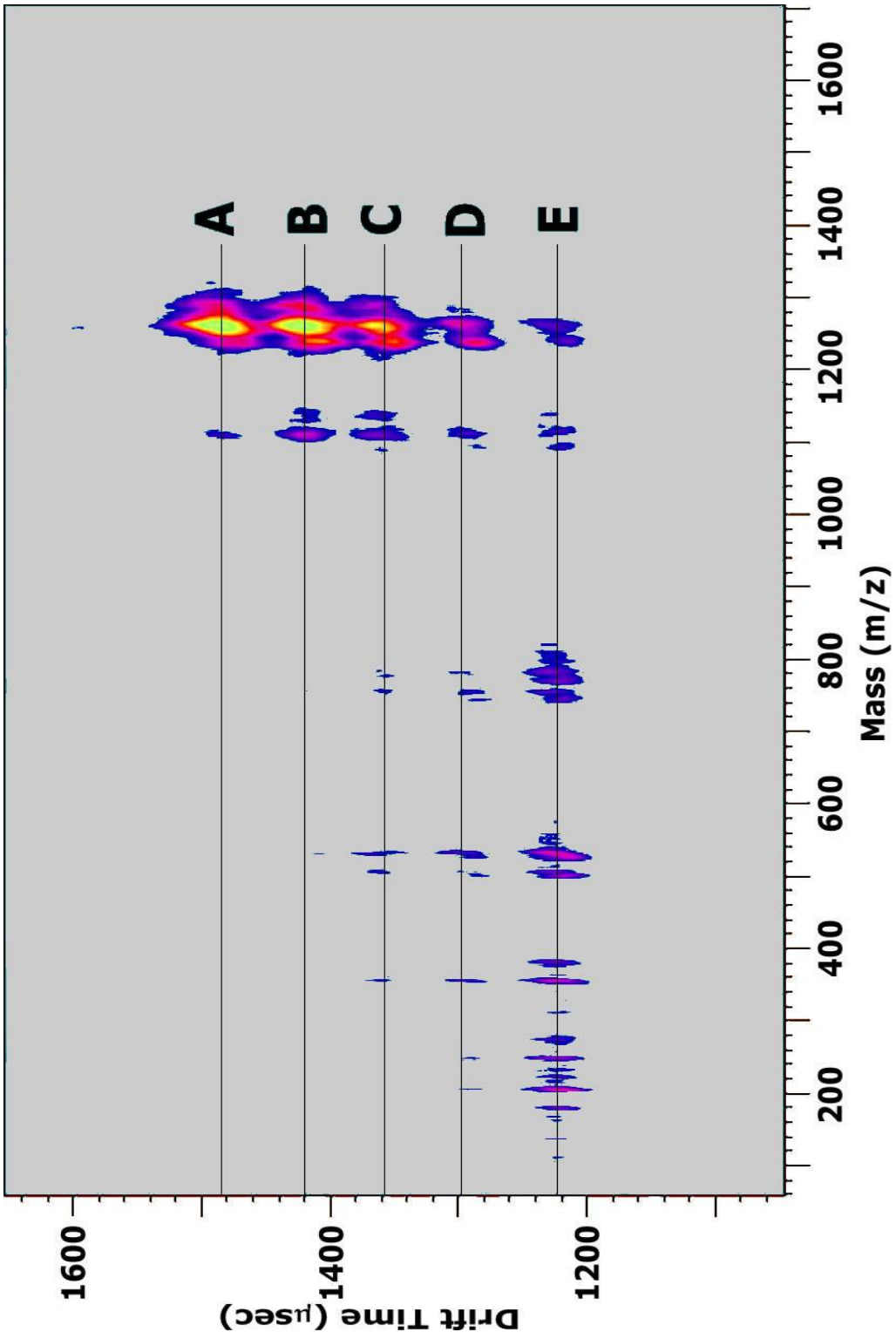

Figure 31: A 2D MALDI-IM-SID-TOFMS plot of a single dendrimer species displaying five mobilities.

The increase in SID fragments and decrease in parent ion observed from mobility correlated series A to E suggests that some of the collision energy goes into an initial fragmentation of an unobserved $[M+H]^+$ increasing by one fixed mass unit (in this case the t-BOC protecting group) for each series. Reductions in the collision energy (from 115 eV to 60 eV) had the expected effect of reducing the SID fragmentation observed for all series, however, the base peak was again the $[M-(tBOC)_4+H]^+$. The sample was then prepared using a MALDI matrix that is known to yield peptide ions with a lower internal energy, trihydoxyacetophenone (THAP) with the expected result being the prevention of the loss of the protecting groups during the MALDI event. Shown in figure 32 is the result of the experiment using THAP as the matrix with a collision energy of 60eV. The base peak was identified as the intact $[M+H]^+$ for series A with each subsequent series (B through E) determined to be the loss of one additional t-BOC group per series. Figure 33 shows the result when the SID energy was increased to 75 eV. The loss of each of the four protecting groups is observed for the series A.

The results of the dendrimer experiments suggest that the five mobility separated bradykinin species separated in mobility observed in Figure 27 are likely to be clusters of bradykinin and a multiple of

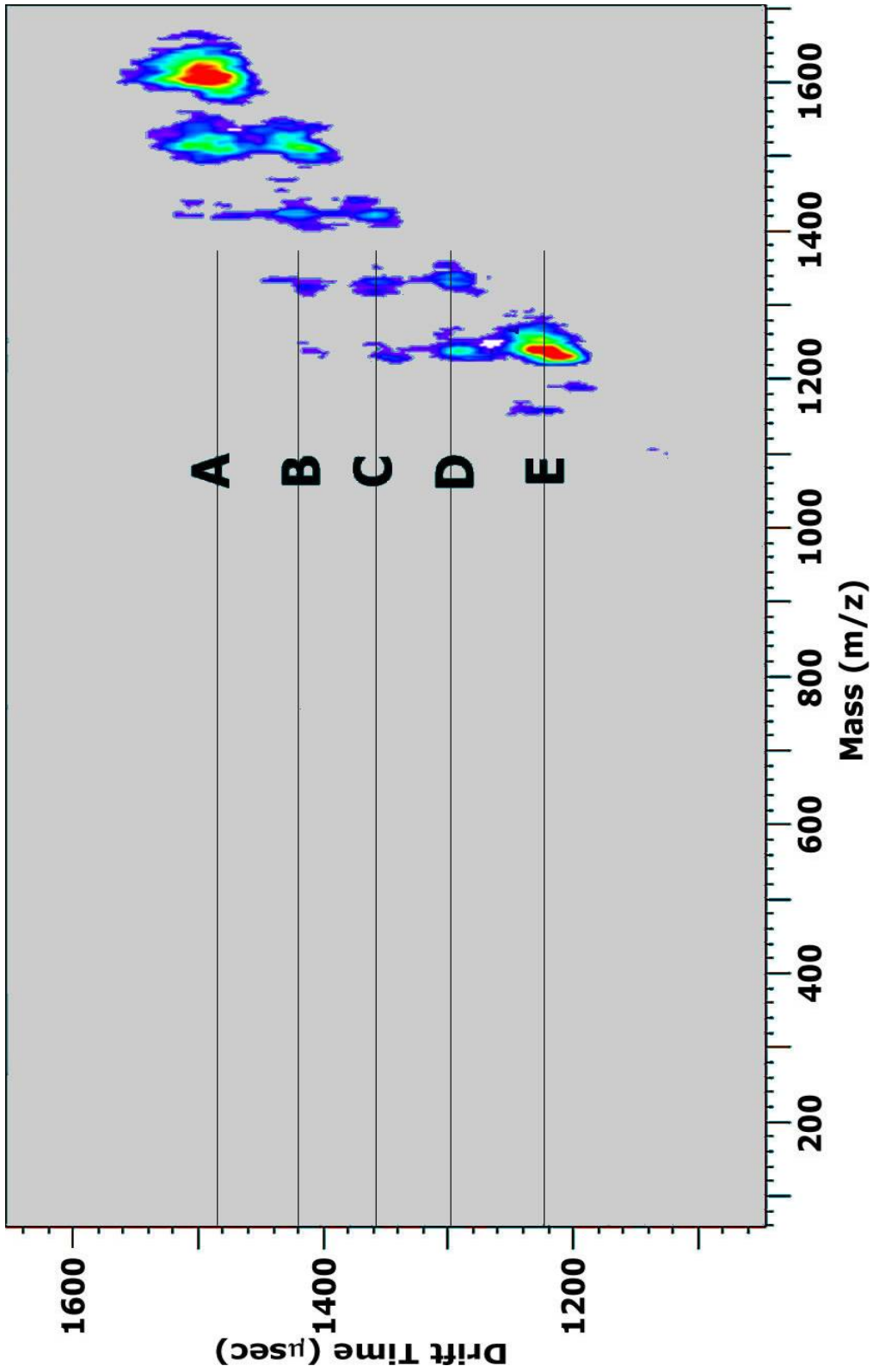

Figure 32: A 2D MALDI-IM-SID-TOFMS plot (SID collision energy 60 eV) of a single dendrimer species displaying five mobilities for a series of parent ions formed during the MALDI event that vary in mass by one repeating unit equivalent in mass to a t-BOC protecting group.

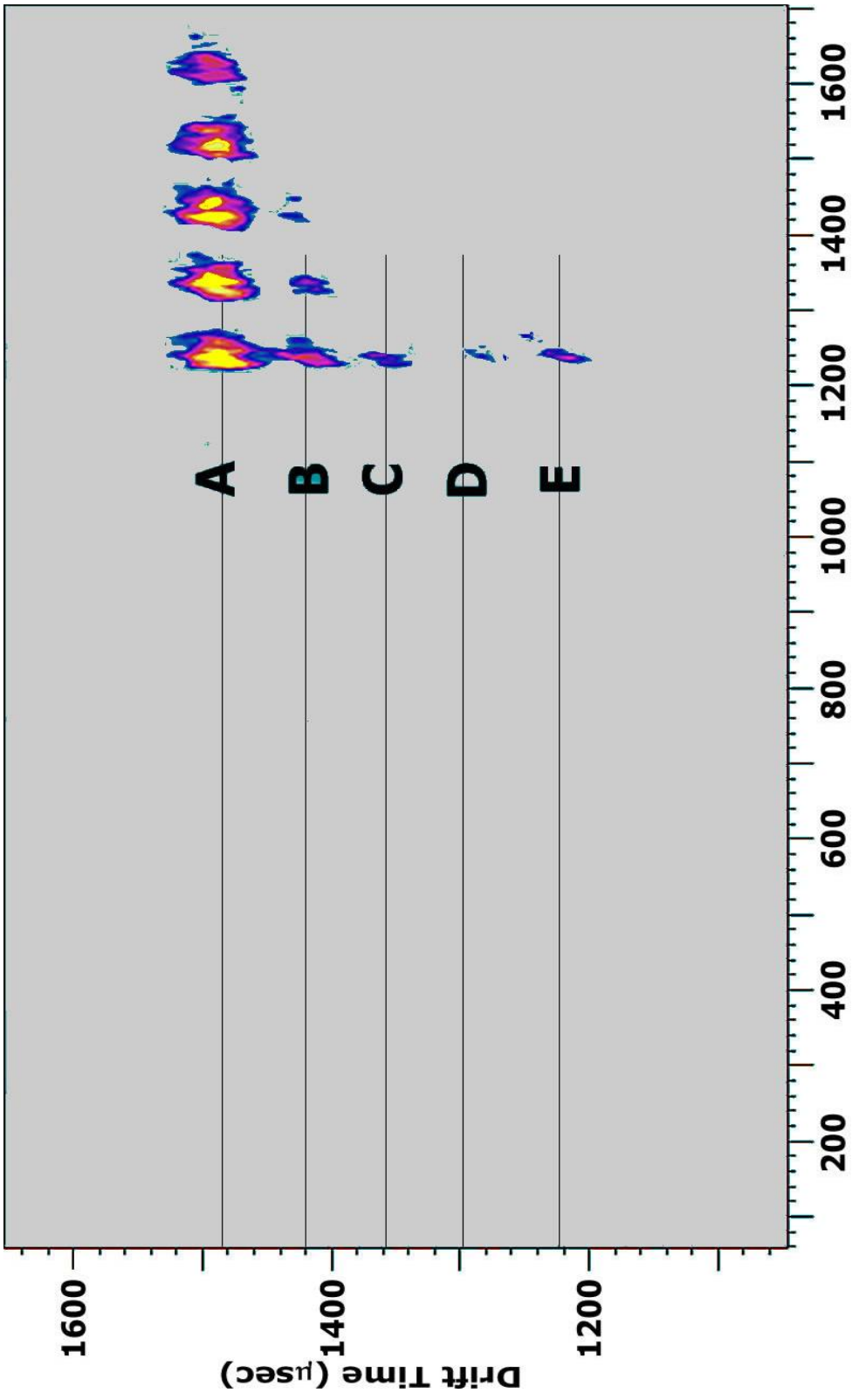

Figure 33: A 2D MALDI-IM-SID-TOFMS plot (SID collision energy 75 eV) of a single dendrimer species displaying five mobilities for a series of parent ions formed during the MALDI event that vary in mass by one repeating unit equivalent in mass to a t-BOC protecting group.

some low mass adduct formed during the desorption event that are stabilized by collisions with the inert buffer gas in the drift cell and survive as intact species during the transit through the drift cell. As the unknown adduct is much more loosely bound to the bradykinin than the labile covalently bound protecting group of the dendrimer it is likely that the intact bradykinin ions are more easily dissociated with the dissociation event occurring in the field free region between the drift cell and the extraction region of the TOF. This also leads to the conclusion that at high field strengths the MALDI formed ions retain sufficient internal energy to contribute to the activation event with the F-SAM surface.

Conclusion

Efforts to optimize the combination of F–SAM SID and IM–TOFMS for proteomics studies are demonstrated. The advantage of the simultaneous acquisition of the peptide mass map and peptide sequence information is greatly facilitated by the use of F–SAM surfaces. The judicious choice of surface composition and collision energy led to significant improvements to the experiment. The implications of the technique include meeting the need for high throughput *de novo* sequencing of peptides and mixtures of peptides resulting from the proteolytic digest of proteins.

CHAPTER V

AN EVALUATION OF MALDI-IM-SID-TOFMS USING A HYBRID DRIFT CELL

The density of the MALDI plume in the previous instrument caused a discharge at the upper end of the range of the designed drift voltage. To overcome the limitation imposed on the drift voltage, which limits mobility resolution, the first ring electrode in the periodic focusing drift cell was enlarged to increase the volume in the area of the MALDI plume. This chapter discusses a combination of the first instrument, which utilized an in-line sample probe and a focusing linear field to focus the MALDI formed ions to the orifice separating the drift cell from the primary ion optics, and the periodic focusing drift cell of the second instrument. The result provides a larger volume for the formation of ions by MALDI, a continuing focus of the ion beam to increase sensitivity, and evaluation of the possibility of incorporating a multi-sample plate similar to that used in other TOFMS instruments in Russell group, *i.e.* ABI 4700 TOF-TOF.

The theoretical resolution for any drift cell operating at the low field limit can be calculated as function of the square root of the drift

voltage, $R=1.84*V^{-2}$. For a drift cell operated at 2400 V (the upper limit of the drift cell under evaluation due to the breakdown characteristics of the bath gas) the theoretical mobility resolution would be 90 $t/\Delta t$ FWHM. Figure 34 contains the mobility spectrum acquired for crystal violet (m/z 374) using the hybrid drift cell operated at 13 V cm^{-1} $Torr^{-1}$ (4.5 Torr He, 2400 V drift potential, and a drift cell length of 40 cm), which is above the low field limit. A mobility resolution of 61 ($t/\Delta t$) at FWHM was achieved. The mobility resolution for 1.3 Torr He (60 V cm^{-1} $Torr^{-1}$) was 21, and for 2.1 Torr He (29 V cm^{-1} $Torr^{-1}$) was 33 (see inset Figure 34.) The slope of the best fit line constructed for the plot of mobility resolution vs. pressure would provide the pressure at which the theoretical mobility resolution would be reached. This pressure was determined to be 7.1 Torr, or 8 V cm^{-1} $Torr^{-1}$, very near the low field limit of 6 V cm^{-1} $Torr^{-1}$. Unfortunately these near ideal mobility resolutions for the drift cells constructed in this laboratory are observed only for neat samples of C_{60} and crystal violet, which can be desorbed and ionized without a matrix, and not with peptide samples which typically do no better than 20 to 30 $t/\Delta t$ at FWHM. The reason peptide samples do not obtain the theoretical resolution like the neat samples of C_{60} and crystal violet is in the dynamics of the MALDI process. Peptides

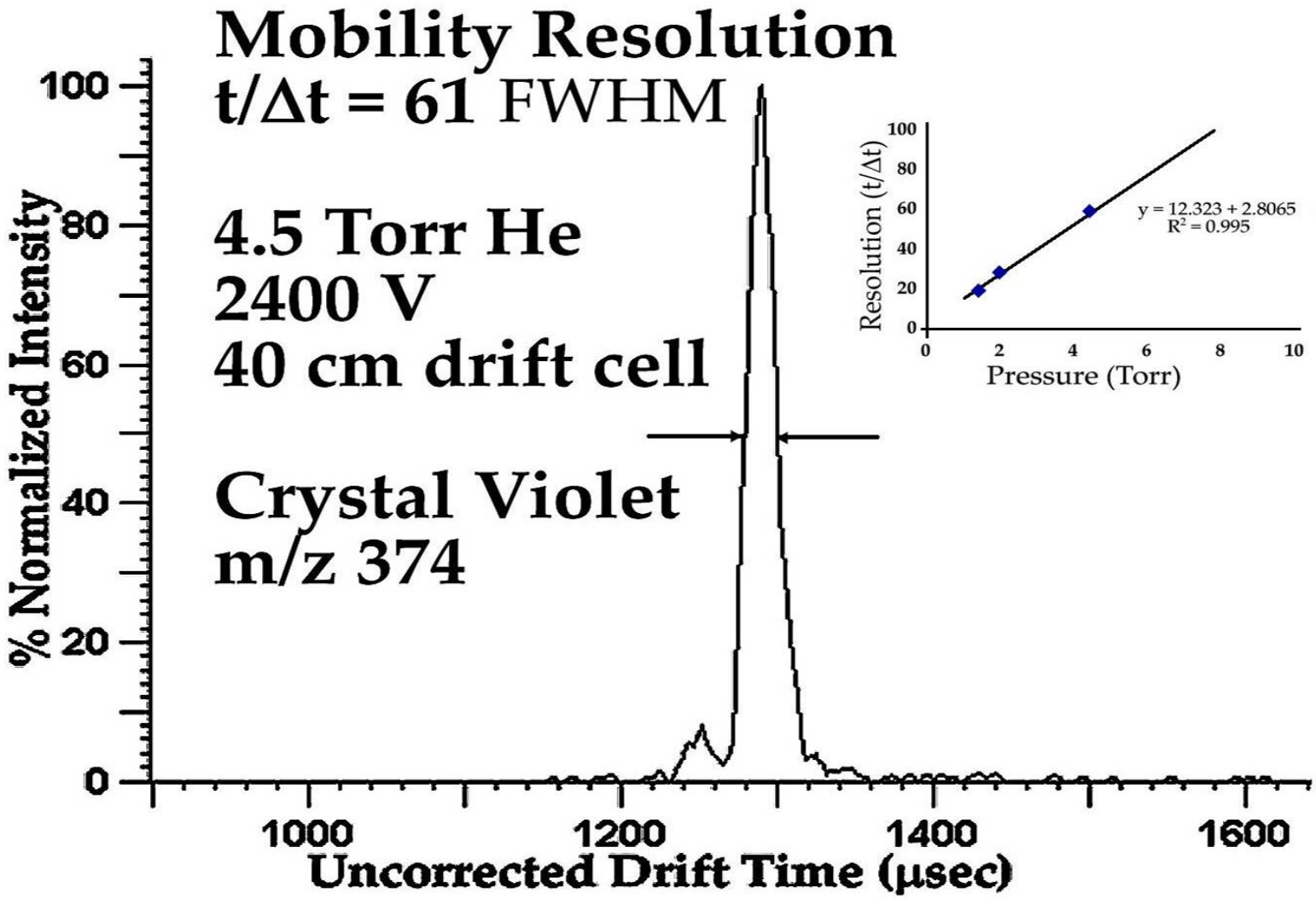

Figure 34: The mobility resolution for crystal violet (m/z 374) obtained using a hybrid drift cell is 61 (t/Δt) at FWHM.

require the presence of a matrix to desorb and it has been shown that the MALDI process is likely to be a cluster emission mechanism.[131] In the case of the mobility drift cell if the cluster does not dissociate promptly, or at least very quickly after desorption, the arrival time distribution will widen as the cluster loses mass and subsequently volume.

The numbers for the hybrid drift cell mobility resolution indicate the marriage of the two technologies should not limit the sensitivity as the second stage periodic focusing drift cell is still able to limit band broadening of the ion packet as it elutes through the drift cell. However, as this experiment includes SID to achieve the simultaneous acquisition of partial sequence information for peptides in the PMM, the SID surface must be considered in the sensitivity issue as collisions with surfaces can and do quench ions. Figure 35 contains the mass spectrum obtained for 60 femtomoles of fibrinopeptide A (m/z 1537, AA sequence ADSGEGDFLAEGGGVR) deposited to the sample probe tip. The probe tip size was 0.125 inches in diameter. Data was acquired for fifty seconds. Abundant $[M+H]^+$ ions where observed as well as $[M+H]^+$-NH_3 ions. The S/N for this short run was insufficient to identify any SID fragments. As the sample was not depleted it was possible to redeposit the sample with methanol and

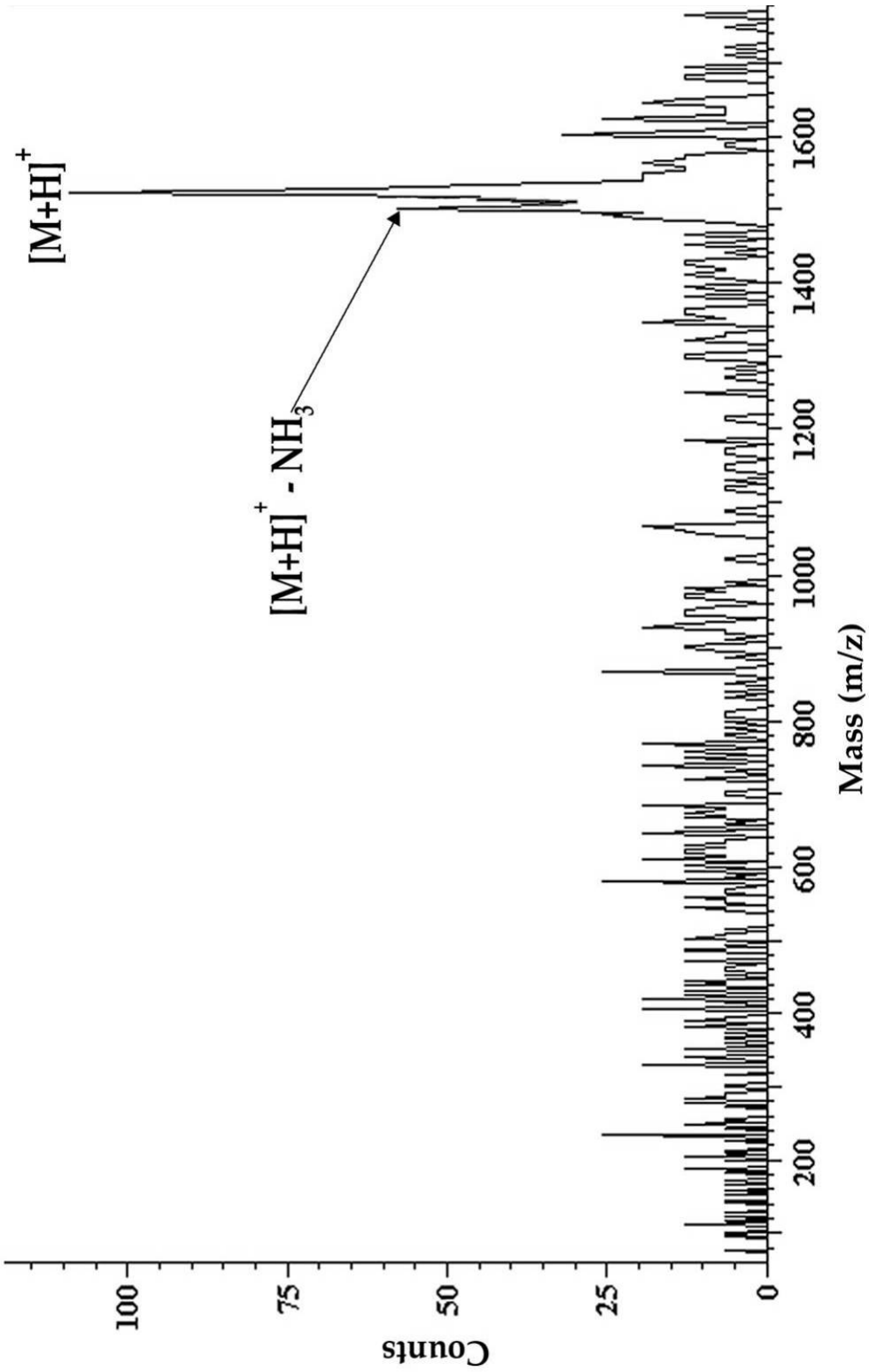

Figure 35: Spectrum of 60 femtomoles deposited of fibrinopeptide A acquired with a MALDI-IM-SID-TOFMS.

the experiment repeated. The redeposition and data acquisition was repeated five times. The resulting spectra for each of the six spectra were similar in appearance with no observable difference in ion intensity. Further modeling of the periodic drift shows that the inner diameter of the rings used in constructing the drift cell for these studies only allows the transmittance of 10% of the total ions through the 300 micron orifice. This transmission efficiency can be increased to nearly 50% by reducing the inner diameter of the rings. The reduction of the ring inner diameter reduces the size of the linear portion of the periodic field before the ions see a focusing or defocusing region, thereby reducing the radial diffusion of the ion beam to a diameter closer in size to the orifice. Further improvements in the transmission efficiency of the drift cell can be realized by increasing the orifice diameter to 500 microns and using a differential pumping region to handle the resulting increased gas flow out of the drift cell. It is also important to note at this time that the design of the probe tip allows the sample deposited to cover almost one eighth of an inch in diameter. It is possible with a redesign of the probe tip to keep the sample spot smaller that ion formation can be improved and consequently the S/N. This demonstrated sensitivity is for ions impinging on the F-SAM SID surface and then entering the extraction

region of the mass analyzer which demonstrates the ability of the FSAM surface to prevent large scale quenching of the ion beam. Of further significance is the age of the surface used for this experiment. The surface used to acquire this spectrum has been in service for two years with the only maintenance being a periodic sonication in ethanol. The extended service life of this surface can be attributed to the robustness of the self assembled monolayer, the pulsed nature of the MALDI experiment, and the ratio of the size of the impinging ion beam to the surface size which permits the movement of the surface relative to the ion beam permitting a large percentage of the surface to be used over time.

Another concern for SID is the run-to-run reproducibility of SID fragmentation spectra. Figure 36 contains a graph for the parent and five selected SID fragment ions of gramicidin S. Twenty replicate runs for each were acquired and the peak heights were compared. The greatest difference is 6% run-to-run for the SID fragment PVO. This reproducibility of fragment ion signatures coupled with the robustness of the FSAM surface makes SID an ideal partner in coupling IM to TOFMS for tandem MS studies.

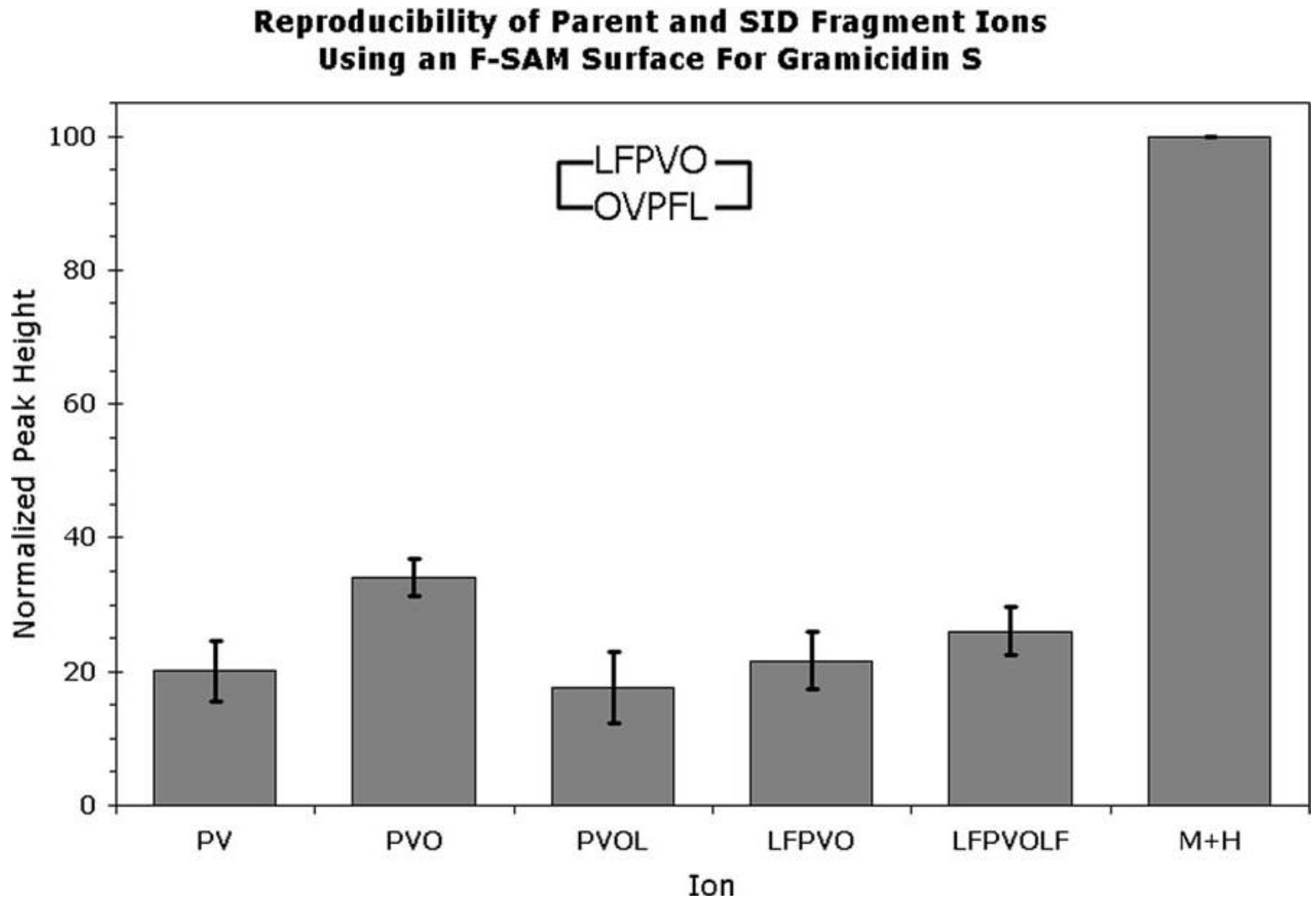

Figure 36: Graph of average peak heights for gramicidin S parent and SID fragment ions. Error bars are for %RSD.

CHAPTER VI

A COMPARISON OF SID, CID, AND PHOTODISSOCIATION FRAGMENT ION SPECTRA FOR MODEL NON-TRYPTIC AND TRYPTIC PEPTIDES

Model Non-tryptic Peptides

To determine the analytical utility of MALDI-IM-SID-TOFMS the SID fragmentation spectra obtained for a series of model peptides was compared to that obtained using photodissociation employing an in-house built MALDI-photodissociation-TOFMS, and with CID obtained using an ABI 4700 TOF-TOF. Figures 37, 38, and 39 contain respectively the SID, CID, and photodissociation fragmentation spectra for RKEVY (RKEVY, 694 m/z). The observed fragmentation is dominated by complete a_n and b_n series fragment ions with the most intense signals observed being from the loss of NH_3. The fragments of greatest abundance are the b_2-NH_3 followed closely by the b_4+H_2O. These fragments are of greater abundance than the immonium ions. At a lower SID collision energy, 20 eV as compared to 50 eV, (see Figure 22) the immonium ion production is much less. With the

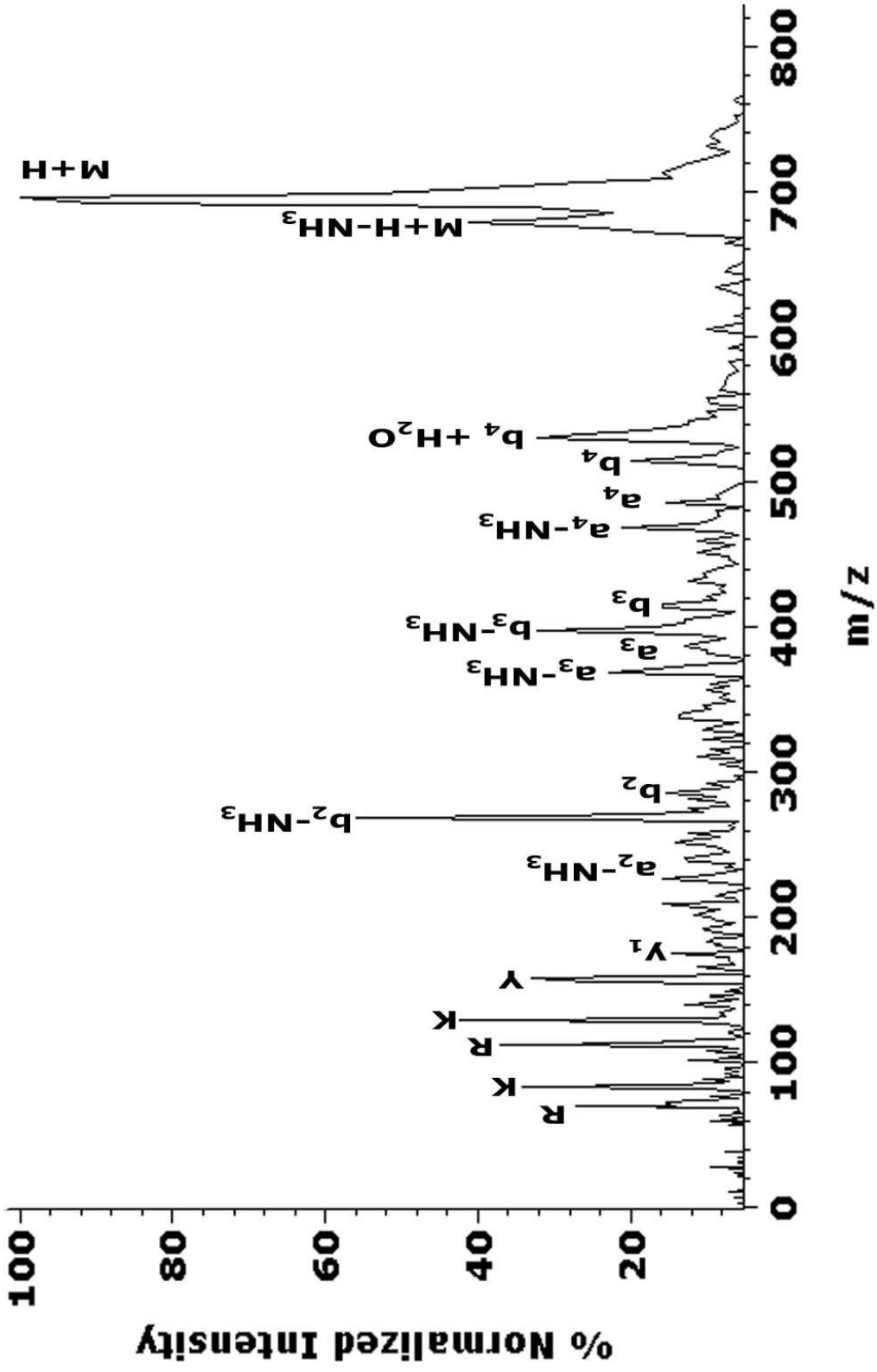

Figure 37: MALDI-IM-SID-TOFMS spectrum of RKEVY (694 m/z), 50 eV SID.

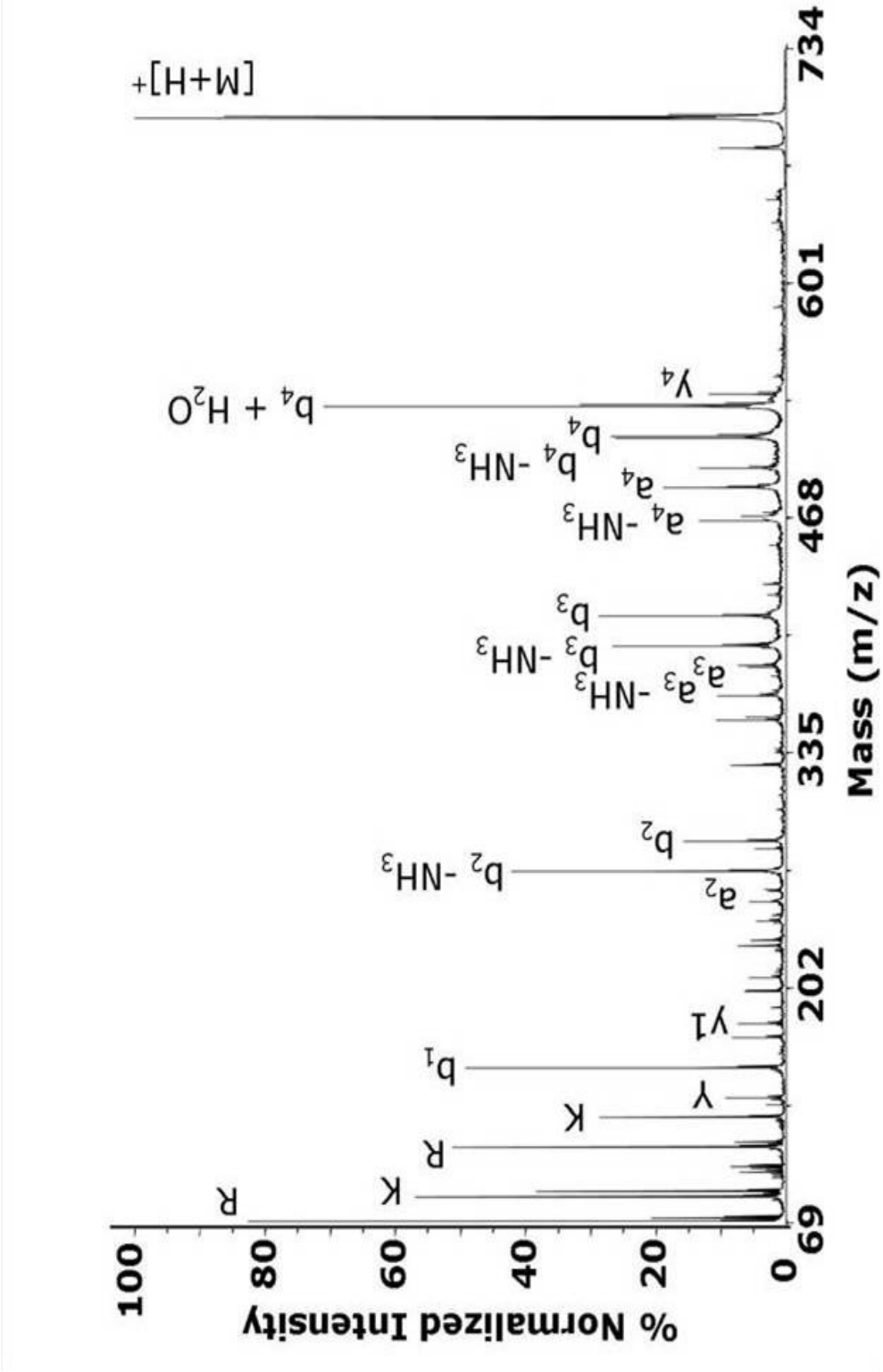

Figure 38: CID spectrum of RKEVY (694 m/z) acquired on an ABI 4700 TOF-TOF.

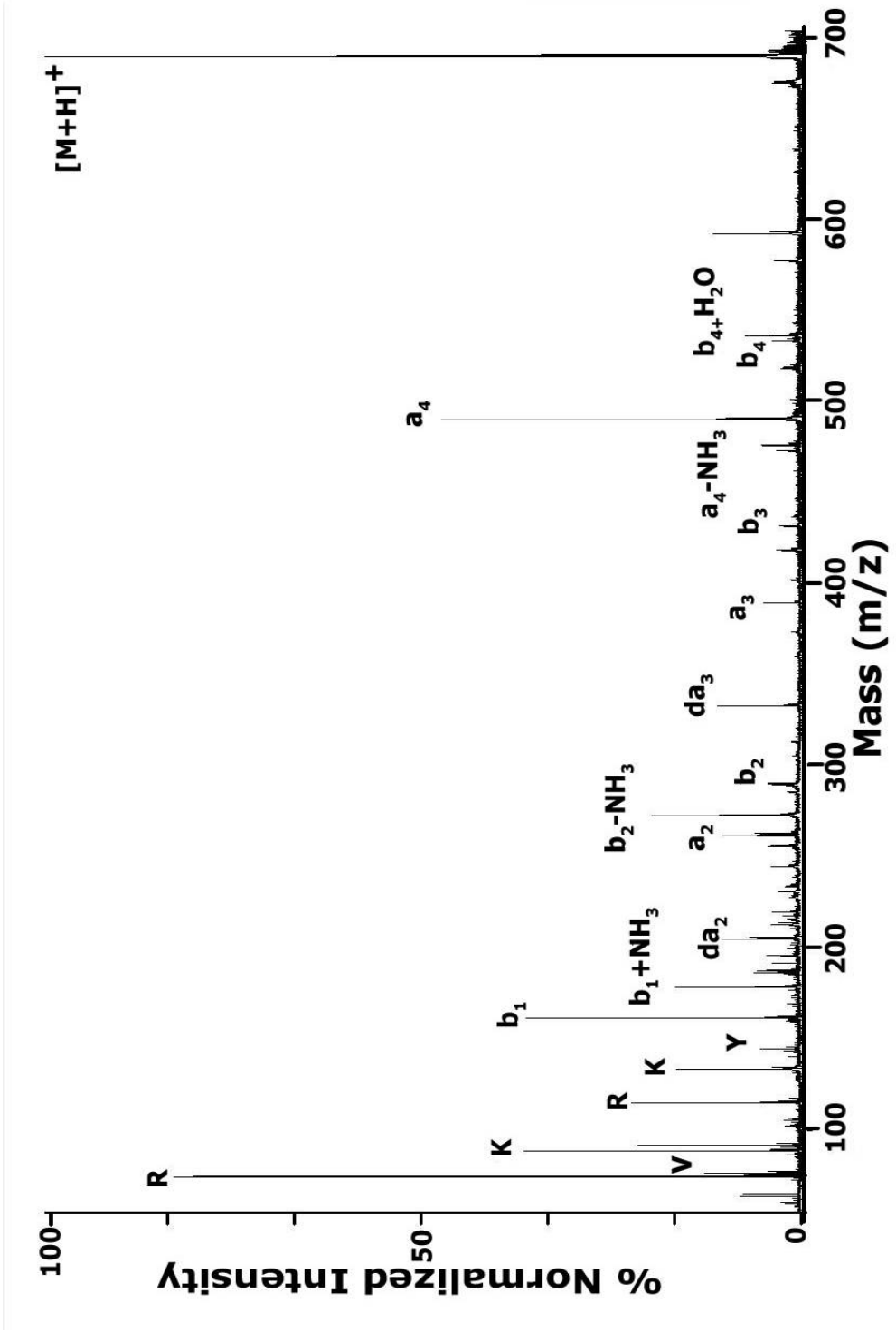

Figures 39: Photodissociation spectrum of RKEVY (694 m/z) acquired on an an in-house built MALDI- Reflectron TOFMS.

exception of the y_1 ion no other y_n series ions were identified in the SID fragmentation of RKEVY.

The CID fragmentation spectrum in Figure 38 is also dominated by complete a_n and b_n series fragment ions with the most intense signals observed being from the loss of NH_3. The fragments of greatest abundance are the b_4+H_2O followed closely by the b_2-NH_3. These fragments are not of greater abundance than the arginine immonium ion and are of comparable intensity to the other immonium ions. With the exception of the y_1 and y_4 ions no other y_n series ions were identified in the CID fragmentation of RKEVY.

The PD fragmentation spectrum in Figure 39 is also dominated by complete a_n and b_n series fragment ions. The fragments of greatest abundance are the a_4 ion and the immonium ions. No y_n series ions were identified in the PD fragmentation of RKEVY. Of much greater abundance are the da_2 and da_4 ions. Immonium ion abundances are most similar to the immonium ion abundances of the CID spectra.

Figures 40, 41, and 42 contain respectively the SID, CID, and photodissociation fragmentation spectra for methionine enkaphalin Arg-Phe (YGGFMRF, 878 m/z.) The SID fragmentation spectrum in Figure 40 is dominated by complete b_n series fragment ions with

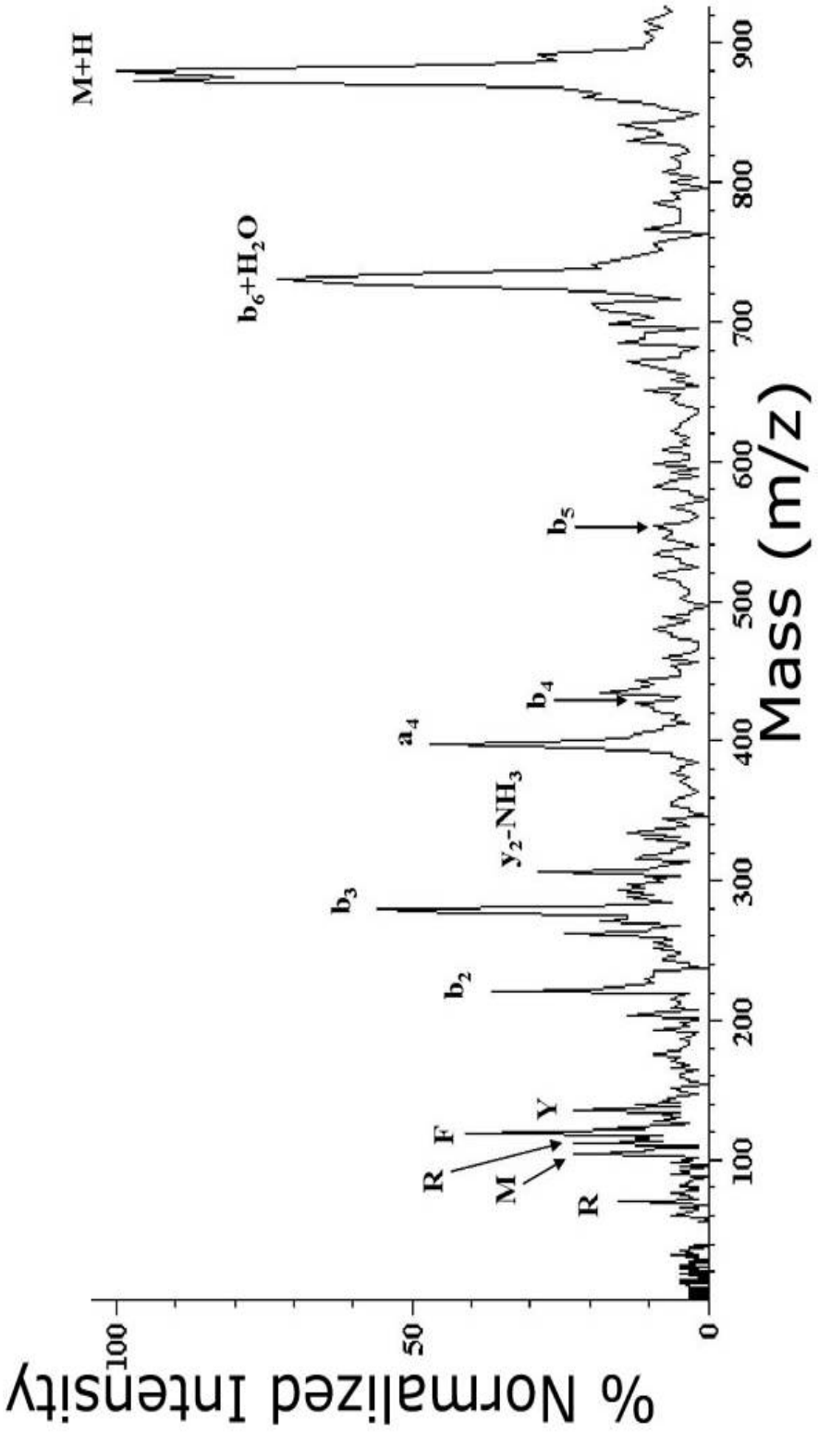

Figure 40: SID ion spectrum of methionine enkephalin Arg-Phe (YGGFMRF, 878 m/z), 50 eV SID, acquired with a in-house built MALDI-IM-SID-TOFMS.

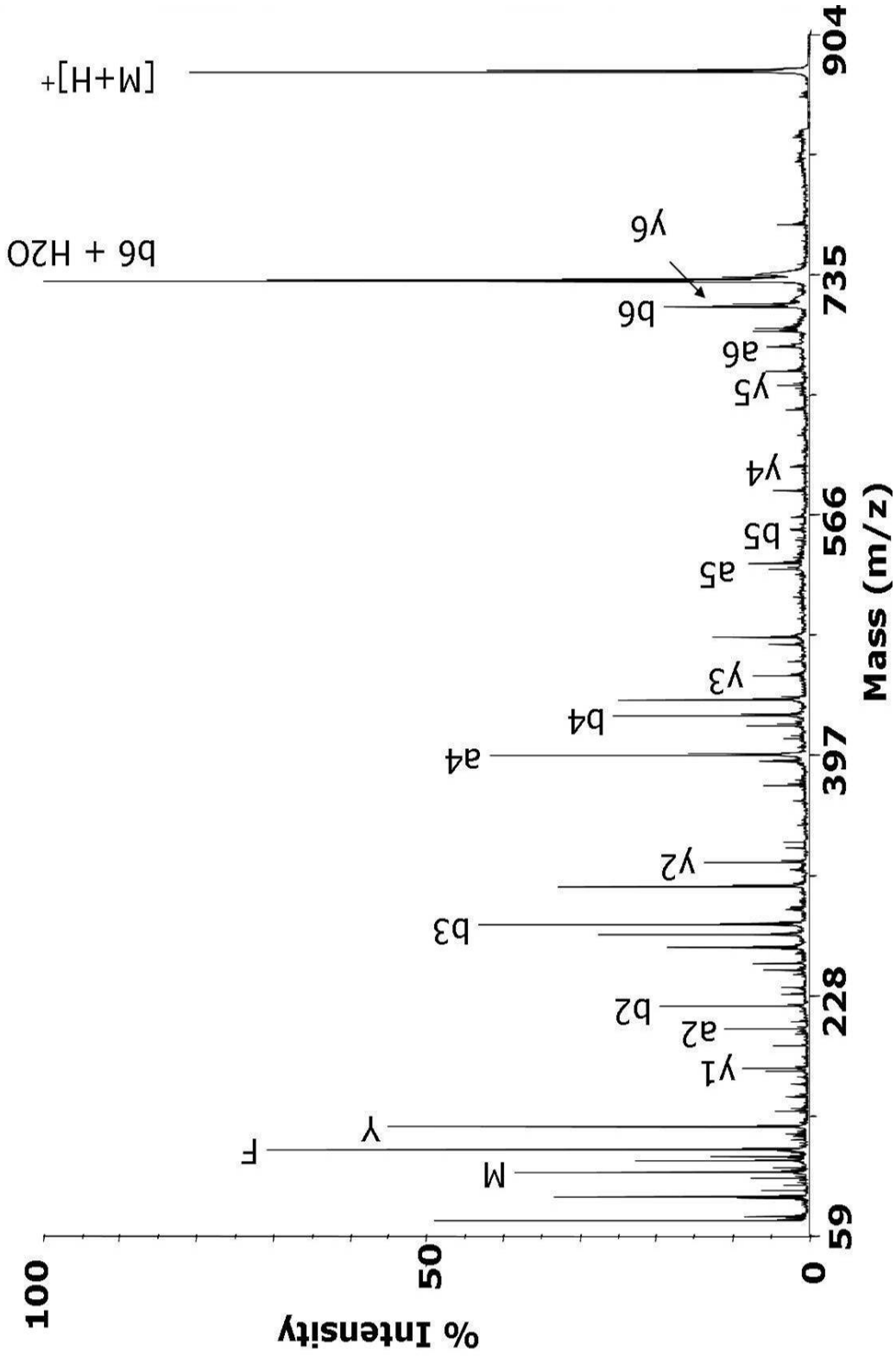

Figure 41: CID spectrum of methionine enkephalin Arg-Phe (YGGFMRF, 878 m/z) acquired on an ABI 4700 TOF-TOF.

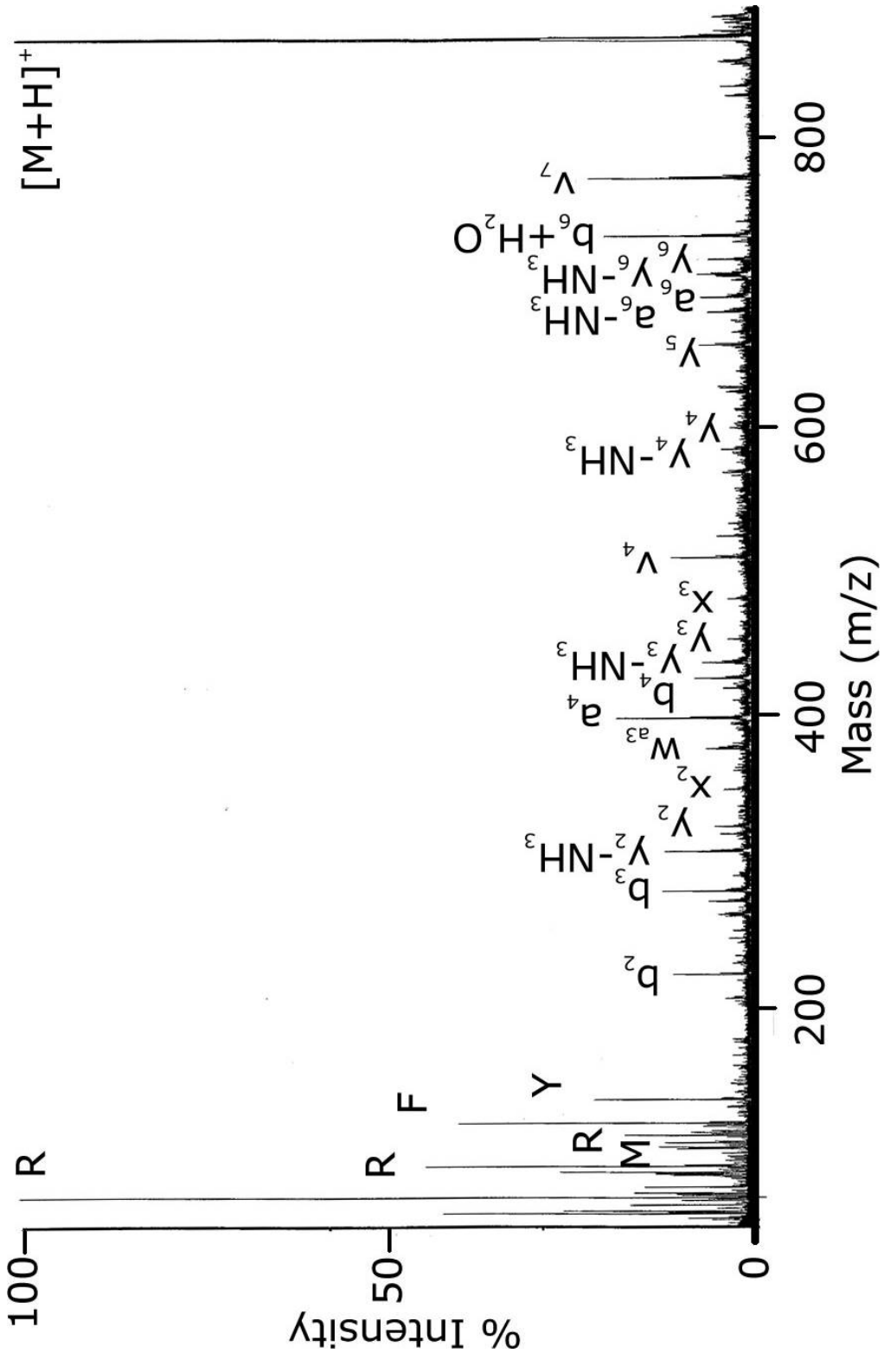

Figure 42: Photodissociation ion spectrum of methionine enkephalin Arg-Phe (YGGFMRF, 878 m/z) acquired on an in-house built MALDI- Reflectron TOFMS.

much less loss of NH_3 being observed. This is as expected from the mass dependence of SID fragmentation as the collision energy used is only 5eV more than that used for RKEVY which is 184 m/z less. The fragments of greatest abundance are the b_6+H_2O followed closely by the b_3 and a_4 ions. These fragments are of greater abundance than the immonium ions. With the exception of the y_2-NH_3 ion no other y_n series ions were identified in the SID fragmentation of methionine enkaphalin Arg-Phe.

The CID fragmentation spectrum in Figure 41 is also dominated by complete b_n series fragment. The fragments of greatest abundance are the b_6+H_2O followed closely by the b_3 and a_4 ions. The b_3 and a_4 fragment ions are not of greater abundance than the arginine immonium ions. The immonium fragment ion abundance pattern is very similar to that of the SID fragmentation pattern. Due to the excellent signal to noise of the ABI 4700 a near complete y_n series ions was identified in the CID fragmentation of methionine enkaphalin arg-phe.

The PD fragmentation spectrum in figure 42 is dominated by complete a_n and b_n series fragment ions with the most intense signals observed being from immonium ions. The a_n, b_n, and y_n fragments are of much lower abundance when compared to the CID and SID spectra

and also the immonium ions present in the PD spectra. Of much greater abundance are the v_7 and v_4 ions. These v_n ions are not present in the SID and CID spectra.

Figures 43, 44, and 45 contain respectively the SID, CID, and photodissociation fragmentation spectra for angiotensin III (RVYIHPF, 932 m/z.) The SID fragmentation spectrum in Figure 43 is composed of complete a_n and b_n series fragment ions with a predominate loss of NH_3 being observed and dominated by smaller m/z a_n series fragment ions. This is not as expected as the same collision energy is used for the angiotensin III peptide as the lower m/z RKEVY peptide (54 m/z less), and is not the fragmentation pattern that is observed in the CID or PD spectra. The fragments of greatest abundance are the a_2-NH_3 followed closely by the b_3-NH_3 and b_2-NH_3 ions. These fragments are of greater abundance than the immonium ions with the exception of the histidine immonium ion. With the exception of the y_2 ion no other y_n series ions were identified in the SID fragmentation of angiotensin III.

The CID fragmentation spectrum in Figure 44 is composed of complete a_n and b_n series fragment ions with a predominate loss of NH_3 being observed. The fragments of greatest abundance are the

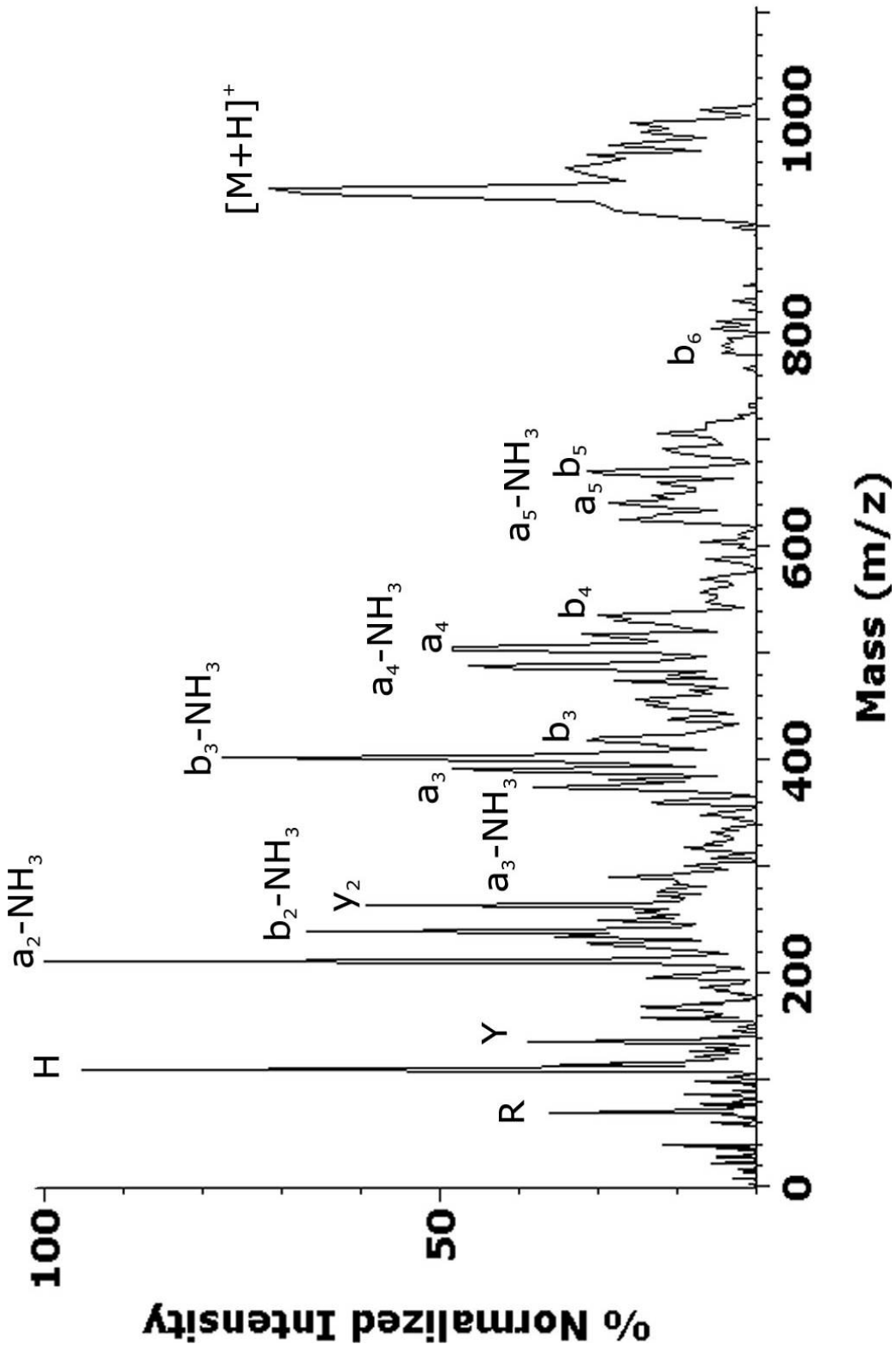

Figure 43: SID ion spectrum of angiotensin III (RVYIHPF, 932 m/z), 50 eV SID, acquired with a in-house built MALDI-IM-SID-TOFMS.

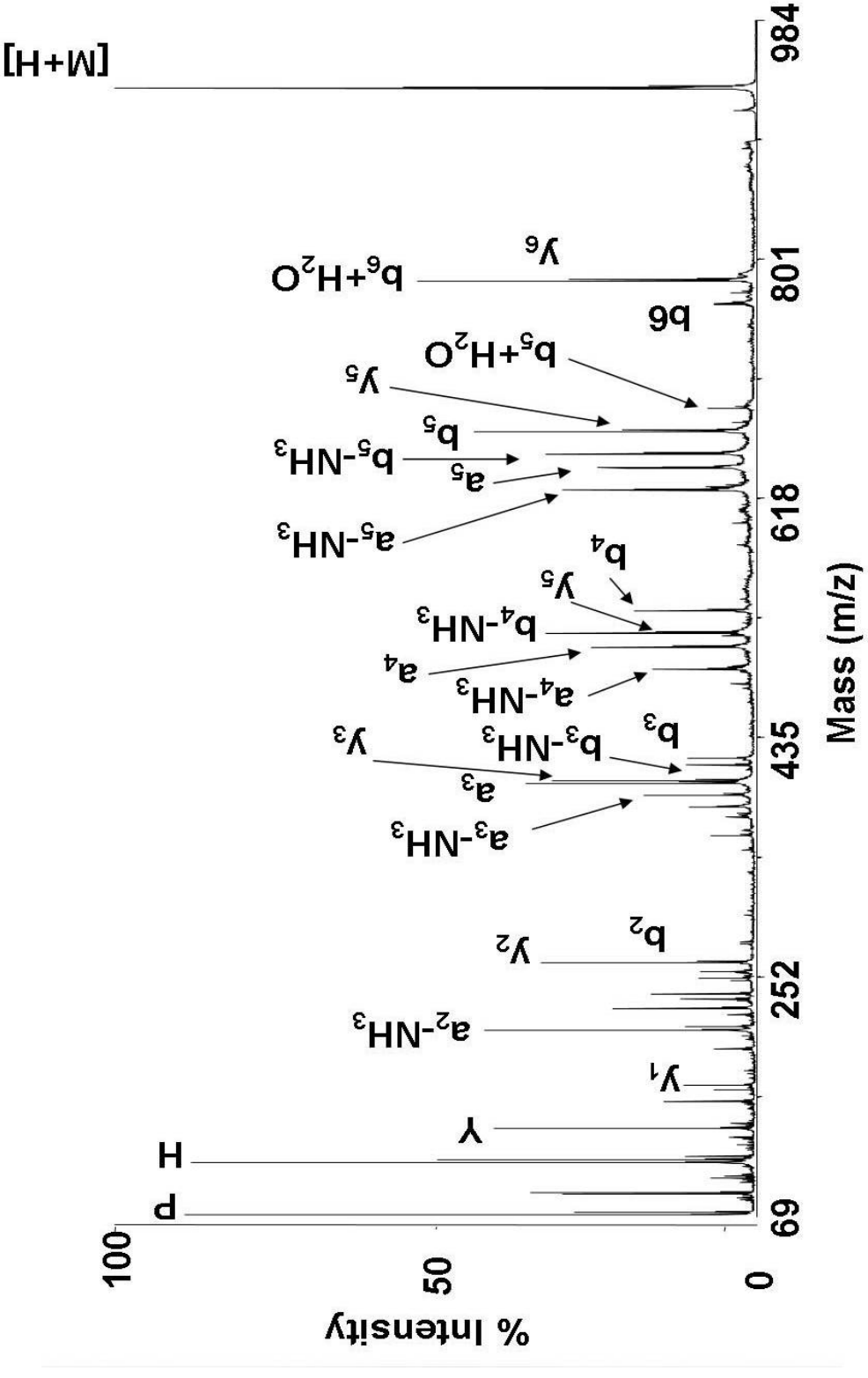

Figure 44: CID ion spectrum of angiotensin III (RVYIHPF, 932 m/z) acquired on an ABI 4700 TOF-TOF.

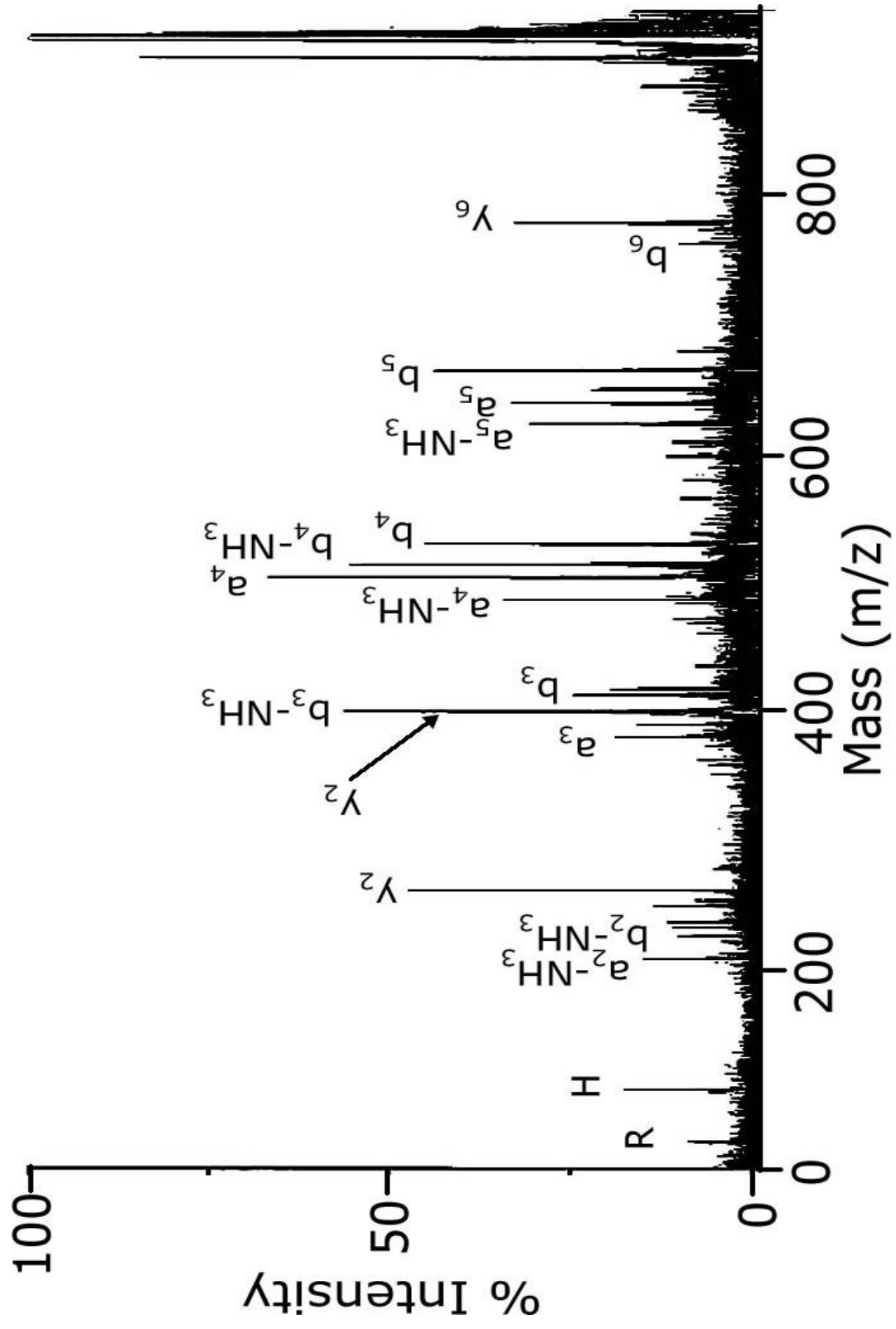

Figure 45: Photodissociation ion spectrum of angiotensin III (RVYIHPF, 932 m/z) acquired on an in-house built MALDI- Reflectron TOFMS.

immonium ions followed by b_6+H_2O and a_2-NH_3 ions. The immonium fragment ion abundance pattern is very similar to that of the SID fragmentation pattern. Again due to the excellent signal to noise of the ABI 4700 side-chain cleavages leading to da_2 and da_4 ions were identified in the CID fragmentation of angiotensin III. A more complete y_n ion series was identified in the SID fragmentation of angiotensin III dominated by the y_2, y_3, and y_6 ions

The PD fragmentation spectrum in Figure 45 is composed of complete a_n and b_n series fragment ions with a predominate loss of NH_3 being observed. The immonium ions present in the PD spectra are of much lower abundance when compared to the CID and SID. The typical appearance of ions resulting from side-chain cleavages were not identified in this spectrum. The fragment ion abundances with the exception of the much lower immonium ions were most similar to the CID spectra. The fragmentation pattern for angiotensin II (not included) follows the trends previously observed for PD induced fragmentation. This indicates that the excitation laser was lower in intensity for this particular peptide.

Tryptic Digest Model Peptide

Figures 46, 47, and 48 contain respectively the SID, CID, and photodissociation ion fragmentation spectra acquired for

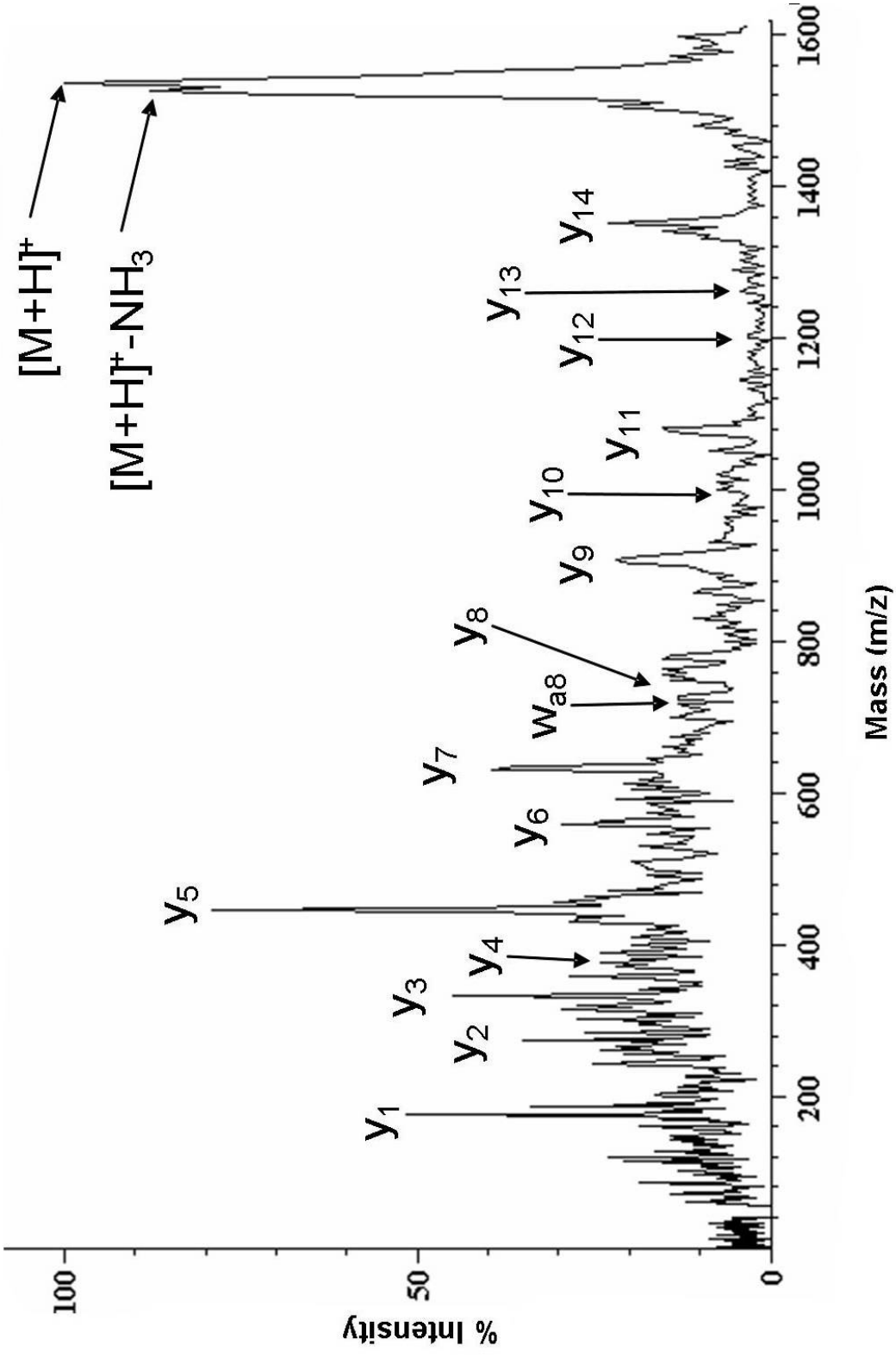

Figure 46: MALDI-IM-SID-TOFMS spectrum of fibrinopeptide A (ADSGEGDFLAEGGGVR, 1537 m/z), 95 eV SID.

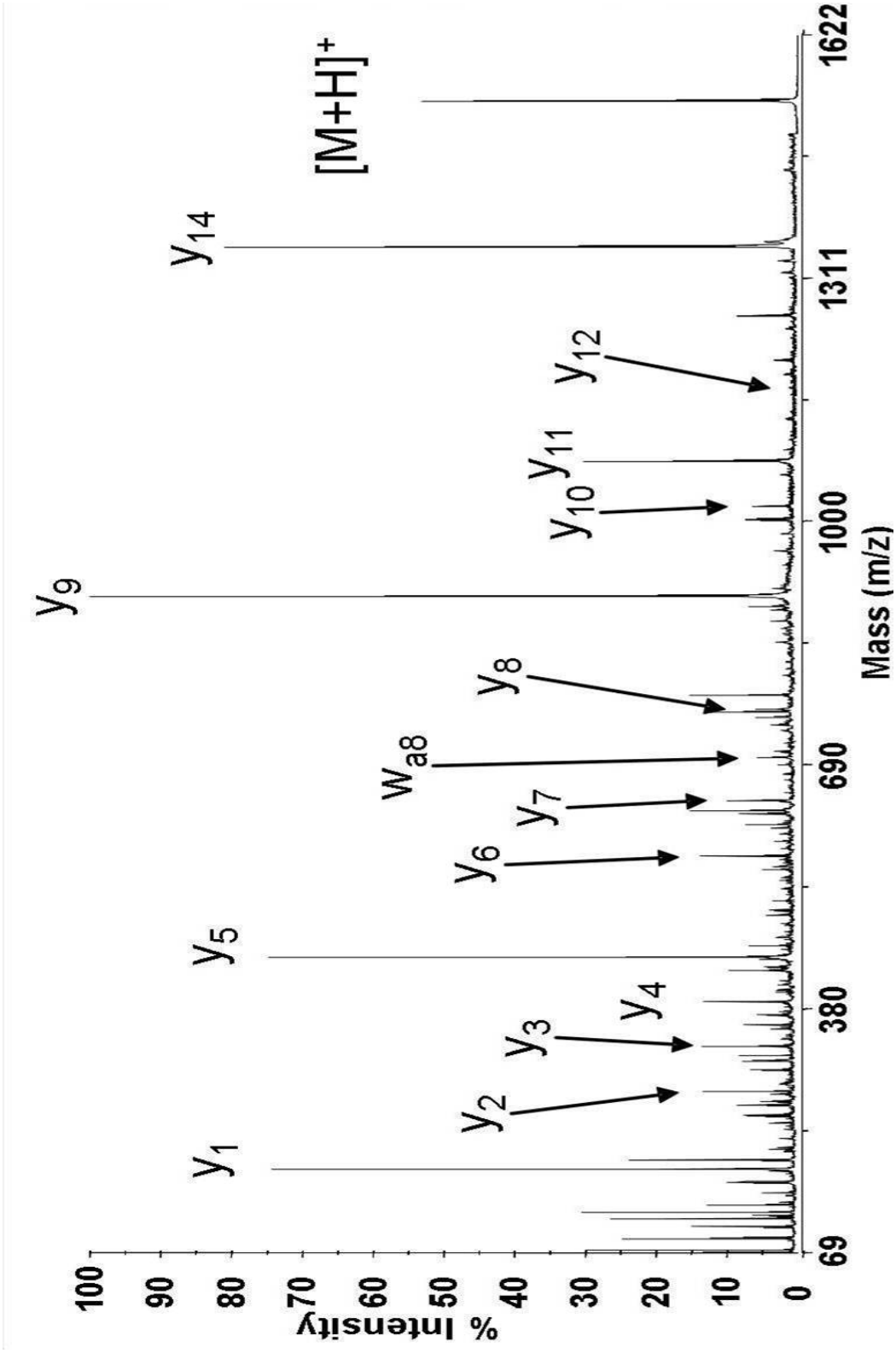

Figure 47: CID spectrum of fibrinopeptide A (ADSGEGDFLAEGGGVR, 1537 m/z) acquired on an ABI 4700 TOF-TOF.

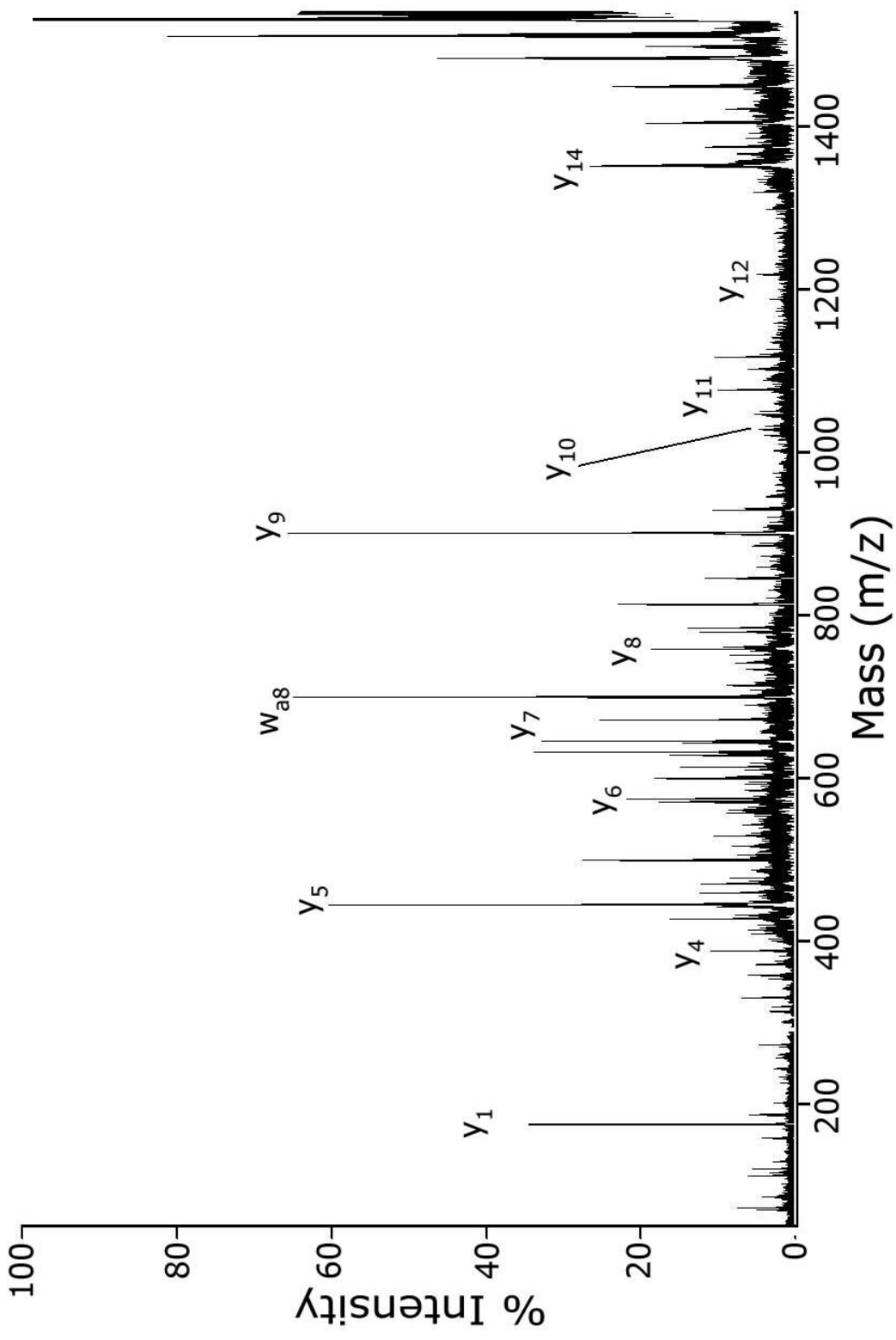

Figure 48: Photodissociation spectrum of fibrinopeptide A (ADSGEGDFLAEGGGVR, 1537 m/z) acquired on an in-house built MALDI- Reflectron TOFMS.

fibrinopeptide A (ADSGEGDFLAEGGGVR, 1537 m/z.) The SID fragmentation spectrum, for 95 eV SID, in Figure 46 is dominated by the almost complete y_n series of ions (only the y_{15} was not identified) as is expected for a C-terminal arginine peptide similar to those formed by tryptic digestion. Internal fragment ions as well as the usual loss of small neutrals for a_n and b_n ions are also observed but of lesser abundance and as such are not labeled in Figure 46 to avoid congestion. Immonium ions at this collision energy are not of significant abundance. Of note is the presence of the w_{a8} ion. This ion which is the result of a side-chain cleavage that is possible using SID permits the identification of the amino acid as leucine rather than isoleucine. The only ambiguity that would remain for determination of the complete peptide sequence would be whether or not the N terminus sequence was AD or DA. The lack of a b_1 or y_{15} ion prevents this determination from being made.

The CID fragmentation spectrum in Figure 47 is also dominated by the almost complete y_n series of ions. The y_9 and y_{14} are of greater abundance than in the SID spectrum, but otherwise the information content is the same. The immonium ion intensity is also very similar to that of the SID spectrum. The side-chain cleavage ion w_{a8} is also observed, but as stated before the lack of a b1 ion or the

y_{15} ion does not allow complete unambiguous sequence identification.

The PD fragmentation spectrum in Figure 48 is also dominated by a near complete y_n series of ions. The w_{a8} ion is of much greater intensity. This is typical for photodissociation experiments. The fragmentation abundances with the exception of the side-chain cleavage products were most similar to that of the SID experiment.

A Special Case – Gramicidin S

The interest in gramicidin S by the pharmaceutical industry as an antibiotic, an immunosuppressant,[132] and a cardiodepressant[133] has elicited greater interest in the biosynthesis of gramicidin S. A particular problem in the biosynthesis of gramicidin S is that five linear analogs as well as the cyclic peptide can be and are produced. Determining the production ratios of these six variants is not an easy analytical task. The application of MALDI-IM-TOFMS to the problem met with some limited success. Encouraged by the results MALDI-IM-SID-TOFMS was applied to the problem with the expectation that the resulting SID fragmentation correlated with the parent ion would make identification both possible and quick.

Figures 49 through 54 contain the SID ion spectra for gramicidin S and five linear analogs that can be made by moving the C-terminal amino acid residue to the N-terminus serially. For each spectrum the

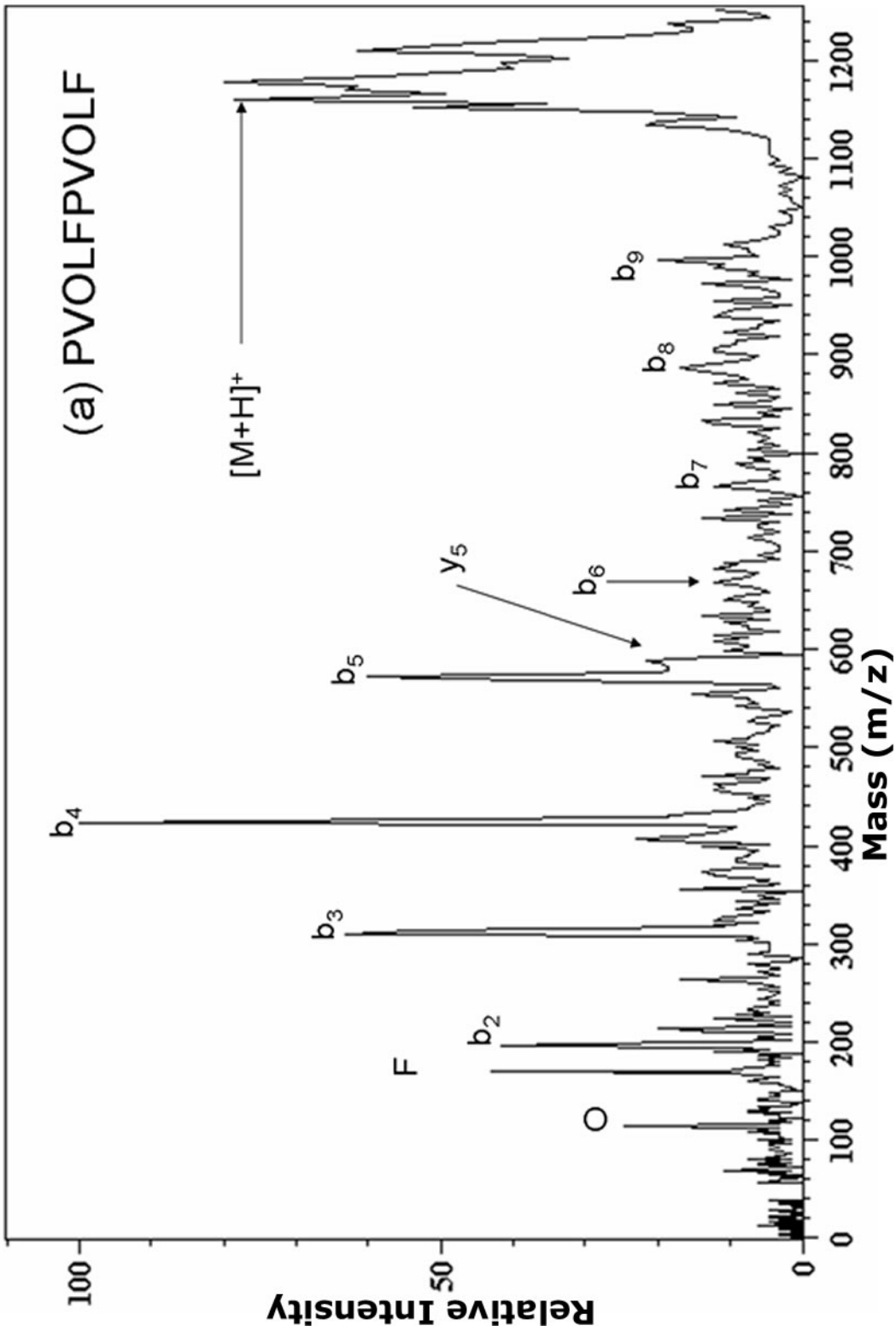

Figure 49: The SID fragment ion spectra for the gramicidin S linear analog PVOLFPVOLF (m/z 1060.)

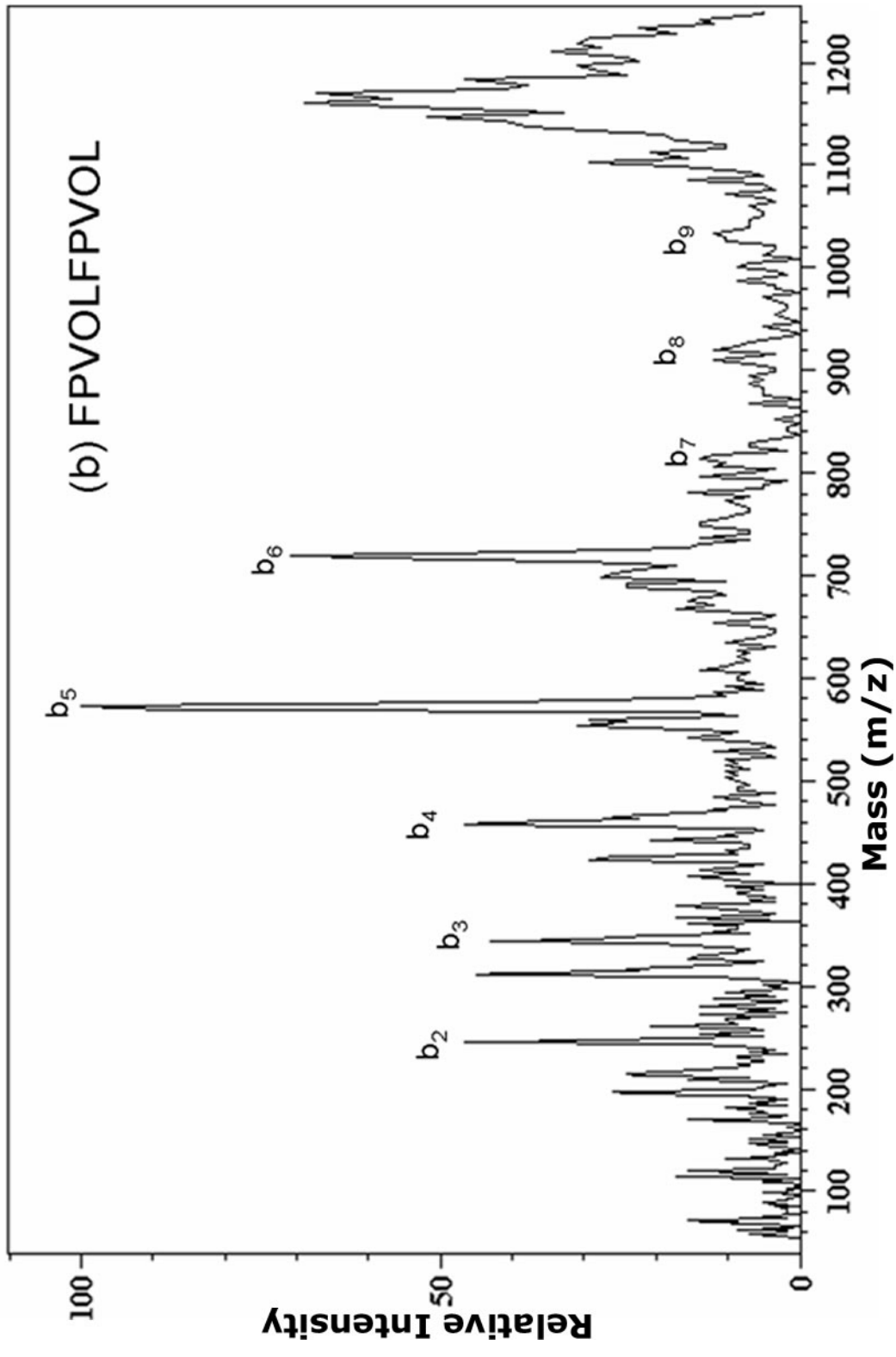

Figure 50: The SID fragment ion spectra for the gramicidin S linear analog FPVOLFPVOL (m/z 1060.)

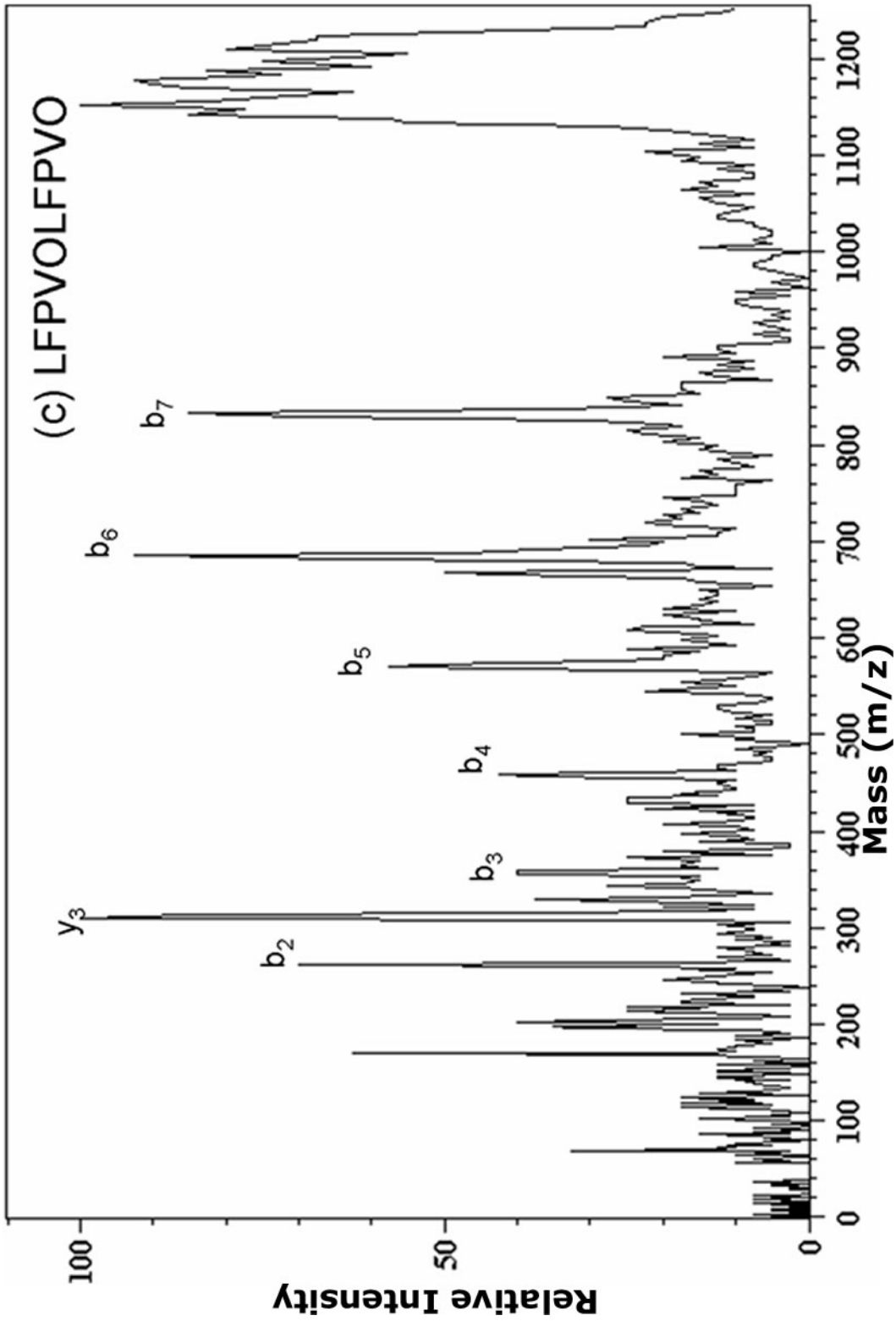

Figure 51: The SID fragment ion spectra for the gramicidin S linear analog LFPVOLFPVO (m/z 1060.)

SID collision energy was 65 eV. The spectrum contained in Figure 49 is of the linear analog amino acid sequence PVOLFPVOLF. A complete b_n ion series is observed and is the dominate SID ion series. Unlabeled peaks in the spectra correspond to lesser abundant internal fragment ions, the y_n fragment ions, and a_n series ions. The proline "proline effect" (the observed dominance of dissociation pathways due to the cleavage of the amide bond to proline attributed to the lower dissociation energies for peptide bonds near proline residues) is observed with the dominate SID fragment ions in the spectra being b_5, b_4, b_3, and b_2. The spectrum contained in Figure 50 is an SID fragment ion spectrum of the linear analog FPVOLFPVOL. A complete b_n ion series is observed and is the dominate SID ion series. Unlabeled peaks in the spectra correspond to lesser abundant internal fragment ions, the y_n fragment ions, and a_n series ions. The "proline effect" is observed with the dominate SID fragment ions in the spectra being b_6, b_5, b_4, b_3, and b_2. As the proline was moved one position further from the C-terminus the intense component of the b_n series of fragment ions increased by one. As the N-terminus is still the more basic than any residue at the C-terminus y_n ions are of low abundance. The spectrum contained in Figure 51 is the spectrum for the linear analog LFPVOLFPVO and continues with the observed trend

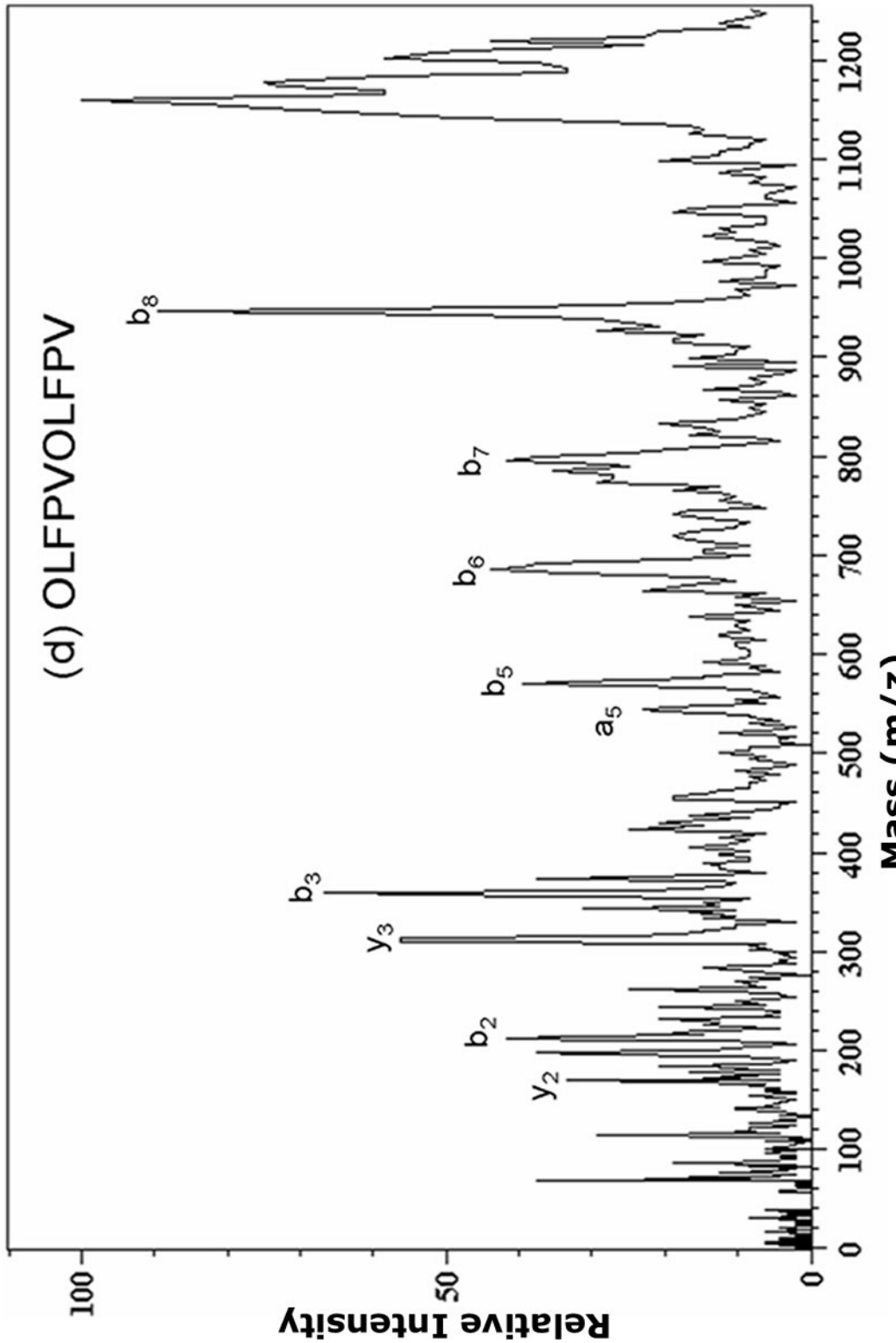

Figure 52: The SID fragment ion spectra for the gramicidin S linear analog OLFPVOLFPV (m/z 1060.)

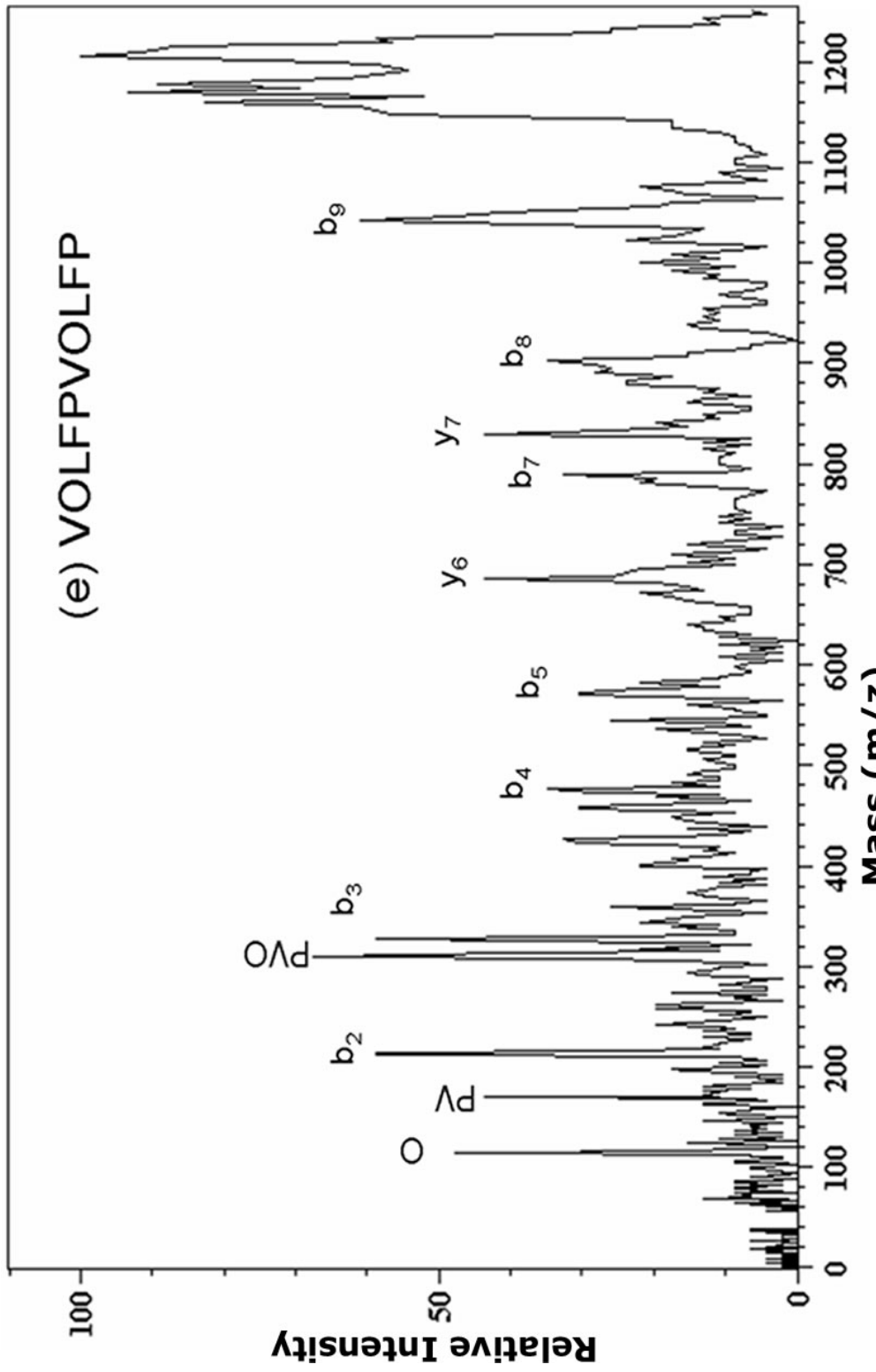

Figure 53: The SID fragment ion spectra for the gramicidin S linear analog VOLFPVOLFP (m/z 1060.)

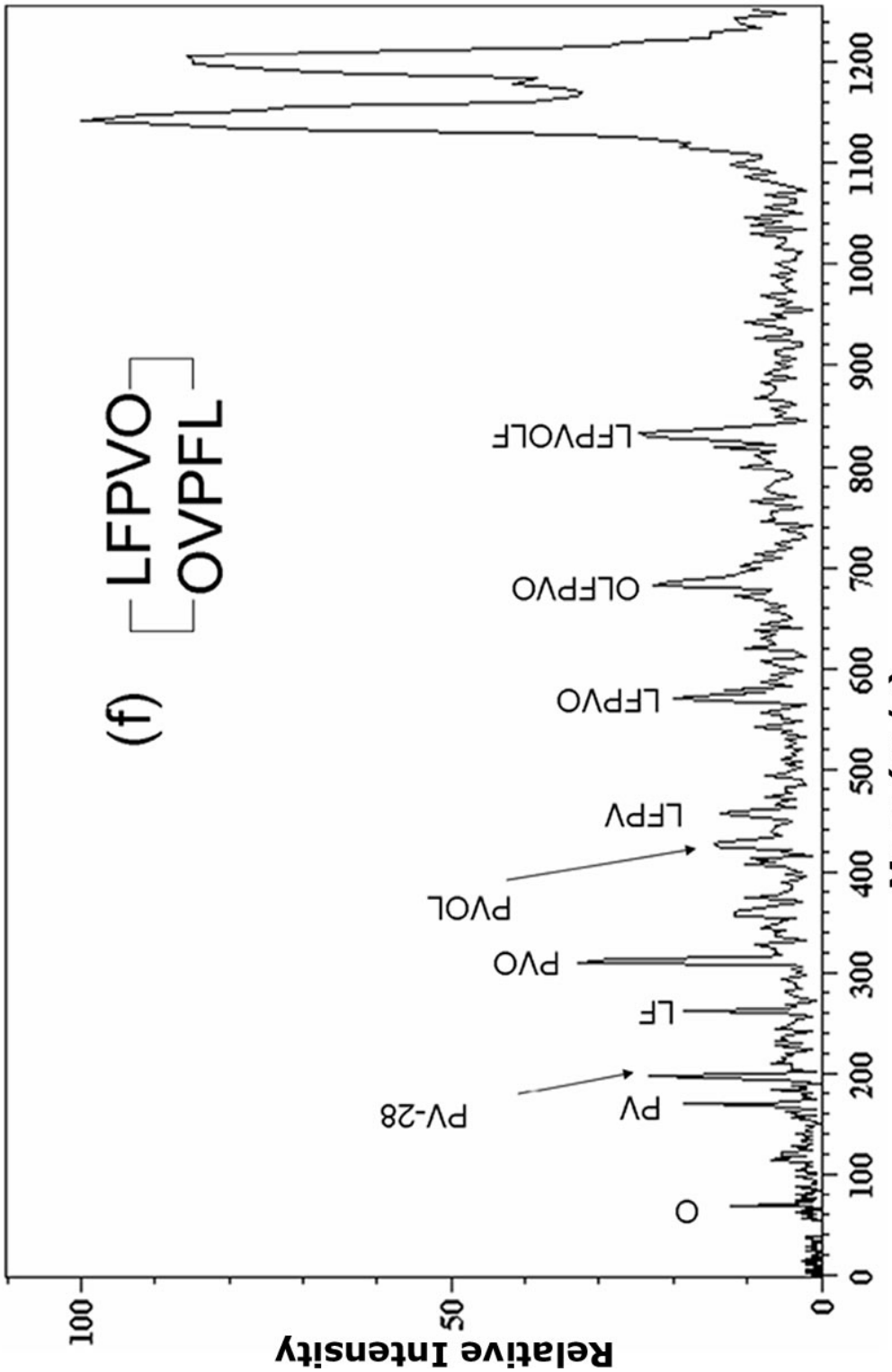

Figure 54: The SID fragment ion spectra for gramicidin S LFPVO-cyclo (m/z 1048.)

in b_n ions. However a very abundant y_3 ion is observed. This is due to the fact that the C-terminal residue is now basic enough to compete with the N-terminus for charge retention and with the help of the proline at that position becomes a favorable bond for cleavage. The spectrum contained in Figure 52 is the SID fragmentation spectrum for the linear analog OLFPVOLFPV which continues the observed trend for b_n ions but has an additional y_2 ion which is favored by the location of the second proline. Also seen is that the steady increase from low mass b_n ions to high mass b_n ions is not as constant as in the previous linear analogs. Now the charge retention though favored by the N-terminus finds that the two prolines are now very likely to direct the fragmentation that is observed rather than leaving the fragmentation to the proline closest to the C-terminus. This result suggests a series of experiments to be performed at a lower collision energy with the same linear analog series. The expected result would be that the steady increase would return. It is likely that at 65 eV SID that there is sufficient translational energy converted to internal energy for the ion that the observed fragmentation is not the result of a single unimolecular dissociation event but two on the timescale of the reaction. The spectrum contained in Figure 53 is the SID fragmentation spectrum of the linear

analog VOLFPVOLFP. In addition to a near complete b_n SID fragment ion series the y_6 and y_7 SID fragment ions are also observed. This suggests that the basicity of the FP amino acid series competes favorably with the N-terminus to direct the fragmentation.

The spectrum contained in Figure 54 is the SID fragment ion spectra observed for cyclic gramicidin S, LFPVO-cyclo. All SID fragment ions observed are internal fragments. This is as expected as there is no N- or C-terminus. The other major difference between the spectrum for the cyclic gramicidin S and its linear analogs is the ratio of the SID fragment ions and the surviving $[M+H]^+$ parent. The lower SID fragment ion intensities for the cyclic gramicidin S can be easily accounted for by taking into account the amount of energy need for ring opening before the resulting SID fragment ions can be formed. However, it can be seen that once ring opened, as is the case with the linear analogs, the prolines direct the SID fragment ions that are observed. The most likely site of ring opening then can be determined by comparing relative b_n and y_n appearances and intensities it is seen that the SID fragmentation patterns for the linear analogs. It is relatively easy to see that the fragmentation pattern for the linear analog in Figure 51, LFPVOLFPVO. From this result a case

can be made for the ring opening to occur at the ornithines, the most basic amino acid residue in the peptide.

Also of note for these six peptides is the continued low abundance of immonium ions observed for the other peptides in this study. The low abundance of immonium ions is not typical for other groups working with SID. However, as the collision energy is increased with the MALDI-IM-SID-TOFMS instrument the parent is further depleted, SID fragment ion intensities do increase with onset of the appearance of immonium ions and a depletion of higher mass SID fragment ions until only the immonium ion for proline is observed. This is the pattern that is observed by other groups. The difference can be attributed to the instrument geometry and the use of the drift cell. That is the ions are thermalized as they transit through the drift cell. Additionally the current instrument geometry allows for only a very short transit time, less than 2 μsec for an ion of m/z greater than 1000, from the F-SAM surface to the extraction region of the mass analyzer. Laskin et al showed that at such short reaction times for unimolecular decay to occur that higher SID collision energies are required. This observation is in good agreement with our results as we typical use higher collision energies. There is a side benefit that is not obvious in that Laskin has shown that at these

higher collision energies the internal energies of the activated ions possess a thermal distribution. This may be the reason for the very high reproducibility of SID fragment ion spectra observed.

The reproducibility of the SID fragmentation spectra obtained employing MALDI-IM-SID-TOFMS provides quick results with a high confidence in the ability to differentiate between gramicidin S and its five linear analogs. All five linear analogs produced strikingly different SID fragmentation fingerprints. As the SID fragment ion intensities for gramicidin S were lower (and the parent ion intensity higher) at the same collision energy than those for the linear it is clear that some of the translational energy converted to the peptide's internal energy is used to ring open gramicidin S. After ring opening further fragmentation follows the "proline effect:" observed for the linear analogs. Comparison of the SID fragmentation patterns for the linear analogs to gramicidin S suggests that the ring opening most likely occurs at the ornithines residue. Further improvements in the resolving power of the periodic focusing drift cell will enable MALDI-IM-SID-TOFMS to quickly differentiate between the possible products of the biosynthesis of gramicidin S.

CHAPTER VII

TRYPTIC DIGEST OF HEMOGLOBIN, A TALE OF TWO INSTRUMENTS

A tryptic digest of hemoglobin was run on a MALDI-IM-SID-TOFMS and an ABI 4700 TOF-TOF with high repetition rate micro crystal lasers. In both cases the operating conditions of the instruments were adjusted to optimize the SID or CID fragment ions observed. The high rep rate laser on the ABI 4700 TOF-TOF was operated at 200 Hz. An identical micro-crystal laser was used on the MALDI-IM-SID-TOF instrument but operated at 400 Hz. Total acquisition time for the ABI-4700 TOF-TOF was 15 minutes. This time is longer than average as two peptides in the PMM are very close in mass and required significant tweaking to observe separate CID spectra for residues 104-115 β–subunit (m/z 1266.6) and 30-39 β-subunit (m/z 1275.5, see Figures 55 and 56.) The total acquisition time for the SID fragment ion spectra was less than one minute. The same digest and sample preparation was spotted at the same time on the sample plate for the ABI 4700 and the SID instrument. In order

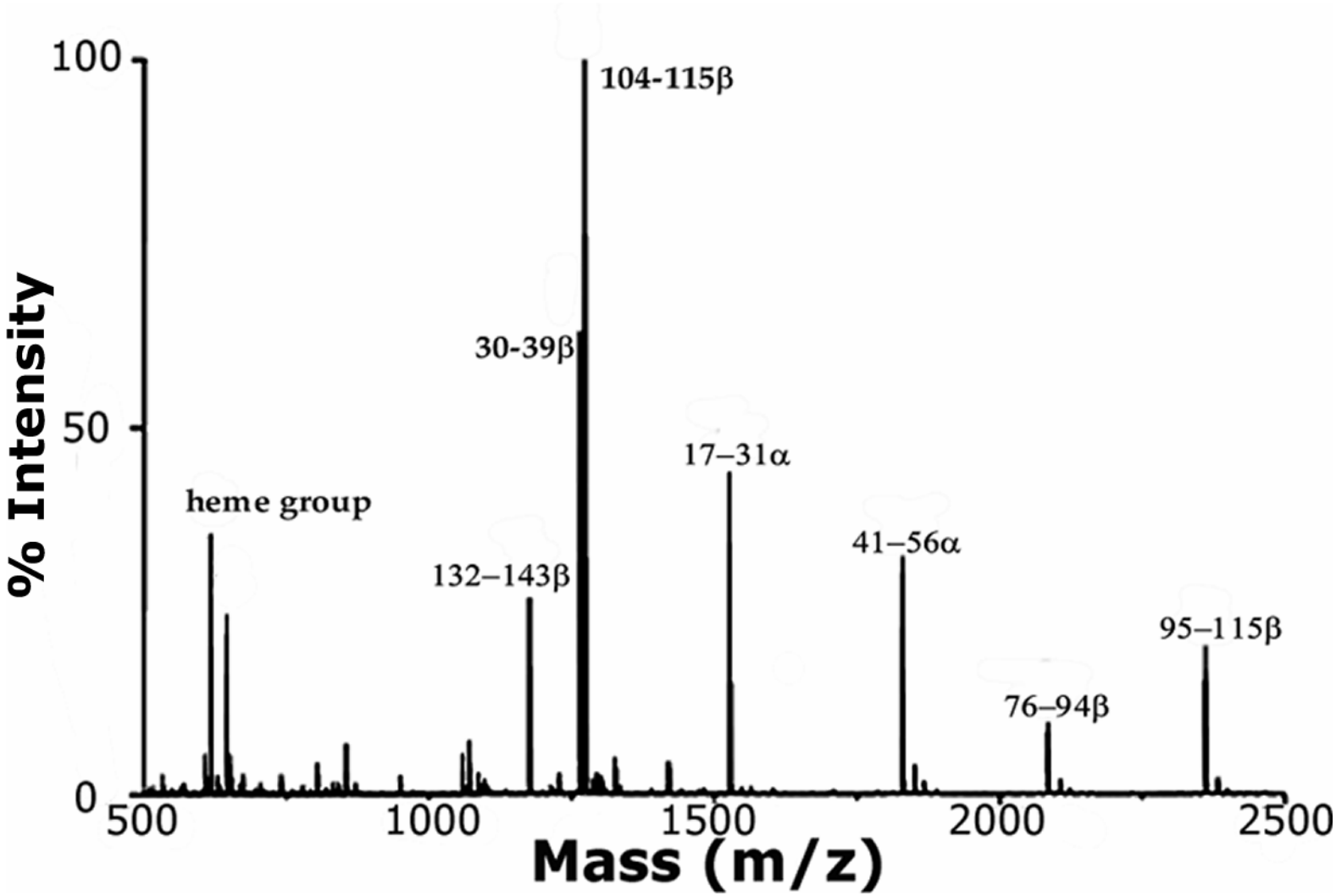

Figure 55: The PMM obtained with an ABI 4700 TOF-TOF containing seven tryptic peptides and the heme group.

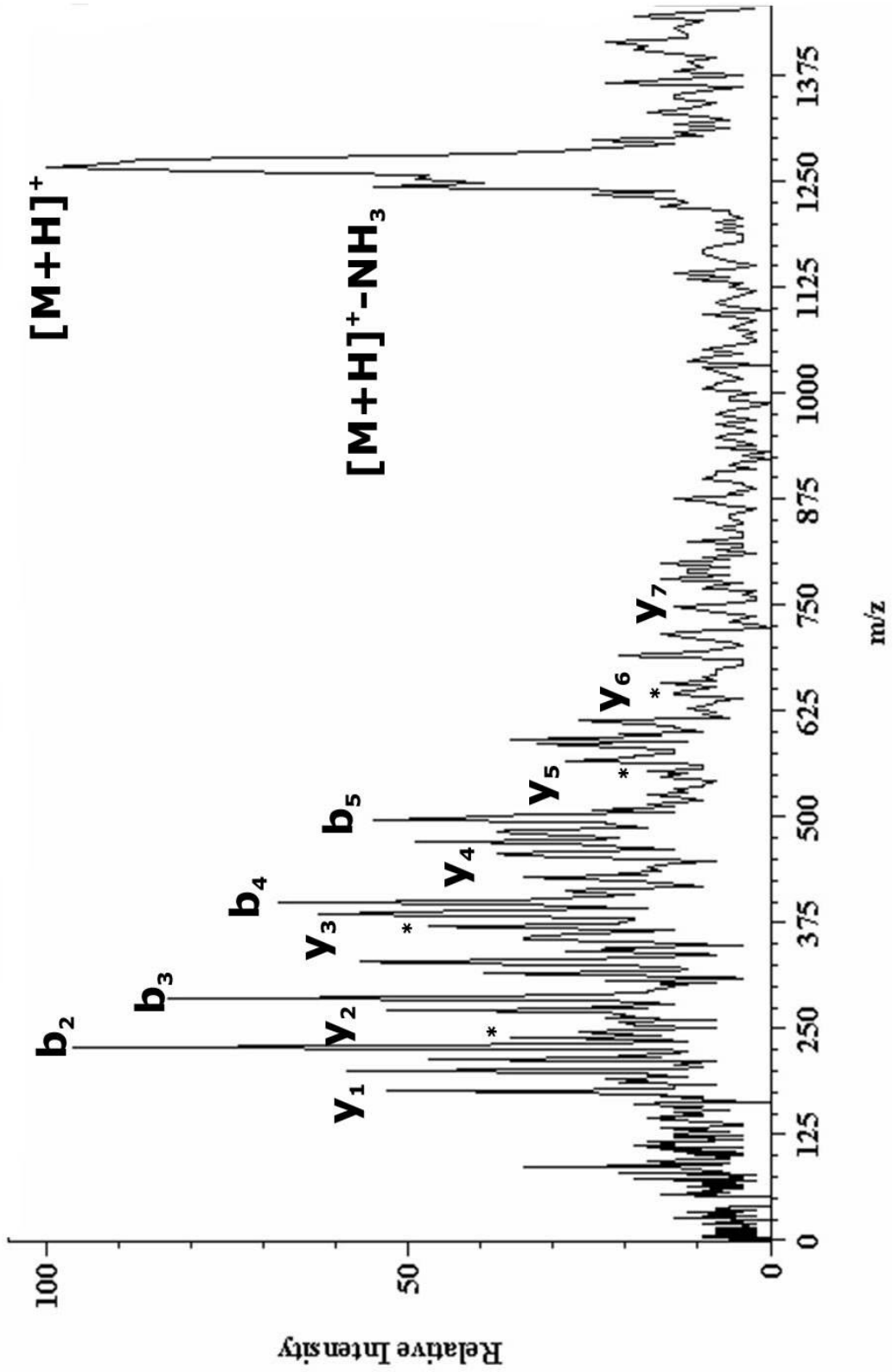

Figure 56: Integrated SID ion mass spectra of residues 104-115 β-subunit, amino acid sequence LLGNVLVVVLAR, for the drift time range from 1125 to 1150 μsec.

to decrease the signal intensity of the heme group the settled digest was not agitated to mix the separated layers, a layer that was more red (higher heme containing fraction) had settled to the bottom. Only the supernatant was used in these experiments.

Figure 55 is the 2D mass-mobility plot for the tryptic digest of hemoglobin. The heme group and eight peptides are observed in the PMM, residues 30-39 β-subunit, 104-115 β-subunit, 17-31 α-subunit, 41-56 α-subunit, 76-94 α-subunit, 95-115 β-subunit, and 41-65 α-subunit, and SID fragment ions are observed for the heme group, residues 30-39 β-subunit, 104-115 β-subunit, -31 α-subunit, and 41-56 α-subunit. Once an updated version of the instrument currently under construction is equipped with the capability to ramp the SID collision energy SID fragments will obtained for all peptides in the PMM.

Figure 56 contains the PMM obtained using the ABI 4700 TOF-TOF. The heme group and seven peptides are observed in the PMM, residues 132-143 β-subunit, 30-39 β-subunit, 104-115 β-subunit, 17-31 α-subunit, 41-56 α-subunit, 76-94 α-subunit, and 95-115 β-subunit with no CID fragment ions identified. Each of these peptides were individually selected and interrogated to obtain sequence

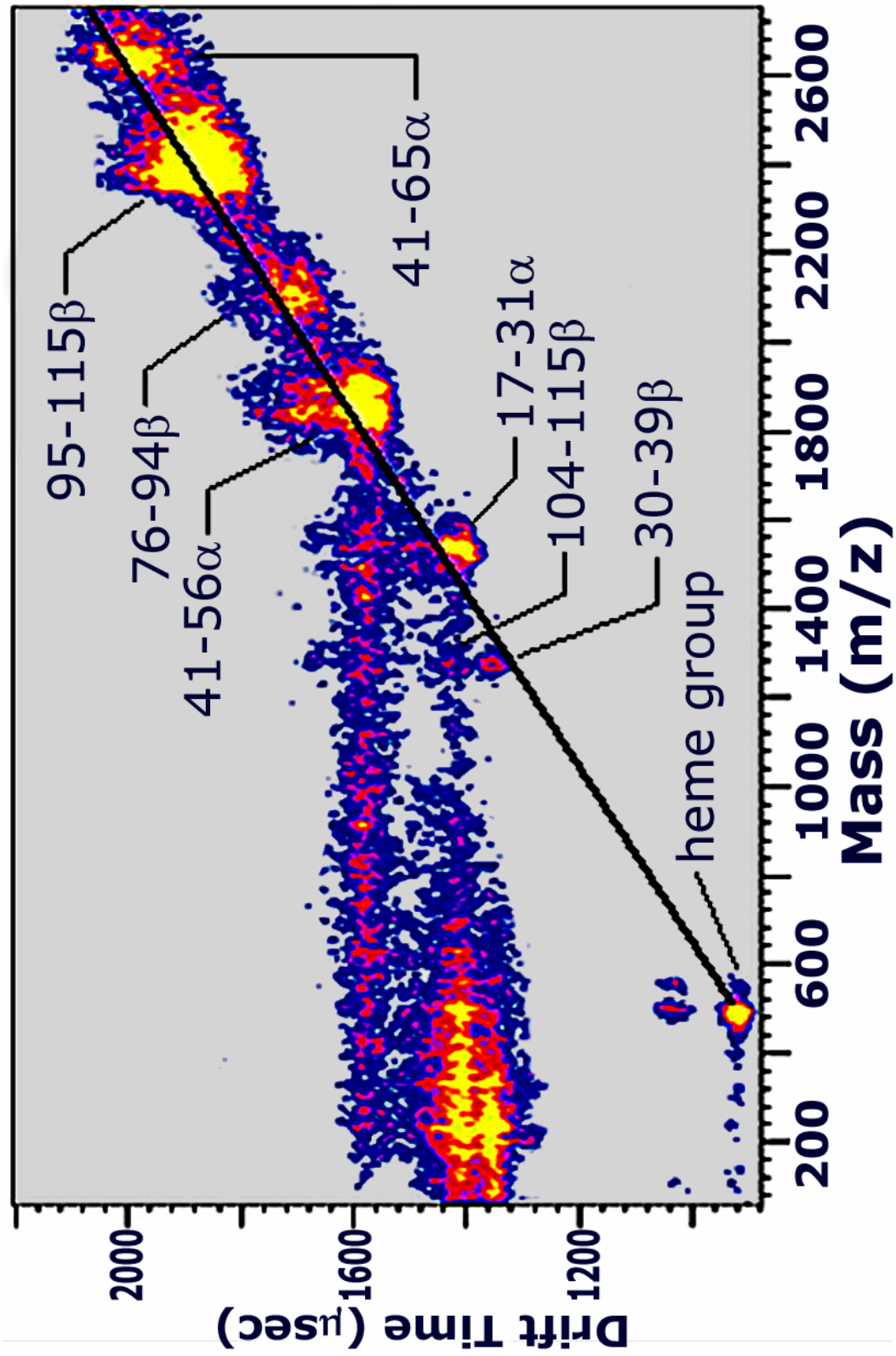

Figure 57: A 2D plot of the PMM and partial sequence information for three of the seven tryptic peptides and heme group assigned observed in the PMM.

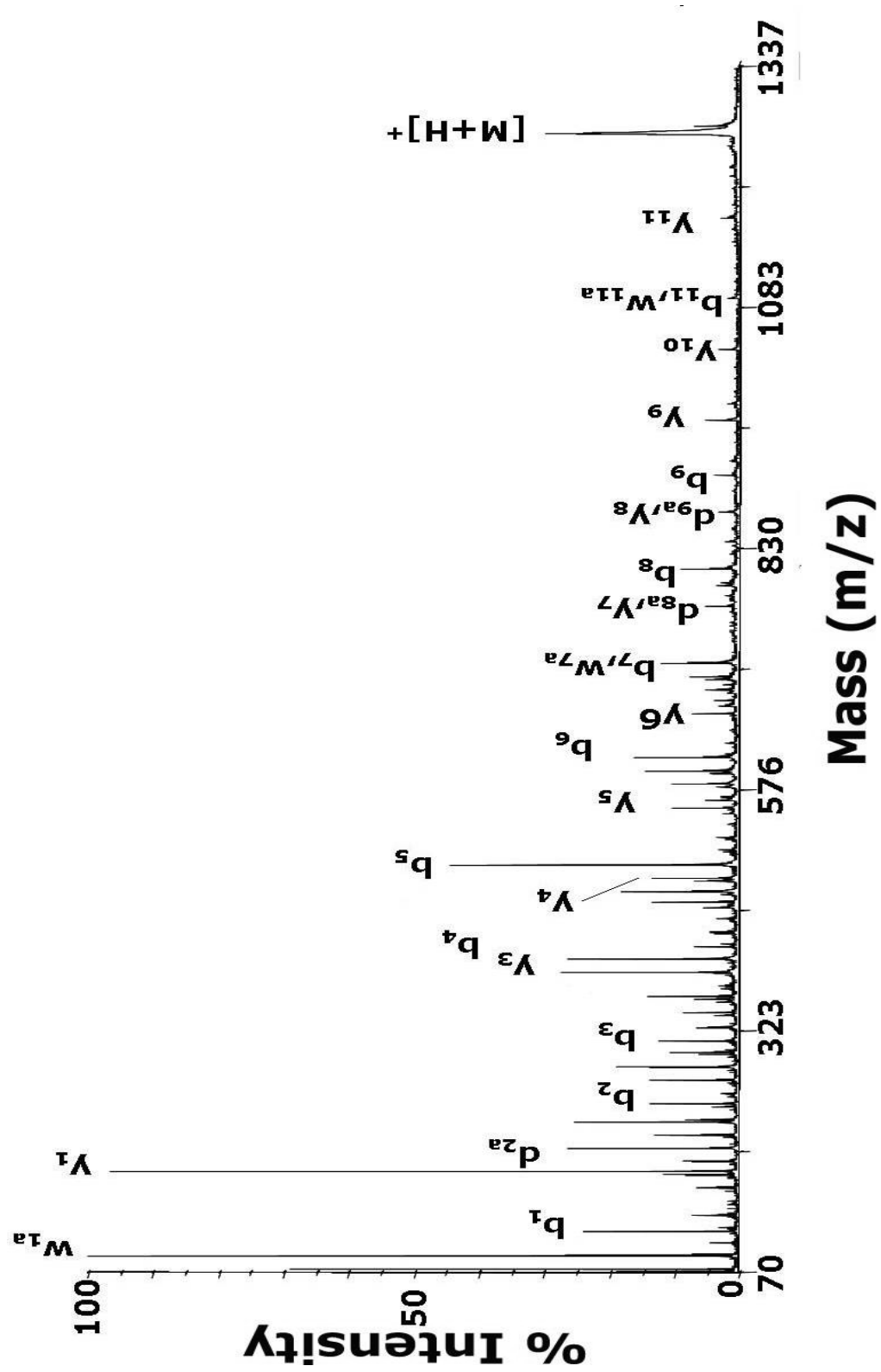

Figure 58: CID ion mass spectra of residues 104-115 β-subunit, amino acid sequence LLGNVLVVVLAR, obtained with an ABI 4700 TOF-TOF.

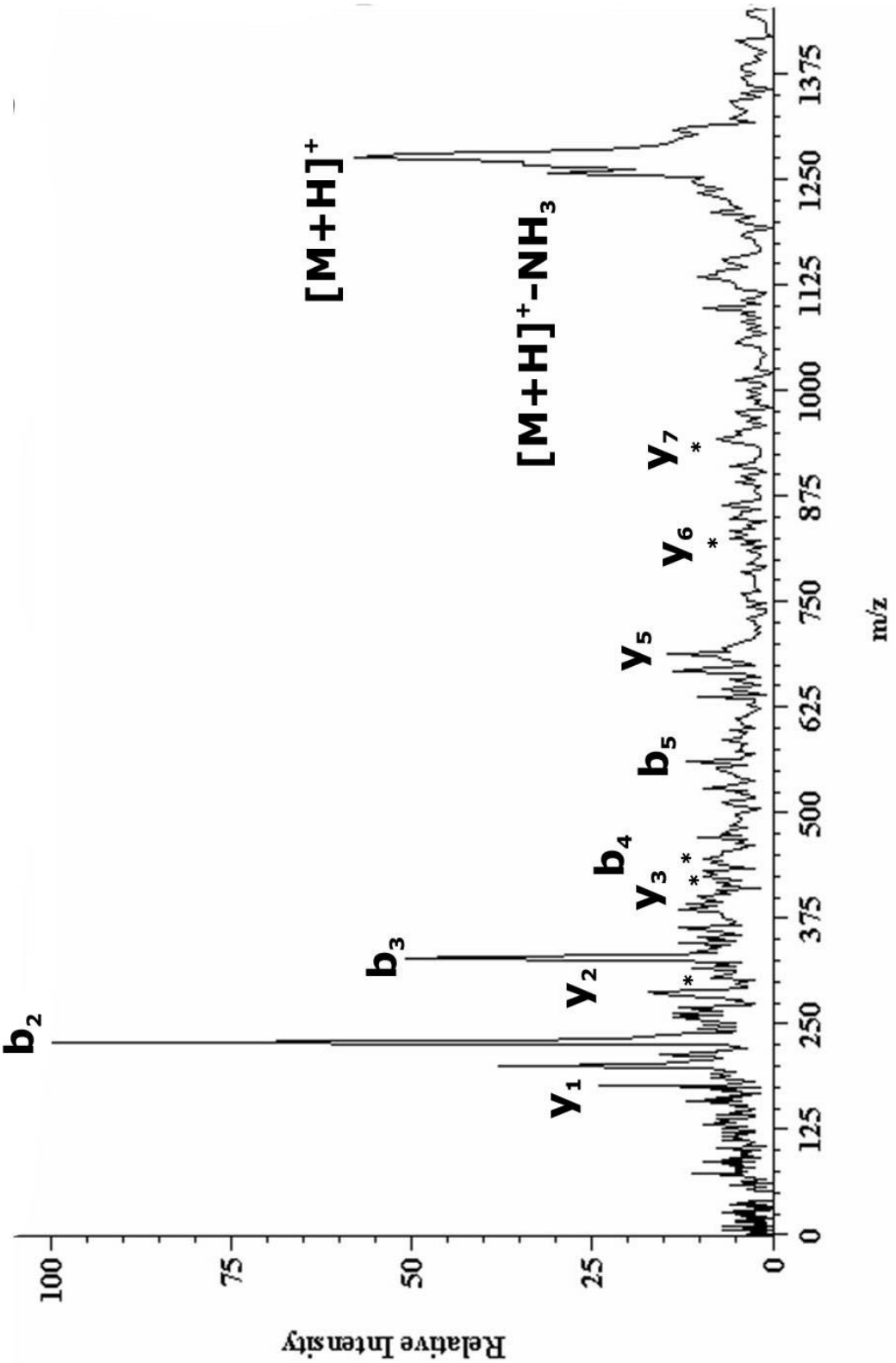

Figure 59: Integrated SID ion mass spectra of residues 30-39 β-subunit, amino acid sequence LLVVYPWTQR, for the drift time range from 1125 to 1150 μsec.

information by CID fragmentation. The 41-56 α-subunit observed in the IM-MS 2D plot was not observed as the mass range for the TOF-TOF was not extended to include it. The 132-143 β-subunit tryptic peptide may have been present in the IM-MS plot but as only a single SID fragment and no conclusive assignment was made.

Figure 57 contains the integrated mass spectra of residues 104-115 β-subunit for the drift time range from 1125 to 1150 μsec. SID fragments identified are b_2 through b_5 and y_1 through y_7. This sequence information is sufficient to identify the entire sequence with the exception of the differentiation of between leucine and isoleucine. The S/N achievable with the 30 cm linear TOF was not high enough to make any unambiguous identification of any side-chain cleavages necessary to identify these amino acids as leucine. Figure 58 contains the CID spectrum residues 104-115 β-subunit for the drift time range from 1125 to 1150 μsec. The S/N is sufficient to add identify a complete y_n series of ions and side-chain cleavages to identify all but the leucine in the b_2 position can unequivocally be assigned as leucine, the remaining side-chain cleavages are either isomass with other CID fragment ions or are not observed. Even had the side-chain cleavage product ions been observed in the SID fragment ion spectra the information thus obtained would also have been

insufficient to make any unambiguous determination as to the complete sequence.

Figure 59 contains the integrated mass spectra of the tryptic peptide residues 30-39 β-subunit for the drift time range from 1125 to 1150 μsec. SID fragments identified are b_2 through b_5 and y_1 through y_7. This sequence information is also sufficient to identify the entire sequence with the exception of the differentiation of between leucine and isoleucine. The S/N achievable with the 30 cm linear TOF was not high enough to make any unambiguous identification of any side-chain cleavages necessary to identify these amino acids as leucine. Figure 60 contains the tryptic peptide residues 30-39 β-subunit obtained with the ABI 4700 TOF-TOF. The only useful side-chain cleavage was to determine an unequivocal sequence for the tryptic peptide is the d_{2a} which allows assignment of the second amino acid residue from the N-terminus to be leucine.

The information content of the MS/MS spectra was equivalent for the CID and SID experiments. The advantage of SID with respect to CID is the simultaneous acquisition of the PMM and partial sequence. The utility of the MALDI-IM-SID-TOFMS will be extended with better mass resolution, the ability to ramp the SID energy, and the addition of a multi-sample plate.

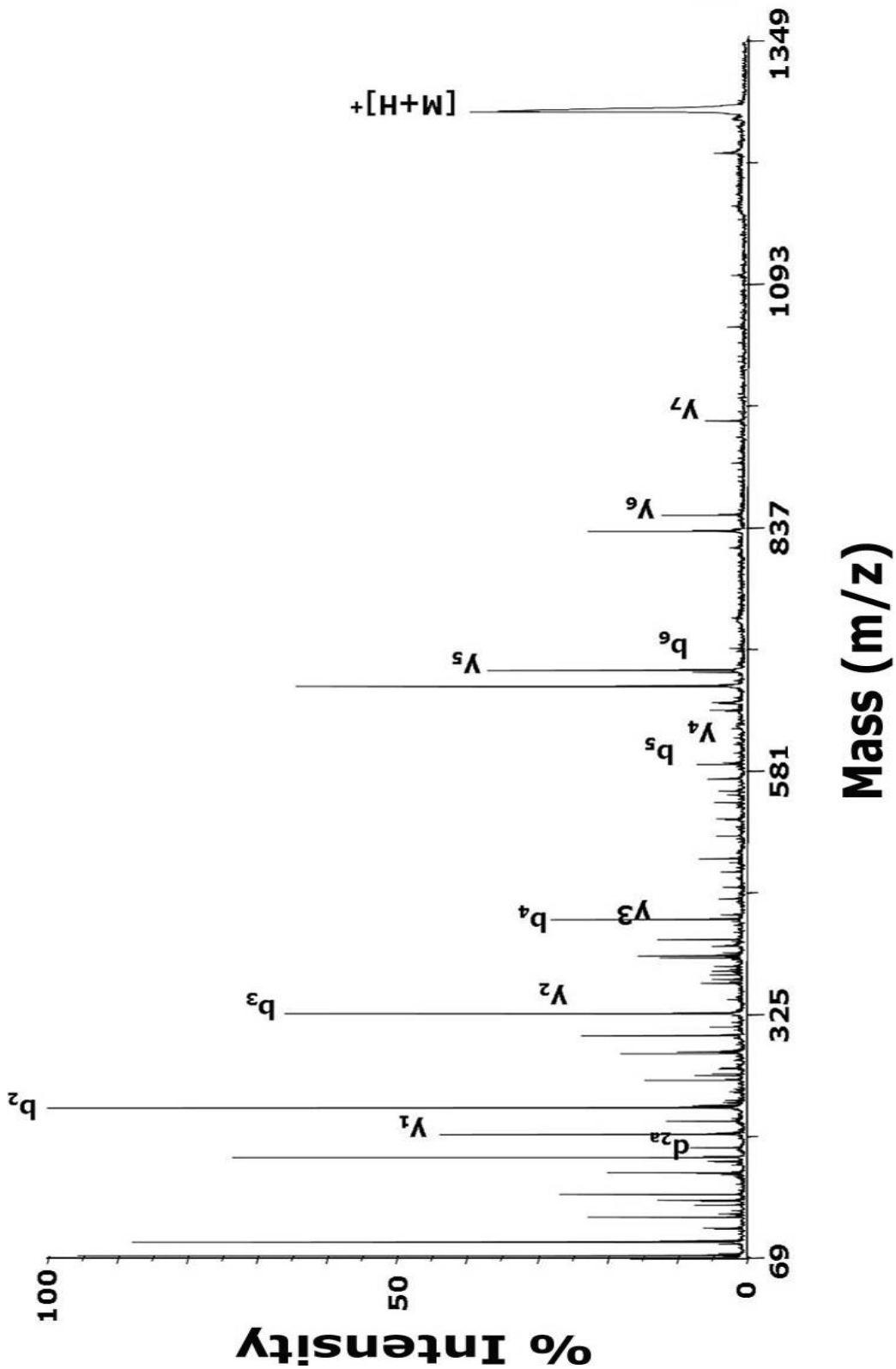

Figure 60: CID ion mass spectra of residues 30-39 β-subunit, amino acid sequence LLVVYPWTQR, obtained with an ABI 4700 TOF-TOF.

CHAPTER VIII

SUMMARY

One of the current challenges of bio-analytical chemistry is the analysis of exceedingly complex mixtures of biological macromolecules. Time-of-flight (TOF) mass spectrometry combined with MALDI has unique potential for such studies. Ion mobility spectrometry (IMS) combined with TOF-MS can be used for rapid, high-sensitivity analysis of proteins. This dissertation describes efforts to develop an advanced IM-TOF-MS instrument to carry out high throughput analysis of peptides and protein digests.

This dissertation also describes development of IM-TOF-MS for tandem MS using SID, for high throughput analysis of complex mixtures of biological samples. It has been demonstrated that IM—SID-TOF-MS provides rapid, high sensitivity (low femtomole) analysis of purified proteins and complex protein mixtures. When coupled with high repetition rate lasers the data acquisition is improved by an order of magnitude; hundreds of seconds using a 30 Hz nitrogen laser and tens of seconds using the kHz Nd:YAG laser. The IM-SID-TOF-MS apparatus is unique because the sample is ionized and the individual

analytes are separated on the basis of ion mobility. The separated analyte ions are then activated by SID and analyzed by TOF-MS. This instrument configuration possesses the same analytical advantages of GC- or LC-MS; however, separations using IM are very rapid, requiring 10 ms-10 ms, and the elution time can be correlated to the mass of the ion. Thus, IM-SID-TOF-MS can be used as a tandem mass spectrometer. The proposed IM-TOF-MS instrument represents a “paradigm shift” in protein identification methodology. The simultaneous acquisition of the peptide mass map and peptide sequence information for rapid, sensitive, high-throughput applications has been demonstrated.

REFERENCES

(1) M. Senda, T. Hiyama, T. Okuyama, *Chrom*., **19**, 19, (1998).

(2) A. Pandey, M. Mann, *Nature*, **405**, 837, (2000).

(3) J.R. Chapman (Ed.), *Methods Mol. Biol. Vol.* 146, Humana, Totowa (2000).

(4) M. Chalmers, S. Gaskell, *Curr. Opin. Biotechnol*., **11**, 384, (2000).

(5) R. Bakhtiar, F. Tse, *Mutagenesis*, **15**, 415, (2000).

(6) R. Bakhtiar, R. Nelson, *Biochem. Pharmacol*., **59**, 891, (2000).

(7) S. Beale, *Anal. Chem*., **70**, 279R, (1998).

(8) C. Larive, S. Lunte, M. Zhong, M. Perkins, G. Wilson, G. Gokulrangan, T. Williams, F. Afroz, C. Schoeneich, T. Derrick, C. Middaugh, S. Bogdanowich-Knipp, *Anal. Chem*. **71**, 389R, (1999).

(9) W. Niessen, A. Tinke, *J. Chromatogr. A* , **703**, 37, (1995).

(10) J. Slobodnik, B. van Baar, U. Brinkman, *J. Chromatogr. A*, **703**, 81, (1995).

(11) F. Regnier, G. Huang, *J. Chromatogr. A*, **750**, 3 , (1996).

(12) E. Gelpi, *J. Chromatogr. A* **703**, 59, (1995).

(13) P. Cao, M. Moini, *J. Am. Soc. Mass Spectrom*., **9**, 1081, (1998).

(14) J.-T.Wu, L. He, M. Li, S. Parus, D. Lubman, *J. Am. Soc. Mass Spectrom*., **8**, 1237, (1997).

(15) M. Karas, F. Hillenkamp, *Anal. Chem*., **60**, 2299, (1988).

(16) M. Karas, U. Bahr in *Mass Spectrometry in Biomolecular Sciences*, edited by R.M. Capprioli, A. Malorni, G. Sindona, NATO ASI Ser., Ser. C, Vol 475, Kluwer Academic Publishers, London, England, p. 33, (1996).

(17) R. Zenobi, R. Knochenmuss, *Mass Spectrom. Rev.*, **17**, 337, (1999).

(18) Cotter, R.J. (Ed.) *Time-of-Flight Mass Spectrometry: Instrumentation and Applications in Biological Research*. ACS, Washington, DC, (1997).

(19) G. Kinsel, L. Preston, D. Russell, *Biol. Mass Spectrom*., **23**, 205, (1994).

(20) A. Vertes, R. Gijbels, F. Adams (Eds.) *Chemical Analysis,* p. 124 Wiley, New York, (1993).

(21) F. Strobel, T. Solouki, M. White, D. Russell, *J. Am. Soc. Mass Spectrom.,* **2**, 91, (1991).

(22) T. Laurell, J. Nilsson, G. Marko-Varga, *J. Chromatogr., B: Biomed. Sci. Appl.,* **752**, 217, (2001).

(23) J. Preisler, P. Hu, T. Rejtar, B. Karger, *Anal. Chem*.,**72**, 4785, (2000).

(24) S. Jespersen, W. Niessen, U. Tjaden, J. van der Greef, E. Litborn, U. Lindberg, J. Roeraade, *Rapid Commun. Mass Spectrom.*, **8**, 581, (1994).

(25) K. Gillig, B. Ruotolo, E. Stone, D. Russell, K. Fuhrer, M. Gonin, A. Schultz, *Anal Chem.*, **72**, 3965, (2000).

(26) J. Ragas, T. Simmons, P. Limbach, *Analyst*, **125**, 575, (2000).

(27) R. Bagshaw, J. Callahan, D. Mahuran, *Anal. Biochem.*,**284**, 432, (2000).

(28) Z.-Y. Park, D. Russell, *Anal. Chem.*, **73**, 2558, (2001).

(29) G. Porter, R. Luedke, *Amer. Biotech. Lab.*, **21**, 70, (2003).

(30) L. Li, E. Romanova, S. Rubakhin, V. Alexeeva, K. Weiss, F. Vilim, J. Sweedler, *Anal. Chem.,* **72**, 3867,(2000).

(31) A.L. Burlingame, S.A. Carr, in *Mass Spectrometry Biological Science*, Vol. 151, edited by J. Stults, W. Henzel, S. Wong, C. Watanabe p. 234, Springer-Verlag, New York (1996).

(32) J. Selley, J. Swift, T. Attwood, *Bioinformatics*, **17**, 105,(2001).

(33) J. Yates III, *Electrophoresis* **19**, 893, (1998).

(34) P. Kowalski, J. Stoerker, *Pharmacogenomics*, **1**, 359, (2000).

(35) A. Shevchenko, A. Loboda, A. Shevchenko, W. Ens, K. Standing, *Anal. Chem*., **72**, 2132, (2000).

(36) I. Humphery-Smith, S. Cordwell, W. Blackstock, *Electrophoresis* **18**, 1217, (1997).

(37) G. Corthals, S. Gygi, R. Aebersold, S. Patterson, in *Proteome Research: Two-Dimensional Gel Electrophoresis Detection Methods,* edited by T. Rabilloud, Springer-Verlag, Berlin, p. 197, (2000).

(38) R. Aebersold, M. Mann, *Nature,* **422**, 198, (2003).

(39) E. Murphy, R. Edmondson, D. Russell, S. Colles, F. Schroeder, *Biochimica et Biophysica Acta,* **1436**, 413,(1999).

(40) K.R. Jennings, *Int. J. Mass Spectrom.*, **200**, 479, (2000)

(41) A.K. Shukla, J.H. Futrell, *J. Mass Spectrom*., **35**, 1069,(2000)

(42) F.W. McLafferty (Ed.), *Tandem Mass Spectrometry,* Wiley, New York, (1983).

(43) K. Gillig, B. Ruotolo, E. Stone, K. Fuhrer, M. Gonin, A. Schultz, D. Russell, *Anal. Chem*. **72**, 3965, (2000).

(44) K.M. Downard (Ed.) *New Advances in Analytical Chemistry*, Harwood Academic Publishers, Amsterdam, (2000).

(45) R.J. Cotter (Ed) *Time-of-Flight Mass Spectrometry: Instrumentation and Applications in Biological Research.*, ACS, Washington DC, (1997).

(46) F.W. McLafferty (Ed.), *Tandem Mass Spectrometry*, John Wiley and Sons, New York, p. 1 (1983).

(47) D. Figeys, G. Corthals, B. Gallis, D. Goodlett, A. Ducret, M. Corson, R. Aebersold, *Anal. Chem*., **71**, 2279, (1999).

(48) H. Cooper, P. Derrick, in *Mass Spectrometry in Biomolecular Sciences*, edited by R.M. Caprioli, A. Malorni, G. Sindona, NATO ASI Ser., Ser. C, Vol 475, Kluwer Academic Publishers, London, p. 201, (1996).

(49) D. Barbacci, D. Russell, *J. Am. Soc. Mass Spectrom.,* **10**, 1038, (1999).

(50) B. Spengler, D. Kirsch, R. Kaufmann, *Rapid Commun. Mass Spectrom*., **5**, 198, (1991).

(51) V. Grill, J. Shen, C. Evans, R. Cooks, *Rev Sci Inst,* **72**, 3149, (2001).

(52) L. Lingjun, C. Masselon, G. Anderson, T. Conrads, K. Alving, L. Pasa-Tolic, T. Veenstra, R. Smith, in *Proceedings of the 2001 Pittsburgh Conference* New Orleans, LA, March 2001, p 1183.

(53) J. Holland, C. Enke, J. Allison, J. Stults, D. Pinkston, B. Newcome, J. Watson, *Anal. Chem*., **55**, 997A, (1983).

(54) J. Banks Jr., T. Dresch, *Anal. Chem*., **68**, 1480, (1996).

(55) E. W. McDaniel, E.A. Mason, (Eds.) *The Mobility and Diffusion of Ions in Gases.* Wiley-Interscience, New York, (1973).

(56) E. Stone, K. Gillig, B. Ruotolo, Z.-Y. Park, D. Russell, K. Fuhrer, A. Schultz, in *Proceedings of the 48th ASMS Conf. on Mass Spec. and Allied Topics*, Long Beach, CA. 2000, p. 318.

(57) S. Valentine, A. Counterman, D. Clemmer, *J. Am. Soc. Mass Spectrom*. **10**, 1188, (1999).

(58) a) B. Ruotolo, G. Verbeck IV, L. Thompson, K. Gillig, D. Russell, *J. Am. Chem. Soc.*, **124**, 4214, (2002), b) B. Ruotolo, G. Verbeck IV, L. Thompson, A. Woods, K. Gillig, D. Russell, *J. Proteome Res.*, **1**, 303, (2002), c) B. Ruotolo, K. Gillig, E. Stone, D. Russell, *J. Chrom. B.* 2002, **782**, 385, d) B. Ruotolo, D. Russell, Submitted to Biochemistry, 2003.

(59) S. Valentine, A. Counterman, D. Clemmer, *J. Am. Soc. Mass Spectrom,* **10**, 1188, (1999).

(60) (a) C. Creaser, M. Benyezzar, J. Griffiths, J. Stygall, *Anal. Chem*., **72**, 2724, (2000), b) G. Eiceman, J. Bergloff, J. Rodriquez, W. Munro, Z. Karpas, *J. Am. Soc. Mass Spectrom.*, **10**, 1157, (1999), c) C. Hoaglund-Hyzer, J. Li, D. Clemmer, *Anal. Chem*., **72**, 2737,(2000).

(61) B. Ruotolo, K. Gillig, E. Stone, D. Russell, K. Fuhrer, M. Gonin, A. Schultz, *Int. J. Mass Spectrom.*, **219**, 253,(2002).

(62) H. Revercomb, E. Mason, *Anal. Chem*., **47**, 970, (1975).

(63) H. Tammet, *J. Aerosol Sci.*, **26**, 459,(1995).

(64) G. Griffin, I. Dzidic, D. Carroll, R. Stillwell, E. Horning, *Anal. Chem.,* **45**, 1204*,* (1973).

(65) Z. Berant, Z. Karpas, *J. Am. Chem. Soc*., **111**, 3819, (1989).

(66) B. Ruotolo, K. Gillig, E. Stone, D. Russell, *J. Chrom. B*, **782**, 385, (2002).

(67) B. Ruotolo, J. McLean, K. Gillig, D. Russell, Submitted to J. Mass Spec. 2003.

(68) R. Beavis, B. Chait, *Anal. Chem,.* **62**, 1836, (1990).

(69) R. Cotter, *Anal. Chem.,* **64**, 1027A, (1992)

(70) G. Montaudo, M. Montaudo, C. Puglisi, F. Samperi, *Rapid Commun. Mass Spectrom.*, **8**, 981,(1994).

(71) G. Montaudo, M. Montaudo, C. Puglisi, F. Samperi, *Anal. Chem.*, **66**, 4366,(1994).

(72) J. Lewis, J. Krone, R. Nelson, *Biotechniques,* **24**, 102, (1998).

(73) d. Despeyroux, A. Wright, K. Jennings, *Int. J. Mass Spectrom. Ion Processes,* **126**, 95, (1993).

(74) R. Cooks, T. Ast, M. Mabud, *Int. J. Mass Spectrom. Ion Processes,* **100**, 209, (1990).

(75) D. Schultz, H. Lim, S. Garbis, L. Hanley, *J. Mass Spectrom*. **34**, 217, (1999).

(76) Jennings, K.R., (Ed.) R. Cooks, S. Miller, in *Fundamentals and Applications of Gas Phase Ion Chemistry,* NATO ASI Ser., Ser. C, edited by K.R. Jennings, Kluwer Academic Publishers, London, p. 55, (1999).

(77) ProteoMetrics, 1997 http://prowl.rockefeller.edu/.

(78) D. Pappin, P. Hojrup, A. Bleasby, *Curr. Biol.*, **3**, 327, (1993).

(79) G. Kinsel, L. Preston, D. Russell, *Biological Mass Spec.,* **23**, 205, (1993).

(80) H. Cooper, P. Derrick, in *Mass Spectrometry in Biomolecular Sciences*, edited by R.M. Caprioli, A. Malorni, G. Sindona, NATO ASI Ser., Ser. C, Vol 475, Kluwer Academic Publishers, London, England, p. 201, (1996).

(81) D. Barbacci, D. Russell, *J. Am. Soc. Mass Spectrom*., **10**, 1038,(1999).

(82) Jennings, K.R., (Ed.) R. Cooks, S. Miller, in *Fundamentals and Applications of Gas Phase Ion Chemistry,* NATO ASI Ser., Ser. C, edited by K.R. Jennings, Kluwer Academic Publishers, London, p. 55, (1999).

(83) E. Denisov, J. Laskin, A. Shukla, J. Futrell, in *Proceedings of the 49th ASMS Conf. on Mass Spectrom. and Allied Topics*, Chicago, IL, 2001, p. 961.

(84) I. Humphery-Smith, S. Cordwell, W. Blackstock, *Electrophoresis,* **18**, 1217, (1997).

(85) (a) G. Corthals, S. Gygi, R. Aebersold, S. Patterson, (Eds.) *Identification of Proteins by Mass Spectrometry*. , Kluwer Academic Publishers, London, (1998) (b) Rabilloud, T. (Ed.) *Proteome Research: Two-Dimensional Gel Electrophoresis Detection Methods*, Springer-Verlag, Berlin, p. 204, (2000).

(86) A. Ducret, I. Van Oostveen, J. Eng, J. Yates III, R. Aebersold, *Protein Sci.,* **7**, 706, (1998).

(87) R. St. Louis, H. Hill Jr., *Crit. Rev. Anal. Chem*., **21**, 321, (1990).

(88) B. Ruotolo, K. Gillig, E. Stone, D. Russell, *J. Chrom. B,* **78**, 385, (2002).

(89) E.A. Mason, E.W. McDaniel, *Transport Properties of Ions in Gases,* John Wiley and Sons, Inc., New York (1988).

(90) E. Stone, K. Gillig, B. Ruotolo, K. Fuhrer, M. Gonin, A. Schultz, D. Russell, *Anal. Chem*., **73**, 2233, (2000).

(91) C. Hoaglund-Hyzer, J. Li, D. Clemmer, *Anal. Chem*. **72**, 2737, (2000).

(92) K. Gillig, D. Russell, K. Fuhrer, M. Gonin, A. Schultz, in *Proceedings of the 47th ASMS Conf. on Mass Spec. and Allied Topics*, Dallas, TX, (1999), p. 1047.

(93) V. Laiko, M. Baldwin, A. Burlingame, *Anal. Chem.,* **72**, 652*,* (2000).

(94) J. Bai, S. Fischer, J. Flanagan, Eur. Pat. No. 964427 (1999).

(95) B. Erickson, *Anal. Chem.,* **72**, 186A, (2000).

(96) C. Hoaglund-Hyzer, J. Li, D. Clemmer, *Anal. Chem.,* **72**, 2737, (2000).

(97) E. Williams, K. Henry, F. McLafferty, J. Shabanowitz, D. Hunt, *J. Am. Soc. Mass Spectrom.*, **1**, 413, (1990).

(98) B. Spengler, D. Kirsch, R. Kaufmann, M. Karas, F. Hillenkamp, U. Giessmann, *Rapid Commun. Mass Spectrom.,* **4**, 301, (1990).

(99) A. Wieghaus, L. Schmidt, A. Popova, V. Komarov, H. Jungclas, *Rapid Commun. Mass Spectrom.,* **14**, 1654, (2000).

(100) M. Bier, J. Amy, R. Cooks, J. Syka, P. Ceja, G. Stafford, *Int. J. Mass Spectrom. Ion Processes* **77**, 31*,* (1987).

(101) Z.-Y. Park, D. Russell, *Anal. Chem.,* **72**, 2667, (2000).

(102) T. Solouki, K. Gillig, D. Russell, *Rapid Commun. Mass Spectrom.,* **8**, 26*,* (1994).

(103) R. Edmondson, D. Russell, in *Mass Spectrometry of Biological Materials,* edited by C. McEwen, B. Larsen, Marcel-Dekker, New York, (1998).

(104) C. Hoaglund-Hyzer, J. Li, D. Clemmer, *Anal. Chem.*, **72**, 2737, (2000).

(105) A. Dongre, A. Somogyi, V. Wysocki, *J. of Mass Spec.*, **31**, 339, (1996).

(106) K. Paech, R. Jockusch, E. Williams, *J. Phys. Chem. A*, **106**, 9761, (2002).

(107) R. Kaiser Jr., R. Cooks, J. Syka, G. Stafford Jr., *Rapid Commun. Mass Spectrom.,* **4**, 30*,* (1990).

(108) R. Chorush, D. Little, S. Beu, T. Wood, F. McLafferty, *Anal. Chem.*, **67**, 1042, (1995).

(109) M. Mabud, T. Ast, R. Cooks, *Org. Mass Spectrum.*, **22**, 418, (1987).

(110) A. Counterman, S. Valentine, C. Srebalus, S. Henderson, C. Hoaglund, D. Clemmer, *J. Amer. Soc. Mass Spectrom.*, **9**, 743,(1998).

(111) Z.-Y. Park, D. Russell, *Anal. Chem.*, **72**, 2667, (2000).

(112) J. Hettick, D. Russell, *Anal. Chem.*, **73**, 5378, (2001).

(113) D. Reiderer, L.Haney, A. Hilgenbrink, J. Beck, in *Proceedings of the 48th ASMS Conf. on Mass Spectrom. and Allied Topics* Long Beach, CA, 2000, p. 883.

(114) D. Russell, R. Edmondson, *J. Mass Spectrom.*, **32**, 263, (1997).

(115) J. Loo, C. Edmonds, R. Smith, *Anal. Chem*., **65**, 425, (1993).

(116) S.Shields, B. Bluhm, D. Russell, *J. Am. Soc. Mass Spectrom.,* **11**, 626*,* (2000).

(117) A. Dongre, A. Somogyi, V. Wysocki, *J. Mass Spectrom*., **31**, 339, (1996).

(118) M. Mak, G. Mezo, Zs. Skribanek, F. Hudecz, *Rapid Commun. Mass Spectrom.*, **12**, 837, (1998).

(119) K. Gillig, E. Stone, G. Verbeck IV, B. Ruotolo, D. Russell, Submitted to Rev. Sci. Inst. 2003.

(120) T.W. Carr (Ed.), *Plasma Chromatography.* Plenum Press, New York, (1984).

(121) D. Riederer, L. Haney, A. Hilgenbrink, J. Beck in *Proceedings of the 48th ASMS Conf. on Mass Spectrom. and Allied Topics*, Long Beach, CA, 2000, p. 1245.

(122) S. Miller, H. Luo, X. Jiang, H. Rohrs, R. Cooks, *Int. J. Mass Spectrom. Ion Processes,* **160**, 83, (1997).

(123) J. Callahan, A. Somogyi, V. Wysocki, *Rapid Commun. Mass Spectrom.,* **7**, 693, (1993).

(124) M. Meot-Near (Mautner), A. Dongree, A. Somogyi, V. Wysocki, *Rapid Communications in Mass Spectrometry*, **9**, 829, (1995).

(125) W. Price, E. Williams, *J. Phys. Chem. A,* **101**, 8844,(1997).

(126) T. Baer and W. Hase*, Unimolecular Reaction Dynamics, Theory and Experiments.* Oxford University Press, New York, (1996).

(127) J. Laskin, J. Futrell, *J. Chem. Phys*., **119**, 3413, (2003).

(128) J. Laskin, T. Bailey, J. Futrell, *J. Amer. Chem. Soc.,* **125**, 1625, (2003).

(129) J. Laskin, J. Futrell, *J. Phys. Chem. A*, **107**, 5836, (2003).

(130) A. Counterman, S. Valentine, C. Srebalus, S. Henderson, C. Hoaglund, D. Clemmer, *J. Amer. Soc. Mass Spectrom.*, **9**, 743, (1998).

(131) M. Karas, R. Krueger, *Chem. Rev.*, **103**, 427, (2003).

(132) S. Matsushima, H. Shichi, *J. Ocular. Pharm.*, **5**, 261, (1989).

(133) D. Zhao, N. Dhalla, *Canadian J. Phys. Pharm.* **67**, 546, (1989).

VITA

Earle Gregory Stone

5646 Sir Gareth

San Antonio, Texas 78218

PRIOR EDUCATION

Associate of Applied Science, Machining Technology, (summa cum laude), St. Philip's College, San Antonio, Texas, December, 1994

Bachelor of Science, Chemistry, (cum laude), University of Texas at San Antonio, San Antonio, Texas, May 1997